EFFECTS OF UNDRAINED SHEAR STRENGTH PROFILE ON RETROGRESSIVE LANDSLIDES IN SENSITIVE CLAYS

by

© PIASH SAHA

A thesis submitted to the

School of Graduate Studies

in partial fulfillment of the requirements for the degree of

Master of Engineering (Civil)

Faculty of Engineering and Applied Science

Memorial University of Newfoundland

February 2023

St. John's Newfoundland and Labrador Canada

ABSTRACT

The undrained shear strength of normally and lightly overconsolidated clays generally increases with depth, which could significantly influence the failure of a slope. Large-scale landslides in sensitive clays generally occur by a successive failure of soil blocks, and the maximum depth of the sliding plane of these failure blocks typically reaches the level of the toe or slightly below the toe. The traditional limit equilibrium (LE) methods cannot model the progressive failure, and the typical Lagrangian-based finite element (FE) modelling technique cannot simulate the complete process of sensitive clay landslides because of significant mesh distortion around the failure planes. Eulerian-based FE simulations are performed in this study to investigate whether the initial undrained shear strength profile and strain-softening could be the cause of failure observed in sensitive clay landslides.

To investigate the effects of the initial shear strength profile, the analyses are performed first for linearly increasing shear strength with depth for elastic perfectly plastic soil (i.e., no softening) with a relatively stronger soil layer below the toe. It is found that the shear strength gradient and depth of the stronger soil layer below the toe affect the location of the critical failure plane, the factor of safety, and the strength reduction factor in finite element analysis.

For sensitive clay landslides, in addition to the depth and strength increase in the stronger clay layer below the toe, the rate of softening affects the failure plane formation and landslide extent. Higher strength and slower softening rate could be the cause of shallower failure of the soil blocks and a larger retrogression distance.

ACKNOWLEDGEMENTS

To begin, I want to express my heartfelt gratitude to Almighty God for providing me with good health throughout my research period and for allowing me to be a part of Memorial University of Newfoundland.

I would like to express my heartfelt appreciation to my supervisor, Dr. Bipul Hawlader, Professor at Memorial University of Newfoundland (MUN), Newfoundland, Canada, for his constant guidance, insightful suggestions, motivation, and encouragement throughout the research study. I consider myself extremely fortunate to have him as a supervisor. Without his immense support and constant guidance, this thesis would not have been possible.

Additionally, I would like to express my heartiest gratitude to Dr. Ripon Karmaker, Dr. Jin Chen, Pritam Kundu, and Dr. Chen Wang for their insightful advice, suggestions, and time that helped in the advancement of my research. I would like to express my appreciation to previous and current students working under Dr. Hawlader for their cooperation throughout various difficulties and for their constant encouragement and knowledge sharing.

I would not have been able to study at MUN if it hadn't been for Dr. Md. Rokonuzzaman and Dr. A.B.M Saifullah's recommendations. I will be eternally grateful for their assistance. Thank you, Riju Chandra Saha, for sharing your experiences with me during the application and visa process. Sudipta Bhowmick was extremely helpful with his printing resources. I'm also grateful to my St. John's friends for their encouragement, support, and fond memories. Thank you so much to all of the faculty and staff at MUN's Faculty of Engineering and Applied Science.

I would like to express my gratitude to the School of Graduate Studies at MUN, the Natural Sciences and Engineering Research Council of Canada (NSERC), Equinor, Petroleum Research

Newfoundland and Labrador (PRNL), and Mitacs for their financial support in conducting this research.

Last but not least, I am eternally grateful to my parents, better half, and all of my family members for their unending love, constant encouragement, and spiritual support throughout this study. I would not be able to complete my research without their assistance.

This thesis is dedicated to all of them.

Table of Contents

List of Figures

List of Tables

List of Symbols

c	Constant $= (1 - s_{uR}/s_{u0})e^{-6}$
E_u	undrained Young's modulus
f_1	strain-softening factor
f_2	strain-rate factor
S_t	sensitivity = s_{u0}/s_{uR}
s_u	mobilized undrained shear strength
s_{u0}	s_u before strain softening and at $\dot{\gamma}_{ref}$
$s_{u,ref}$	undrained shear strength at $\dot{\gamma}_{ref}$
s_{uh}	maximum value of shear stress on the horizontal surface
s_{uld}	s_u at large displacements
s_{uR}	s_u mobilized in shear band at considerable shear displacement
t_{FE}	thickness of finite element
v_x	velocity along x-axis
v_y	velocity along y-axis
v_z	velocity along z-axis
β	soil parameter for strain-rate effect in power-law model
γ	total unit weight of soil
γ^p	engineering plastic shear strain
$\dot{\gamma}$	shear strain rate
$\dot{\gamma}_{ref}$	reference shear strain rate
δ	plastic shear displacement
δ_{95}	δ at which s_u reduced by 95% of $(s_{u0} - s_{uR})$

δ_{ld}	δ at large displacements
ε_q^p	equivalent plastic shear strain
η	soil parameter for strain-rate effect in additive power-law model
μ	soil parameter for strain-rate effect in semi-logarithmic model
ν_u	undrained Poisson's ratio

Chapter 1: Introduction

1.1 General

In the early stages, analytical methods are used to evaluate the stability of slopes, and the analyses are performed for idealized conditions (Fredlund and Krahn 1977; Han and Leshchinsky 2004; Cheng et al. 2007; Ho 2014), assuming a circular failure plane and uniform shear strength profile. However, in many practical situations, such idealization might be questionable. For example, shear strength might vary with depth and a non-circular failure plane might form. Several computer programmes, such as SLOPE/W, were developed based on the limit equilibrium (LE) approach to accommodate complex geometry and shear strengths. These programs were successfully used to calculate the factor of safety (F_s) of embankments and cut slopes based on the equilibrium of the single soil block above the potential failure plane. However, many large-scale landslides in sensitive clays involve the failure of a number of soil blocks, and the failed blocks displace tens to hundreds of meters in some cases, which cannot be modelled using these LE-based computer programs. The finite element (FE) method could be a better approach to model such problems as it provides deformation; advanced soil models could be implemented and the analyses could be performed for complex geometry and failure conditions. Unfortunately, Lagrangian-based FE techniques, as commonly used in geotechnical engineering, cannot simulate such landslides because of large plastic shear strain development around the failure planes. Therefore, in the present study, a Eulerian-based FE method is used, which does not have any numerical issue related to mesh distortion.

Stability analysis of clay slopes is generally performed for both drained (long-term and slow loading) and undrained (short-term and rapid loading) conditions. Although the initiation of failure might be a slow loading process (e.g., toe erosion), the failure of subsequent soil blocks in a sensitive

clay landslide generally occurs rapidly, in a matter of a few minutes. Locat et al. (2011) schematically showed the mechanisms of shear band propagation with the dislocation of soil blocks with time. Several studies numerically simulated the undrained progressive formation of shear bands (Dey et al. 2015; Wang et al. 2021; Karmaker et al. 2022). Progressive failure of the soil blocks occurs due to the strain-softening behaviour of sensitive clays.

Different types of failure surfaces are considered in slope stability analysis (e.g., circular or non-circular). The formation of the failure plane is more complex in sensitive clay landslides, and, depending upon the progressive formation of the failure plane, different types of landslides occur in the field (e.g., flowslide and spread). The extent of sensitive clay landslide (retrogression and runout) depends on the type of landslide.

Many post-slide investigations were conducted in the past which identified the type of landslides and their soil profiles (Bélanger et al. 2017; Locat et al. 2017; Kvalstad et al. 2005). The variation of undrained shear strength was measured not only in the intact soil behind the backscarp but also through the debris (Demers et al. 2014; Thakur et al. 2014; Wang et al. 2021). One of the main objectives of such investigations was to find the relationship between the failure pattern (including the location of the sliding plane) and the soil shear strength profile.

Post-slide field investigations show a constant undrained shear strength profile up to the failure plane in some cases (Perret et al. 2019); however, in many cases, the undrained shear strength increases with depth, at least up to the maximum depth of the sliding plane (e.g., Saint-Jude landslide, Locat et al. 2017; Rigaud landslide, Carson 1979). In some cases, different soil units were obtained above and below the failure plane, although the undrained shear strength of soil units may not have

been significantly different. Therefore, a question that remains unanswered is whether the variation of shear strength could affect the failure pattern and thereby the landslide extent.

The effects of shear strength variation on failure patterns for non-sensitive clays could be investigated using computer programs developed from the limit equilibrium approach or typical Lagrangian-based finite element (FE) programs. Analytical approaches could be also used for simplified conditions (Han and Leshchinsky 2004; Cheng et al. 2007). However, those approaches cannot be used for sensitive clay landslide analysis because the soil has strain-softening behaviour, failure occurs by progressive formation of failure planes, and debris flows over a large distance. For example, a large landslide occurred in the municipality of Saint-Jude, Quebec, about 50 km northeast of Montréal, on May 10, 2010, at 20:25 p.m. The landslide occurred along the Salvail River in a sensitive Champlain Sea clay deposit. The landslide affected a 275 m-long section parallel to the river. The landslide retrogression distance was 80 m from the initial crest of the slope to the backscarp of the landslide. The total debris volume was approximately 520,000 m^3. Since it occurs suddenly, without warning, and can cover large areas, this type of catastrophic landslide affects human life and infrastructure in many cases. Figure 1.1 shows a view of the south part of the Saint-Jude landslide, highlighting the complex displacement of debris.

Figure 1.1: South part of Saint-Jude landslide (Locat et al. 2017)

Another example is the 1908 landslide in Notre-Dame-de-la-Salette, Québec shown in fig. 1.2. It was one of the deadliest incidents in the history of sensitive clay landslides in eastern Canada, and was the cause of 33 deaths, in addition to other damages. Twenty six of those deaths were associated with the tsunami-generated impact of water and ice on the opposite bank. A total of 6.5 ha was covered by the failed soil mass, which was roughly 1.2 million m^3 in volume.

Figure 1.2: Aerial map of the Notre-Dame-de-la-Salette landslide, Québec (Perret et al. 2013)

Another important observation in post-slide investigations is that soil units are not similar above and below the failure plane. For example, the post-slide investigation of the St. Jude landslide area shows different soil units above and below the failure planes. Bélanger et al. (2017) found two sensitive clay layers in a landslide area: (i) below the crust, the soil is highly sensitive, with high clay content, less silt content, high liquidity index and low residual shear strength, and (ii) below the failure plane (~ 22 m depth), the soil is less sensitive.

A weathered crust is commonly observed near the ground surface. The behaviour of such surficial crust is relatively complex as it is affected by seasonal effects (e.g., freezing and thawing). An extensive fracture might occur due to repeated periods of wetting and drying (Rayhani et al. 2007). The surficial crust is relatively difficult to model because the shear strength depends on many variables, including desiccation, pore water pressure response, groundwater level, and anisotropy (Sully 1993). While many studies were dedicated to clay slopes, a very limited number of studies are available in the literature that investigated the effects of surficial crust on sensitive clay landslides.

1.2 Rationale

Post-slide investigations of large-scale landslide areas show that, for similar geometry and potential triggering factors, the failure pattern varies. For example, flowslide occurs by successive rotational failure of soil blocks in some cases, while in other cases spread type failures occur by formation of triangular failure blocks. In spreads, a quasi-horizontal failure surface is formed around the depth of the toe of the slope. The failure pattern has a significant practical implication as it affects the landslide extent and thereby potential hazards. The mechanisms and potential causes of such varying failure patterns could not be explained using typical limit equilibrium or Lagrangian-based FE analyses. Therefore, advanced numerical analysis that can handle large deformation of soil, as presented in this thesis, is required.

Another challenge in stability analysis of sensitive clay slope is modelling of surficial crust. This soil layer could considerably affect the landslide pattern. Unfortunately, the stress-strain response of the crust is complex, as geological and seasonal effects change its behaviour. Therefore, by modelling the crust for varying conditions, critical scenarios could be identified, which could also provide further insights into overall failure mechanisms.

1.3 Objectives

The main objective of this research is to investigate the effects of soil shear strength on the failure pattern of sensitive clay slopes. The following steps are taken to achieve that objective.

- Develop a large deformation FE modelling technique for slope stability analysis using the Eulerian-based FE modelling approach in the commercially available Abaqus FE software.
- Incorporate strain-softening, strain-rate and depth-dependent undrained shear strength model using user subroutines.
- Calibrate the developed FE model by comparing the results with available analytical solutions and LE analyses for simplified soil behaviour (elastic–perfectly plastic material).
- Examine the role of shear strength variation, including the rate of strain softening and the existence of different soil units, in the progressive formation of the failure plane, and thereby, the failure pattern and landslide extent.
- Examine the role of surficial crust on failure patterns by modelling the crust in undrained conditions.

1.4 Outline of the thesis

The thesis consists of the following five chapters.

Chapter 1 highlights the background and objectives of the research.

Chapter 2 provides a comprehensive literature review. The literature review covers the studies mainly related to the shear strength profile of clay and surficial crust, especially focused on sensitive clay. The literature review also includes studies on the behaviour of sensitive clay and its role in the retrogressive failure. The findings from field investigations and numerical simulations are discussed. Moreover, the limitations of previous studies are summarized in this chapter.

Chapter 3 presents LE and FE analyses of elastic perfectly plastic clay slopes. The primary goal of this chapter is to investigate the stability of a linearly increasing clayey soil profile and to compare the results of analytical solutions, LE analysis and FE simulation.

Chapter 4 presents large-deformation FE modelling of sensitive clay landslides. The effect of an undrained shear strength profile on retrogressive landslides in sensitive clays is investigated in this chapter. A part of this work has been published as Saha, P., Karmaker, R. and Hawlader, B. 2022. "Effect of undrained shear strength profile on retrogressive landslides in sensitive clays" 8th Geohazards Conference, Quebec City, Quebec, Canada.

Chapter 5 summarises the findings of the study and makes some recommendations for future research.

Chapter 2: Literature Review

2.1 General

Slope failure is a well-known problem and is a critical issue for many engineering designs. Historically, slope stability has been assessed using limit equilibrium (LE) methods, and the analyses are performed for idealized conditions. For example, several slope stability analysis methods have been developed to investigate the homogeneous undrained shear strength of soil (e.g., Taylor 1937) although some studies considered linearly increasing shear strength profiles (Gibson and Morgenstern 1962; Hunter and Schuster 1968). In many cases, analyses are performed assuming a circular failure plane. Landslides in sensitive clay are the focus of the present study that involves the following features, which are different from those considered in typical slope stability analysis: (i) undrained shear strength is not uniform; rather, it increases with depth, and a relatively stronger surficial crust of several meters exists in many cases; (ii) soil exhibits strain-softening behaviour, and the shear strength could be very small at large shear strains; (iii) failure surface generates progressively; (iv) landslide occurs by successive failure of a number of soil blocks; (v) upslope retrogression and failure patterns depend on the displacement of the failed soil block (tens to hundreds of meters in some cases), and (vi) failure planes are not circular in many cases. These features cannot be incorporated in the existing LE methods. In the following sections, a critical review of existing methods (analytical, LE and FE) is presented. The literature review primarily focuses on undrained failure of clay slopes, and more specifically, landslides in sensitive clays. The literature review is organized as follows. First, the advantages and limitations of available limit equilibrium methods are discussed. Second, as the LE method cannot accommodate soil deformation and strain-softening, the available FE methods that could consider these aspects in slope stability analysis are reviewed. Third, as the focus of the present study is to investigate the effects of shear strength on a landslide, the shear

strength profiles reported from field and laboratory investigations in sensitive clay landslide areas are presented. Finally, the large-deformation FE modelling and its application to sensitive clay landslides is presented.

2.2 Limit Equilibrium Methods

Limit equilibrium (LE) methods are widely used to check the stability of slopes in terms of the factor of safety (F_s). They provide reasonable answers, and the analysis is simple enough for typical geotechnical problems. In previous studies, various techniques have been developed in the LE framework, including the shape of the slip surface (e.g., circular and non-circular), soil shear strength profiles (e.g., uniform and varying shear strength), and drainage conditions (i.e., drained and undrained). As this thesis focuses on the undrained behaviour of soil, previous studies on undrained failure of slopes are discussed in the following sections.

2.2.1 LE analysis for homogenous soil

A number of slope stability analysis techniques have been developed for homogeneous soil with uniform soil properties using LE methods. To show the performance of these techniques, some studies conducted FE analysis using the strength reduction method and compared the F_s obtained from LE methods with the Strength Reduction Factor (SRF) obtained from FE or finite difference analysis. Table 2.1 shows some of these analyses.

Table 2.1: Limit equilibrium analysis and comparison with numerical solutions for homogenous clay slope in undrained conditions

References	Method	Remarks
Fredlund and Krahn (1977)	Method of slices using the SLOPE/W program	Compared F_s for various methods for slope stability analysis.
Han and Leshchinsky (2004)	Bishop's method in LE analysis	Verified LE analysis results with continuum mechanics-based finite difference analysis using FLAC 2D.
Zolfaghari et al. (2005)	Morgenstern-Price using SlopeSGA	Developed an algorithm to find the critical noncircular failure surface.
Cheng et al. (2007)	Morgenstern-Price method	Examined the performance of the strength reduction method.
Steward et al. (2011)	Morgenstern-Price using SLOPE/W	Analyzed the stability of c–ϕ soil.
Ho (2014)	Bishop's method using SLOPE/W	Compared F_s obtained from different LE methods with SRF for different geometric conditions.

2.2.2 LE analysis for linearly increasing shear strength profile

A linear increase in undrained shear strength with depth is commonly observed in the field (Gibson and Morgenstern 1962) in normally consolidated clay. One might assume average undrained shear strength of the soil layer and perform stability analysis, as in the previous section; however, such an assumption would lead to inaccurate results (Gibson and Morgenstern 1962). In the field, a strong overconsolidated clay crust is commonly observed near the ground surface. However, in previous studies, the varying strength of crust is neglected, and the analyses are performed assuming a linear increase of undrained shear strength (s_{u0}) with depth (z) as $s_{u0} = s_{ug} + kz$, where s_{ug} is the shear strength

at the ground surface ($z = 0$), and k is the rate of shear strength increase with depth. Typical values of undrained shear strength and strength gradient are shown in Table 2.2.

Table 2.2: Typical values of undrained shear strength and other parameters for normally consolidated clays (Koppula 1984)

Material	Water content %	Plastic limit %	Liquid limit %	Strength at $z = 0$ kPa	Strength gradient k, kPa/m	Reference
Soft clay	40–50	20–30	50–70	2.5	2.5	Bjerrum and Overland (1957)
Sensitive clay	37	18	26	0	1.5	Bjerrum (1961)
New Liskeard varved clay	60	27	65	10	1.83	Lo and Stermac (1965)
Nicolet clay	60	20	40–50	2.5	3.5	Kenney (1965)
Drammen clay	30–40	20	30–40	2.5	1.5	Bjerrum (1967)
Liestranda clay	35	19	25	5.0	0.8	DiBiagio and Aas (1968)
San Francisco Bay mud	55	30	50	7.5	1.25	Duncan and Buchignani (1973)

For normally consolidated clay layers having zero undrained shear strength at the ground surface, Gibson and Morgenstern (1962) developed an analytical solution assuming a circular failure plane and found that the factor of safety against undrained failure of a cut slope depends on the slope height, slope angle, rate of shear strength increases with depth, and bulk unit weight of the soil. The solution developed by Gibson and Morgenstern (1962) is valid for the groundwater table at or above the ground surface. Hunter and Schuster (1968) advanced the solution for common cases of the groundwater table (i.e., below the ground surface). They found that F_s is independent of slope height but might depend on depth of the failure plane. They developed the solutions for varying depth of failure plane locations.

Davis and Booker (1971, 1973) found that the slip circle method seriously overestimates the bearing capacity of a foundation. They examined possible limitations of the slip circle method, as used by Gibson and Morgenstern (1962), by means of the theory of plasticity, and showed that the

difference between the solution obtained from the slip circle and plasticity theory is high for flat slope cases and for many practical cases (e.g., $\beta > 10°$), and that for steeper slopes, both approaches give comparable results (Booker and Davis 1972).

Koppula (1984) developed a slope stability analysis method for normally consolidated clay with non-zero (positive) shear strength at the ground surface, as commonly observed in the field. It has been shown that the stability number decreases with slope angle and increases with the dimensionless cohesion factor $c_R = kH/s_{ug}$, where H is the height of the slope. Koppula (1984) developed the solution assuming that the critical failure plane is circular and passes through the toe. This assumption has been questioned by Shen and Brand (1985) because the failure may not be always at the toe circle, but could be deep-seated for higher values of s_{ug} and lower k.

Yu et al. (1998) compared conventional limit equilibrium analysis results with upper and lower bound solutions obtained by finite element limit analysis. They investigated the effects of the firm stratum based on the depth factor (D) which is the ratio of the firm stratum depth to the slope height. For undrained failure, the stability number slightly decreases with the depth factor and remains constant when $D > 2$. Also, the stability number increases almost linearly with a dimensionless parameter kHF_s/s_{ug}. Griffiths and Yu (2015) assumed a circular failure plane tangential to the given depth ratio. Developing an optimization program in MATLAB, the location of the center of the circle that gives minimum F_s was calculated. Some FE analyses were also performed for verification purposes. Unlike some previous studies (e.g. Gibson and Morgenstern 1962; Koppula 1984) who assumed failure through the toe only, Griffiths and Yu (2015) found four types of failure planes, namely slope circle, toe circle, base circle and deep circle, with an increase in the depth factor (Fig. 2.1). The type of failure also depends on slope angle. In addition, the stability number is almost constant for large values of D (Fig. 2.2).

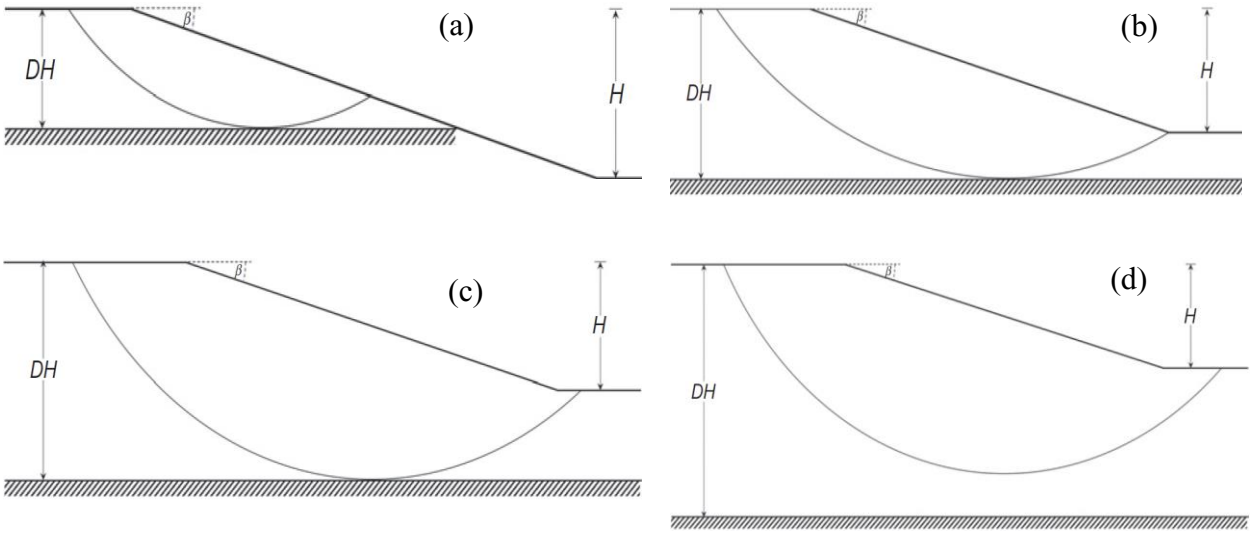

Figure 2.1: Different types of critical failure circles: (a) slope circle; (b) toe circle; (c) base circle; (d) deep circle (after Griffiths and Yu 2015)

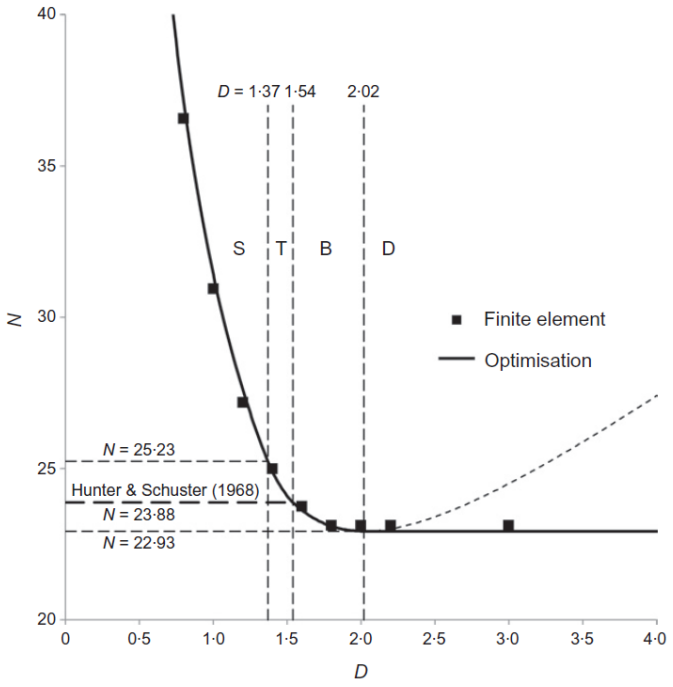

Figure 2.2: Typical result for slope with s_{ug}/kH = 2 and β=15° (S, slope; T, toe; B, base; D, deep failure) (Griffiths and Yu 2015)

Table 2.3 provides a brief summary of the works on slope stability analysis for linearly increasing undrained shear strength with depth.

Table 2.3: Summary of previous limit equilibrium analyses for non-homogenous soil slopes

References	Remarks
Gibson and Morgenstern (1962)	considered linearly increasing strength profile with cohesion at the ground surface (c_{u0}) as zero
Hunter and Schuster (1968)	extended the case of Gibson and Morgenstern. Used $c_{u0} > 0$ at the ground surface
Chen et al. (1975)	obtained the upper-bound solution by employing a kinematic method
Koppula (1984)	analyzed the slope stability of a linearly increasing shear strength profile in the static case
Leshchinsky and Smith (1989)	evaluated the safety factor of embankments built on soft or sensitive clay
Griffiths and Yu (2015)	used MATLAB to evaluate the critical slip surface and factor of safety of the slope with a strong base at the bottom of the slope and linearly increasing undrained cohesion with depth.

2.3 Finite Element Analysis

The commonly used limit equilibrium methods for slope stability analysis cannot simulate progressive failure. The Finite Element (FE) method, on the other hand, may be able to overcome some of the limitations of the LE methods. A wide range of FE modelling techniques have been developed in the past. Some of them which have been used for slope stability analysis are discussed in the following sections.

2.3.2 Small Deformation FE analysis

A number of studies used the Lagrangian-based FE modelling technique to simulate slope failure (Griffiths and Kidger 1995; Dawson et al. 1999). One of the advantages of this FE method is that it can simulate the development of plastic shear strains and deformation of the soil. Many studies conducted the analysis following the strength reduction technique, where the strength of the soil is gradually reduced until a complete failure plane forms. The strength reduction factor (SRF), which defines the ratio between the initial shear strength and the strength when failure of the slope occurs, is compared with the F_s obtained from LE methods (Ho 2014). Table 2.4 presents a brief summary of FE analyses of clay slopes for small deformation problems.

Table 2.4: Summary of FE modelling of slopes for small deformation problems

References	Constitutive model	Type of slopes	Remarks
Ugai and Leshchinsky (1995)	Mohr–Coulomb failure criteria	Homogeneous	Compared the location of the critical slip surface and F_s with the LE method. Failure was defined by the distribution of the maximum shear strain.
Griffiths and Kidger (1995)	Elastic-plastic, von Mises failure criteria	Homogeneous	Slope stability analysis was carried out using the Lagrangian framework. The location of the failure is identified by the deformed mesh.
Dawson et al. (1999)	Elastic-plastic Mohr-Coulomb	Homogeneous	Stability analysis of the embankment was carried out using the Lagrangian framework. There is a good match between the computed F_s and the stability number obtained from the limit analysis.
Huang and Jia (2007)	Strength reduction in SSRFEM	Homogenous	Compared the safety factors derived by LEM and SSRFEM (shear strength reduction technique).
Maula and Zhang (2011)	Strength reduction in Plaxis 2D	Homogenous	Compared F_s or *SRF* for various methods for slope stability analysis. The results from these methods are generally consistent.
Ho (2014)	Elastic-plastic Mohr-Coulomb	Non-homogenous	Compared F_s in LE and SRF in FE analyses in Lagrangian framework. Failure is considered when a sudden increase in displacement causes significant mesh distortion.
Tu et al. (2016)	Elastic-plastic Mohr-Coulomb	3D slopes	Investigated the relation between energy change and slope failure in Lagrangian framework.

2.3.3 Large Deformation FE analysis

One of the limitations of Lagrangian-based FE analysis is that it cannot simulate large deformation because of significant mesh distortion around the failure planes, especially when strain localization occurs in soil exhibiting strain softening behaviour (e.g., sensitive clays). Several attempts were made in the past to overcome the issues related to mesh distortion by developing advanced FE modelling techniques. Table 2.5 shows a brief summary of the FE modelling of slope failure where strain-softening behaviour of soil was incorporated. Some of these studies developed modelling techniques for large deformation of soil (e.g., Dey et al. 2015; Wang et al. 2020).

Table 2.5: FE modelling of slopes considering strain-softening behaviour

References	Method	Constitutive model	Remarks
Potts et al. (1990)	ICFEP FE program by Imperial College	Elastic-plastic strain-softening	Shear band propagation was identified as a factor for progressive failure.
Andresen and Jostad (2002, 2007)	BIFURC	Elastic-plastic soil model with NGIANISOFT	The propagation of the shear band in saturated sensitive clay with finite-thickness interface elements was studied for progressive failure.
Locat et al. (2013)	PLAXIS 2D & BIFURC	Undrained strain-softening	Modelled progressive failure, initiation and formation of a quasi-horizontal shear band for an idealized section of a riverbank slope.
Chai et al. (2013)	CRISP-AIT	Undrained strain-softening	Modelled failure of an embankment on soft clayey soil was investigated using a modified cam clay model.
Dey et al. (2015)	Eulerian FE in Abaqus	Undrained strain-softening	Simulated large deformation and failure of soil block in sensitive clay slopes.
Wang et al. (2015)	Eulerian FE in Abaqus	Undrained strain-softening	Simulated the effect of K_0 on large deformation failure of sensitive clay slopes.
Wang and Hawlader (2017)	Eulerian FE in Abaqus	Undrained strain-softening	Modelled the effect of toe erosion of the slope on the propagation of shear bands.
Wang et al. (2021)	Eulerian FE in Abaqus	Undrained strain-softening and strain rate	Simulated large deformation failure of sensitive clay slopes considering strain softening and strain rate effects on undrained shear strength.

2.4 Typical shear strength profile of sensitive clay

Field investigations show that the undrained shear strength of sensitive clay generally increases almost linearly with depth below the crust (Quinn et al. 2011; Locat et al. 2015; Perret et al. 2019). Post-landslide investigations also show that the soil units above and below the failure planes are somehow different. The majority of FE simulations of landslides assumed an elastic base or ignored the effects of clay layer strength beneath the toe. As mentioned in the introduction (Chapter 1), the present research focuses on the effects of a underlying clay layer on a retrogressive landslide. Therefore, this section presents the shear strength profiles of some sensitive clay layers where large-scale landslides occurred.

2.4.1 Vases Creek valley near Brownsburg, Quebec

Numerous landslides occurred in the Vases creek valley, as indicated by the red line on the topographic map (Fig. 2.3). Along the survey line AA′ in Fig. 2.3, borehole drilling and piezocone penetration tests with pore pressure measurements were performed (Fig. 2.3). Three distinct soil units were identified from this site investigation (Fig. 2.4). Unit C, located at the bottom, contains less clay than Unit B, which is located above C. However, the failure is occurring in the vicinity of the interface zone (Fig. 2.4).

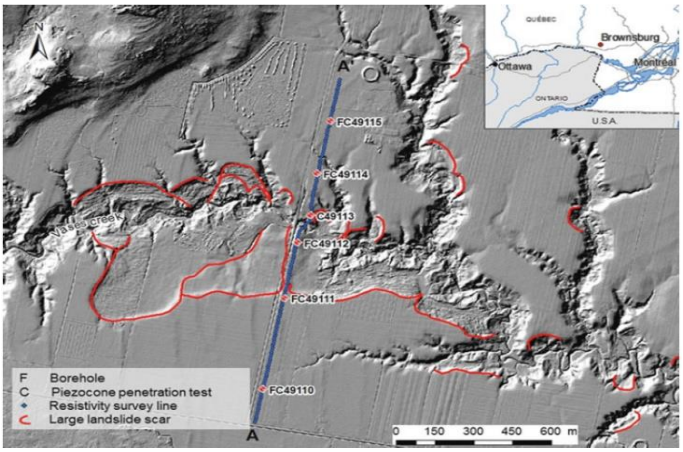

Figure 2.3: Map of the Vases Creek Valley near Brownsburg, Quebec, showing the location of the geophysical and geotechnical investigation. (Bélanger et al 2017)

Figure 2.4 shows the typical shear strength profile in this area, where three distinct units were found. Unit A represents the surficial crust, unit B represents sensitive clay, and unit C represents a strong soil layer composed primarily of clayey silt. The water content and liquidity index are high (> 1) in the sensitive clay of unit B, which decreases rapidly in the soil of unit C. Initial undrained shear strength increases gradually in soil units B and C without showing a significant change in strength between these two soil units. However, an abrupt increase in remoulded shear strength is found between these two soil units. Note that the maximum depth of failure in these cases is located approximately near the interface of these two units.

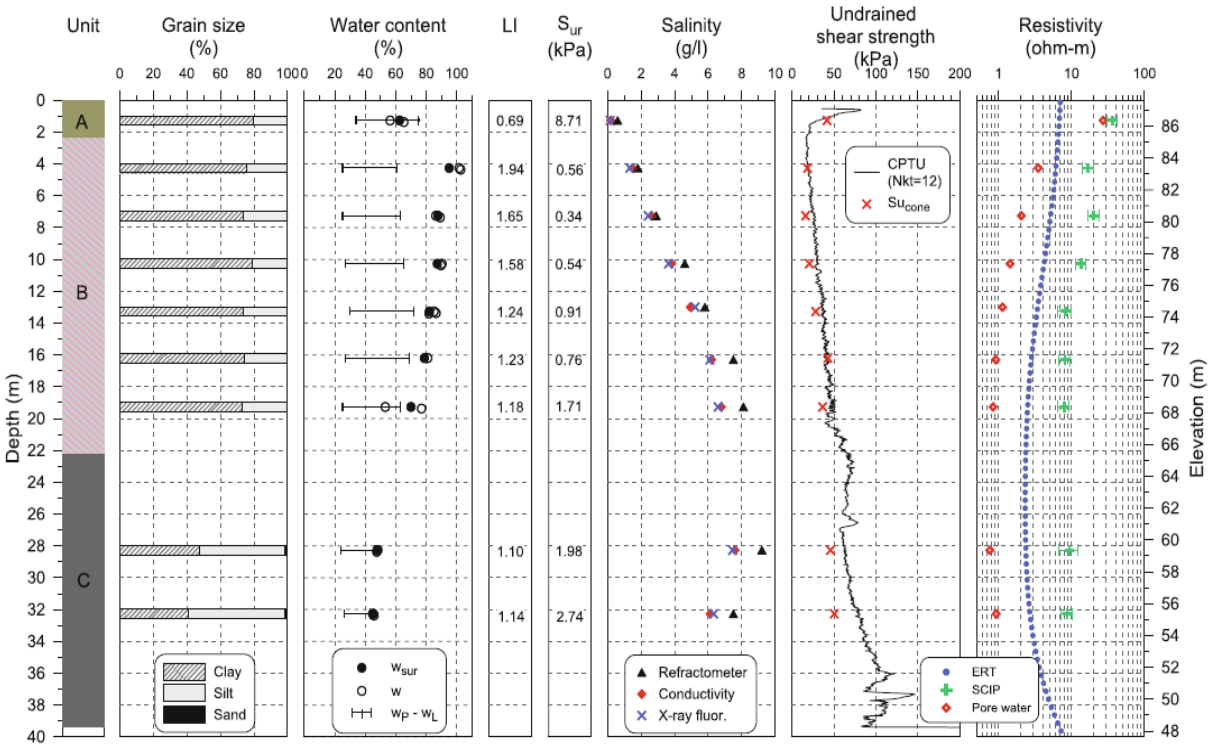

Figure 2.4: Geotechnical and electrical resistivity profiles of borehole F49114 in the marine clay deposit of Brownsburg, Quebec. (Bélanger et al 2017)

2.4.2 Disaster of Notre-Dame-de-la-Salette, Québec, Canada

The geotechnical profile of this landslide reveals observations similar to the previous case described by Bélanger et al. (2017). The failure plane is located near 22 m depth, as shown in Fig. 2.5. The soil unit above the approximate depth of the failure surface contains a high proportion of clay and a low proportion of silt. In contrast, below the failure surface, the clay content is low while the silt content is high. Above the failure depth, the water content and plasticity index are high, whereas they decrease below the failure depth. Below and above the failure plane, the liquidity index and remoulded shear strength do not show a significant pattern. Furthermore, a gradual increase in undrained shear strength is observed near the failure depth. A pattern was found in this sensitive clay landslide area, where the soil layer below the failure plane is somewhat different in terms of clay content, water content and plasticity index. That means, the location of the failure plane may have been influenced by the different behaviours of the two soil units above and below it.

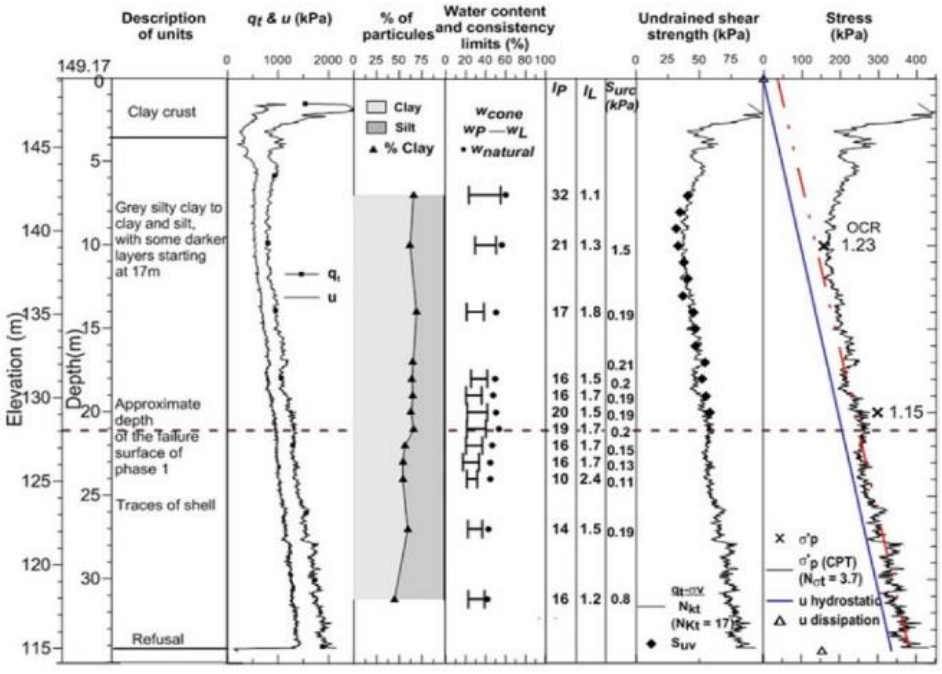

Figure 2.5: Geotechnical profile of soil at Notre-Dame-de-la-Salette (Locat et al. 2017)

2.4.3 Mont-St-Hilaire landslide

The failure plane of the 1859 Mont-St-Hilaire landslide is 16 metres below the crest. The shear strength profile of this landslide reveals observations similar to the previous case described by Bélanger et al (2017). Figure 2.6 shows that near the failure depth, there is almost no change in undrained shear strength with depth. Although the undrained shear strength increased almost linearly with depth, no significant pattern was found in this sensitive clay landslide soil profile near the sliding plane. More geotechnical information may reveal a possible factor in determining the failure plane.

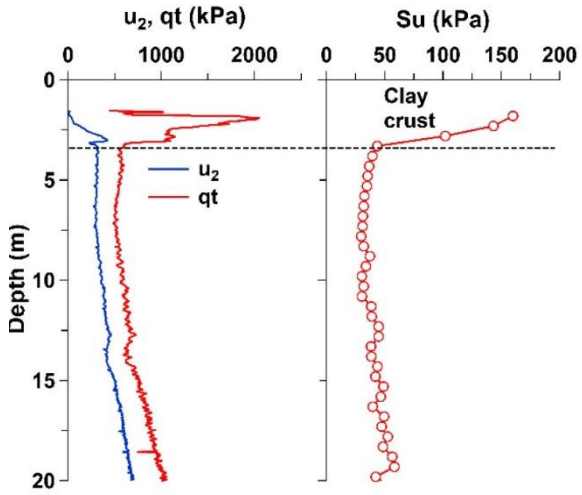

Figure 2.6: Geotechnical soil profile of the 1859 Mont-St-Hilaire landslide (Perret et al 2019)

2.4.4 Saint-Alban test site

The failure occurred at around 9.5 m depth at the Saint-Alban test site. The geotechnical profile of this landslide shown by Roy et al. (1981) in Fig. 2.7 reveals observations similar to the previous case described by Bélanger et al. (2017). The soil unit above the approximate depth of the failure surface contains a high proportion of clay and a low proportion of silt. In contrast, below the failure surface, the clay content is low while the silt content is high. Near the failure depth, the percentage of clay decreases from 35% to 17%, while the percentage of silt increases from 6% to 18%. Above the failure depth, the water content and the liquidity index are high, whereas they decrease below it. The liquidity

index falls to 1.8 from 2.3 at the approximate failure depth. However, there is an increase in shear strength close to the failure depth. There are a number of factors that influence the behaviour of the two soil units located above and below the failure plane. In this sensitive clay landslide region, a pattern has been identified where the soil layer below the failure plane is somehow different in terms of clay content, water content and liquidity index. Again, the location of the failure plane may have been influenced by the different behaviours of the two soil units above and below it.

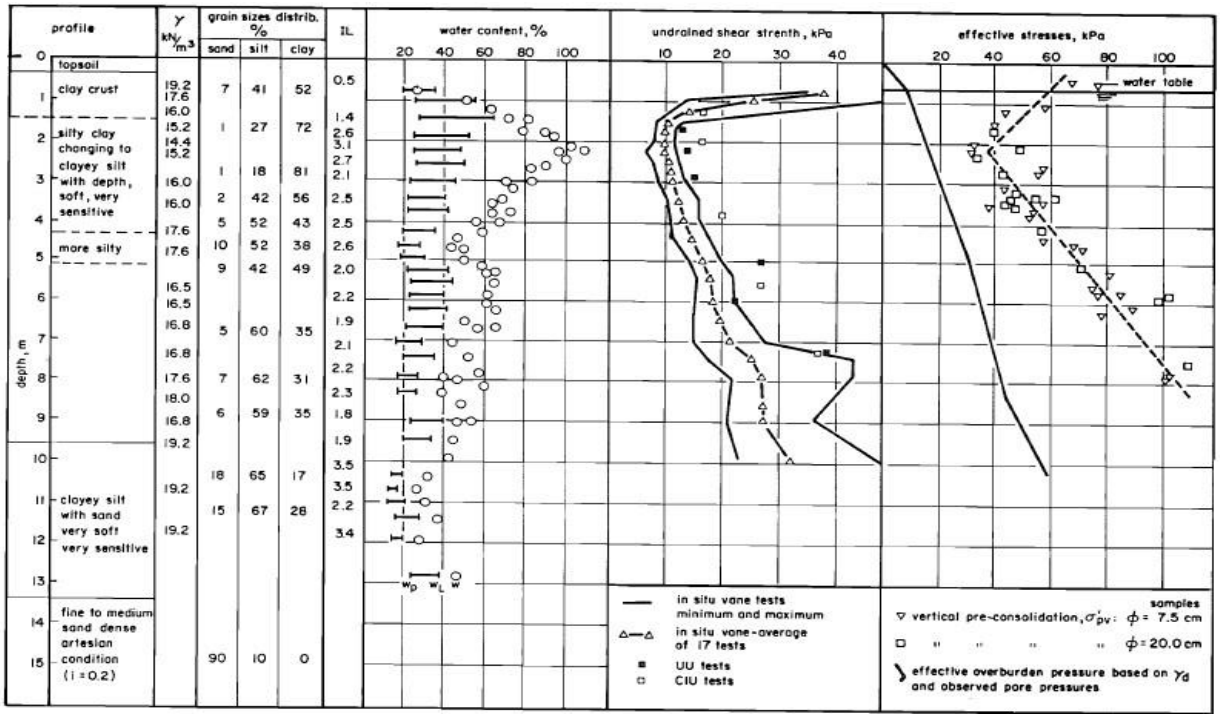

Figure 2.7: Geotechnical soil profile (Roy et al. 1981)

2.4.5 Saint-Jude landslide

At the St. Jude landslide location, the failure occurred at a depth of approximately 27 m depth. The geotechnical profile of this landslide, as depicted in Fig. 2.8 by Locat et al. (2017), reveals observations similar to those described in Roy et al. (1981). There was a slight increase in shear strength near the failure plane, which can be a key variable in predicting the depth of the failure plane. The water content and liquidity index are high above the failure depth but dramatically decrease

below it. The particle size distribution also reveals that the percentage of clay has drastically decreased in the soil unit below the failure plane, while the proportions of silt, sand, and gravel have dramatically increased. In this sensitive clay landslide region, a pattern has been identified where the soil layer below the failure plane is somehow different in terms of clay content, water content and liquidity index. The distinct behaviour of the two soil units located above and below the failure plane could influence the location of the failure plane.

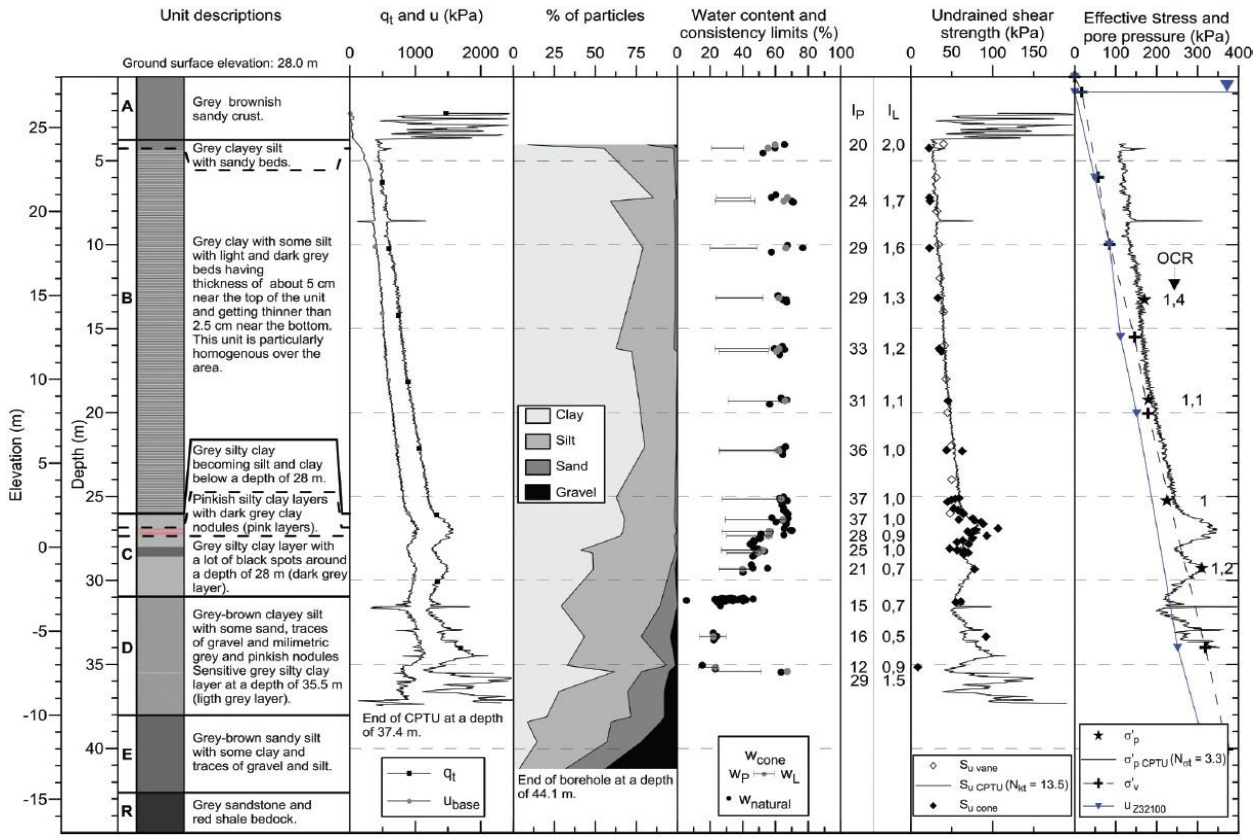

Figure 2.8: Geotechnical soil profile (Locat et al. 2017)

2.4.6 Sainte-Monique landslide, Quebec

The geotechnical soil profile of the 1994 Sainte-Monique landslide is shown in Fig. 2.9. The failure surface starts near the toe of the slope and spreads almost horizontally into the intact deposit at a

depth approximately 17 m from the crest. The geotechnical profile of this landslide reveals observations similar to those described by Belanger et al (2017). Shear strength increases almost gradually throughout the soil depth. The water content is high above the failure depth but decreases dramatically below it. The particle size distribution also reveals that the percentage of clay has decreased significantly in the soil unit below the failure plane, while the proportions of silt, sand, and gravel have increased significantly. Despite a linear increase in shear strength with depth, the two soil units behave differently. In this sensitive clay landslide region, a pattern has been identified in which the soil layer beneath the failure plane differs in terms of clay content and water content. The location of the failure plane may have been influenced by the different behaviours of the two soil units above and below it.

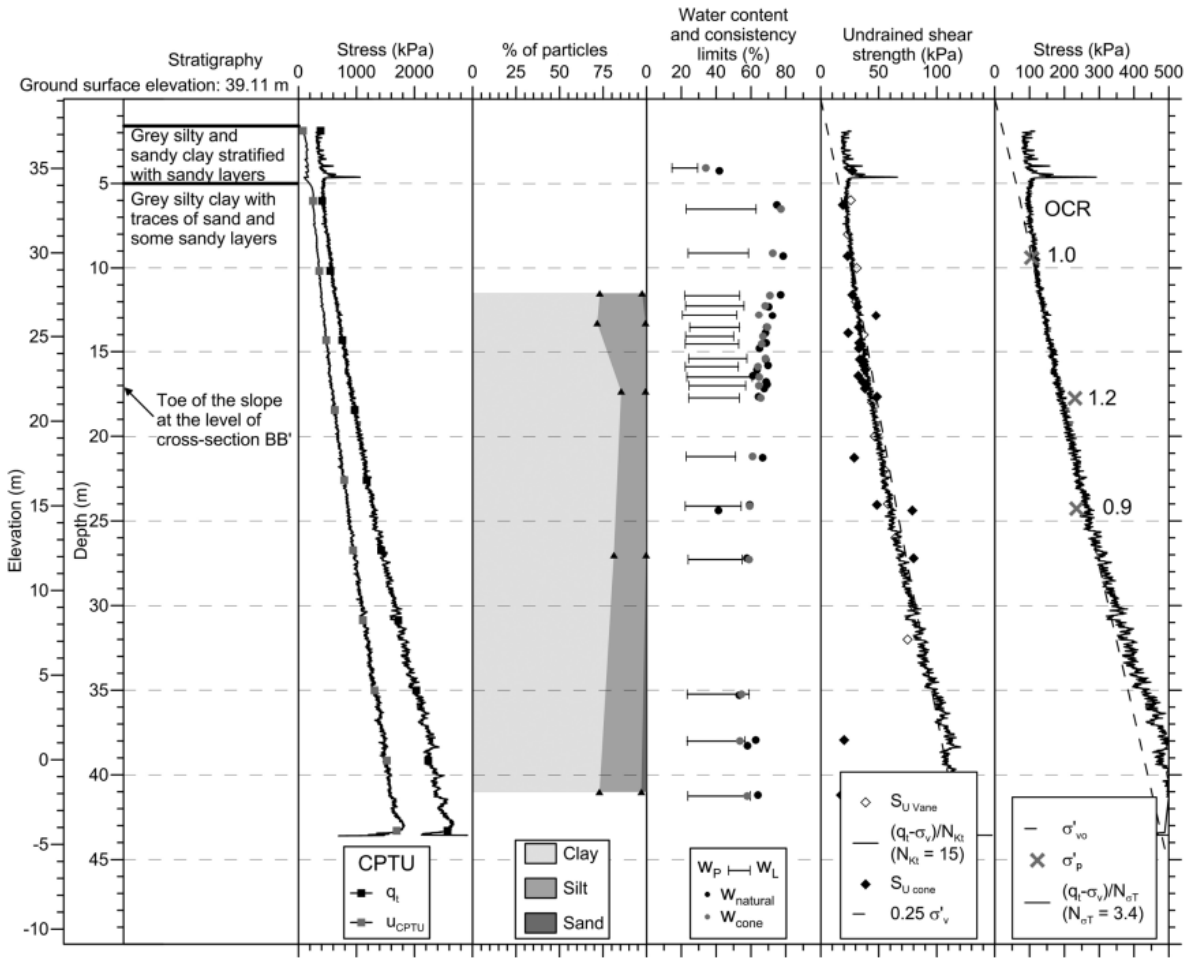

Figure 2.9: Geotechnical soil profile (Locat et al. 2015)

2.5 Shear strength gradient in sensitive clays

Geertsema et al. (2006) compiled data from several sensitive clay landslides with an aim to relate undrained strength gradient (*k*) to failure patterns (Fig. 2.10). Based on a limited number of landslides and shear strength profiles, they showed a trend of flowslides for low *k* while the failure was spread for intermediate *k*, and, for large *k* where the strength increases rapidly with depth, retrogressive failure was not expected.

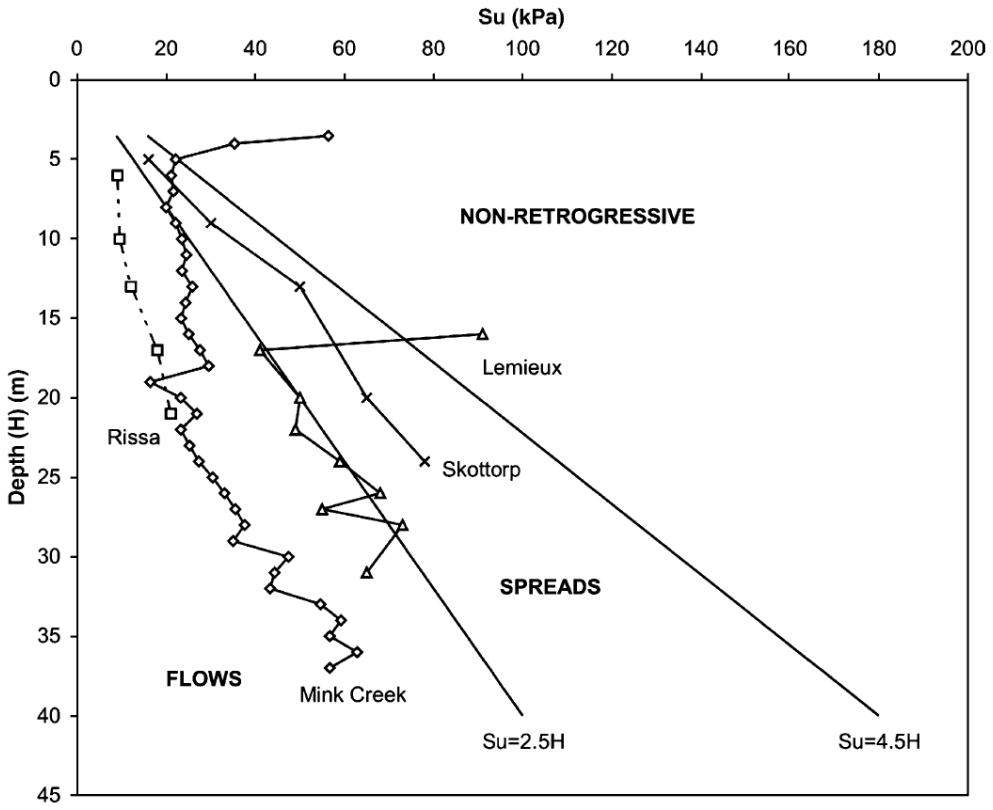

Figure 2.10: Shear strength profile of sensitive clays and failure patterns (Geertsema et al. 2006)

2.6 Surficial crust

Surficial crust of one to several meters thickness is commonly found in many sites. The crust is significantly affected by seasonal effects and generally fissured. While there is a huge uncertainty in determining strength of crust and mode of failure (drained/undrained, failure pattern etc.), vane shear tests are commonly used to determine undrained shear strength. Lo and Hinchberger (2006) suggested that while the failure surface is cylindrical in a field vane test, the fissures of the crust are planar, which affects the mobilized strength. Therefore, for the design of embankments on crust, they recommended to use the mass strength of the crust, which is a reduced value of field vane shear strength. Field tests of crust mass strength are limited; however, Table 2.6 shows the typical reduction factor for some clays.

Table 2.6: Effect of fissures on the intact undrained strength of clays (compiled by Lo and Hinchberger 2006)

Soil Deposit	Depth (m)	S_{ui} (kPa)	$S_{u,m}$ (kPa)	$\frac{S_{u,m}}{S_{ui}}$
Sarnia Till	1.5 (Crust)	280	55	0.20
	3.0 (Crust)	250	104	0.41
	4.5 (Transition)	150	85	0.56
Olga Sensitive Clay	0.2-1.2 (Crust)	75 ($\pm$ 25)	18	0.24 (east trench)
		80 ($\pm$ 40)	18	0.23 (north trench)
Nanticoke G.S.	3.3	333	56	0.17
Fissured Clay	4.8	390	95	0.24
	6.1	371	97	0.26
Brown London Clay, Maldon	1.4-2.0	77	31	0.40

Note: S_{ui} = "intact" undrained strength from UU tests or vane test
$S_{u,m}$ = undrained mass strength from *in situ* shear box tests

Dey et al. (2015) showed from large deformation finite element simulations that the crust's shear strength significantly affects the failure patterns. Perret et al. (2019) compiled the data on spreads and flows in eastern Canadian sensitive clays; however, they could not find any trend of failure pattern related to crust thickness (Fig. 2.11)

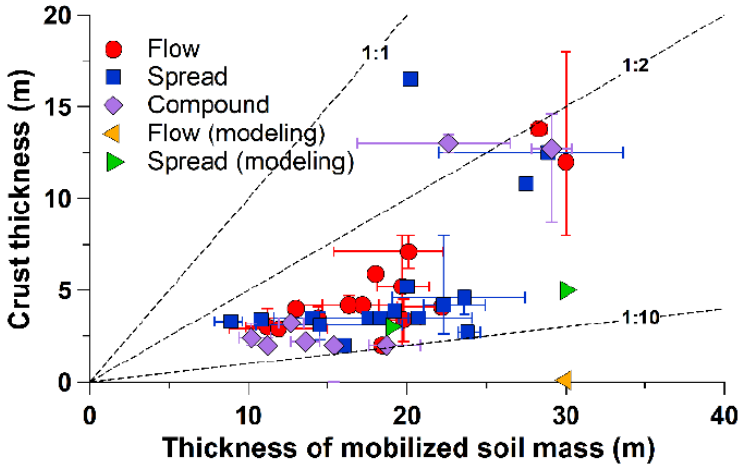

Figure 2.11: Failure pattern of 37 eastern Canadian sensitive clay landslides (Perret et al. 2019)

2.7 Large deformation finite element modelling

Modelling a retrogressive landslide numerically can be challenging due to the large deformations that occur in the failure area. Most of the FE models available in the literature for slope stability analysis were developed in a Lagrangian framework (Griffiths and Lane 1999; Loukidis et al. 2003). In these types of FE models, significant mesh distortion occurs, particularly near the failure planes (Griffiths and Lane 1990). When simulating large deformation problems, the mesh and material move together simultaneously, and cause non-convergence at large deformations (Griffiths and Lane 1999). The present study utilizes the Eulerian-based FE technique in Abaqus 6.19 software in which the Eulerian material (soil) can flow through the fixed mesh without causing numerical issues related to mesh distortion, even at very large deformations. In the Eulerian formulation, the mesh is fixed as the background, and the material flows through the fixed mesh (Fig. 2.12). The Eulerian Volume Fraction (EVF) tool is used to define the soil and voids: EVF = 1 for the elements filled with Eulerian material (clay), EVF = 0 for the void, and 0 < EVF < 1 for the elements partially filled with soil.

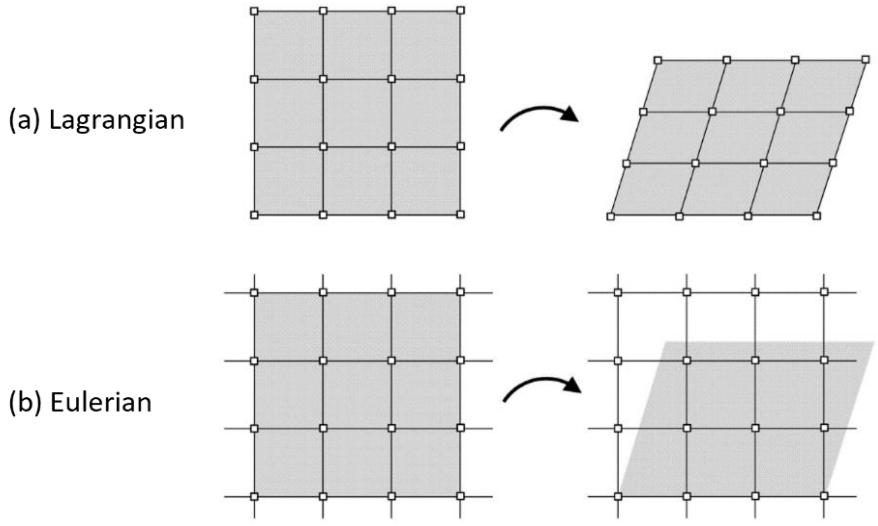

Figure 2.12: Finite element modelling approaches: (a) Lagrangian; and (b) Eulerian (Benson and Okazawa 2004)

2.8 Summary

The literature review presented in this chapter shows that the mechanisms of a sensitive clay landslide are not well understood. The observation of several post-slide investigations suggests that the failure process may be affected by different soil units above and below the maximum depth of the failure plane. The undrained shear strength could be slightly higher in the lower clay layer, as observed in some field investigations. The failure depth could also be influenced by factors such as clay content, water content, or liquidity index. Thus, it is necessary to study the effects of the shear strength profile on slope failure and retrogressive landslides.

Very few numerical studies are available in the literature for modelling progressive failure. Most of them are limited to idealized conditions. Traditional limit equilibrium methods for slope stability analysis cannot explain these types of large landslides. Typical finite element methods in a Lagrangian framework also cannot simulate this type of landslide because of mesh distortion. In the present study, a large deformation FE technique is used to investigate several key factors, such as shear strength profile, failure depth, and surficial crust in the slope, as well as strain-rate and strain-softening effects on undrained shear strength for the failure slope caused by toe erosion near the riverbank.

Chapter 3: Effects of Undrained Shear Strength Profiles on Stability Analysis: A Comparative Study

3.1 General

The shear strength profile is a vital geotechnical parameter that influences landslide failure mechanisms. Limit Equilibrium (LE) methods were used to determine the location of the critical failure plane and, in some studies, compared the results with Finite Element (FE) simulation results. For undrained failure of clay slopes, most of those studies used elastic perfectly plastic models for clay, and the analyses were performed assuming uniform undrained shear strength profile, with a firm base. A limited number of LE analyses are available for linearly increasing shear strength profile, again for some idealized conditions. In this chapter, the stability of clay slopes for gradually increasing shear strength profile is determined using LE and FE analyses. Post-slide investigations in sensitive clay landslides show slightly higher shear strength below the failure depth. This soil layer may not be considered a firm base, as is commonly used in LE analysis. The role of this slightly stronger soil layer in failure patterns and the safety factor is also investigated. The analysis in this chapter is focused on investigating failure mechanisms for idealized elastic perfectly plastic soil, while in the following chapter (Chapter 4), the effects of strain-softening and strain rate on progressive formation of failure planes and large-scale landslides in sensitive clays are simulated.

3.2 Introduction

The undrained shear strength profile could have a significant influence on slope failure mechanisms. Historically, many studies used idealized shear strength profiles (e.g. Taylor 1937; Fredlund and Krahn 1977; Han and Leshchinsky 2004), and a limited number of studies considered linearly increasing undrained shear strength (s_{u0}) profiles (e.g., Gibson and Morgenstern 1962; Hunter and

Schuster 1968; Koppula 1984; Griffiths and Yu 2015). Note that mobilized undrained shear strength (s_u) governs the progressive formation of the failure planes, and s_u depends on strain softening and shear strain rate, which have been incorporated in Chapter 4. However, in this chapter, the symbol s_{u0} is used for undrained shear strength, as the soil is modeled as elastic-plastic material without softening and rate effects.

Figure 3.1 shows the conceptual approaches used in previous studies for slope stability analysis. The typical variation of shear strength profile is shown in Fig. 3.1(b). Field investigations show a stronger soil crust near the ground surface, which is generally overconsolidated and formed through desiccation and weathering effects. Below the crust, s_{u0} generally increases linearly with depth (z), at least for normally and lightly overconsolidated clays, as described by the upper clay layer in this study. If one is interested in determining the factor of safety (F_s) of a cut slope, s_{u0} of the crust and upper clay layer should be considered.

For a linearly increasing shear strength profile, the undrained shear strength (s_{u0}) at any depth (z) can be defined as:

$$s_{u0} = s_{ug} + kz \tag{3.1}$$

where s_{ug} is the undrained shear strength at ground surface, and k is the shear strength gradient with depth in kPa/m.

Previous studies conducted such analyses. For example, Gibson and Morgenstern (1962) assumed that the soil is normally consolidated and considered that the undrained shear strength at the ground surface (s_{ug}) is zero, which means that shear strength increases linearly from zero at the ground surface at a constant gradient of k (left line in Fig. 3.1(c)). They developed a closed-form solution assuming a circular failure plane. Koppula (1984) followed a similar approach as Gibson and Morgenstern

(1962) but considered non-zero undrained shear strength at the ground surface. Based on a literature review of research on soft clays, s_{ug} of 0–10 kPa and k of 0–3.5 kPa/m were reported.

In current engineering practice, a firm stratum below the clay layer is commonly assumed, to calculate the factor of safety. The depth of firm stratum is commonly defined using a depth factor (D), which represents the ratio between the firm stratum depth from the crest (DH) and slope height (H) (Fig. 3.1(a)). For a uniform undrained shear strength profile, it has been shown that D has a significant influence on calculated F_s for low slope angle (β) (e.g. $\beta < 30°$), and the effects of D diminish when $D > 3.0$. Griffiths and Yu (2015) investigated the influence of the firm stratum depth on F_s and location of the critical failure plane for linearly increasing shear strength profiles. They identified four models of failure (deep, base, toe and slope circles). The failure mode depends on the slope angle, depth of the firm base and the ratio s_{ug}/kH. All these studies assumed circular failure planes. Steward et al. (2011) used SLOPE/W software to analyze the stability of c–ϕ soil and showed that, when the firm stratum is close to the toe, a segment of failure plane might pass above the firm stratum, which could affect the F_s.

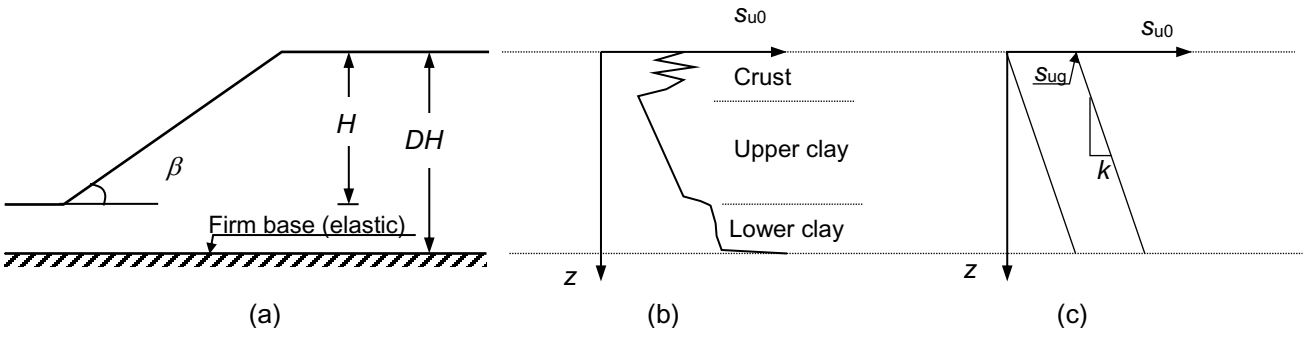

Figure 3.1: Problem statement: (a) notations; (b) typical variation of undrained shear strength; (c) shear strength variations used in previous studies

As mentioned in the abstract and chapter 1, one of the main objectives of this study is to investigate the effects of stronger lower layers on slope failure mechanisms, especially for sensitive clay slopes, and compare them with the observed behaviour in the field. In this chapter, the effects of slope failure for elastic-plastic material (without softening) are shown.

3.3 Problem definition

Numerical simulations are performed for the following geometries of the slope by varying the slope angle (β) and slope height (H).

a) Set A: H = 10 m and β = 2:1

b) Set B: H = 20 m and β = 2:1, 2.5:1 & 3:1

The geometry of natural and cut slopes varies widely. For a cut slope, the depth of the cut and slope angle depend on engineering requirements and geotechnical properties. For example, Griffiths and Yu (2015) analyzed a typical clay slope of 10 m in height. The findings of that study are compared in the present study. For sensitive clays, Demers et al. (2014) reported an average slope height of 27 m (10 m-73 m) where flowslide occurred and for 18 m (9 m–35 m) where spread occurred based on 108 historical landslides and scars in eastern Canada. The above geometry is considered based on those studies.

Although a weathered crust typically exists near the ground surface, in Fig. 3.2, such crust is not considered in the analyses presented in this chapter. Note that the effects of weathered crust on slope failure are discussed in the following chapter. For both sets of analyses, two clay layers are considered: (i) upper clay layer (S1), (ii) lower clay layer (S2) (Fig. 3.2). The top surface of the lower clay layer is at the level of the toe or up to 10 m below the toe of the slope. In other words, the thickness of the upper clay layer is greater than or equal to the height of the slope. The lower clay

layer (S2) has a higher shear strength compared to that of the upper clay layer (S1). The higher shear strength of the lower clay layer is given by increasing the strength by s_{uL} at the interface between the lower and upper clay layers, as shown by the dashed line of the shear strength profile in Fig. 3.2. Note, however, that the strength gradient k remains the same for both upper and lower clay layers. A firm base is placed at a depth of H from the toe of the slope. The soil in the firm base is very strong and is modelled as an elastic material. The depth of the top surface of the lower clay layer below the toe is defined by h_L. Analyses are performed for $h_L = 0$ (i.e., top surface of the lower clay layer S2 is at the level of the toe) and $h_L > 0$. The groundwater table is at the ground surface and along the slope.

The left and right boundaries are placed at 30 m and 50 m for Set A and 100 m and 250 m for Set B from the toe and crest, respectively. Analyses are also performed by placing the left and right boundaries at further distances; however, no significant effects on slope failure mechanisms are found.

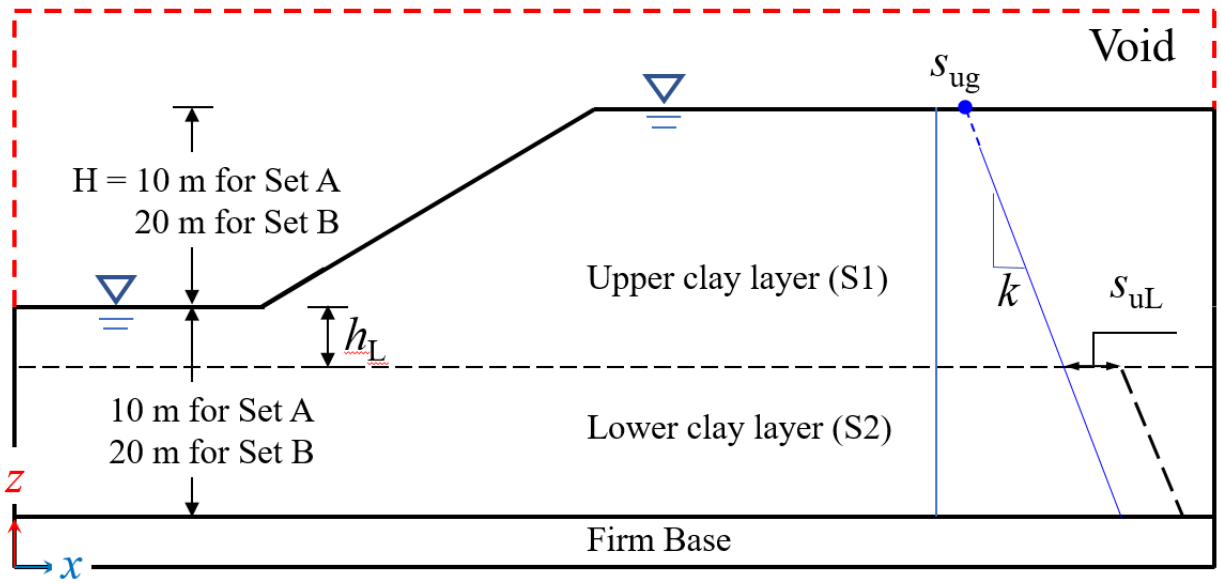

Figure 3.2: Geometry used in finite element analysis (not to scale)

Finite element analyses are performed in two steps. In the first step, the geostatic load is applied to bring the soil to the in-situ stress conditions. The slope is stable at the end of the geostatic step. In

the second step, the undrained shear strength of soil is reduced gradually by a factor, which is commonly known as the strength reduction factor (*SRF*), until sufficient plastic shear strains generate along the failure plane. The mobilized undrained shear strength (s_u) is related to *SRF* as

$$s_u = \frac{s_{u0}}{SRF} \tag{3.1}$$

Various approaches have been used to compare *SRF* in FE with F_s in limit equilibrium methods, which include the *SRF* corresponding to the formation of a complete (global) failure plane, toe displacement, and excessive mesh distortion, after which analysis could not be continued. In the present Eulerian-based FE analysis, mesh distortion is not an issue. In the following sections, the value of *SRF*, when a complete failure plane forms, is compared with F_s in limit equilibrium for the critical failure plane.

3.4 Finite element modelling

As mentioned earlier, most of the FE models available in the literature for slope stability analysis were developed in a Lagrangian framework (Griffiths and Lane 1999; Loukidis et al. 2003). The present study utilizes the Eulerian-based FE technique in Abaqus 6.19 software in which the Eulerian material (soil) can flow through the fixed mesh without causing numerical issues related to mesh distortion.

In numerical modelling, zero velocity boundary conditions are applied in all directions (i.e., $v_x = v_y = v_z = 0$) at the bottom of the soil model (Fig. 3.2). A zero velocity boundary condition is also applied to all of the vertical faces of the domain except for the left side, where $v_x = 0$ is applied only to the elements below the toe level. There is no velocity boundary condition along the soil–void interface, which allows the soil to move into the void space when needed.

Only three-dimensional elements are available for Eulerian FE simulations. Therefore, the modelling is performed with a single element in the out-of-plane direction to simulate the plane strain conditions. The Eulerian domain is discretized into 0.5-m cubical elements using EC3D8R in the software, which are 8-node linear brick elements of multi-materials with reduced integration, and hourglass control. The mesh size regularization technique is used to reduce mesh sensitivity issues (Karmaker and Hawlader 2022). The Eulerian Volume Fraction (EVF) tool is used to define the soil and voids: EVF = 1 for the elements filled with Eulerian material (clay), EVF = 0 for the void, and 0 < EVF < 1 for the elements partially filled with soil.

3.5 Material parameters

Table 3.1 shows the geometry and soil properties used for the FE simulations in this chapter unless otherwise mentioned. Stronger clays are used in Set B analyses to avoid any failure of the slope of larger slope height prior to strength reduction using SRF. Analyses are performed for varying strength gradients (k) and s_{uL}, as commonly observed in the field. Analyses are also performed for $s_{uL} = 0$, which represents the condition of the same linearly increasing soil shear strength profile for both clay layers.

Table 3.1: Geometry and soil properties of the clay layers used for base case simulations

Parameter	Set A	Set B
Total unit weight, γ (kN/m^3)	20	20
Initial undrained shear strength at ground surface, s_{ug} (kPa)	30	40
Slope height, H (m)	10	20
Undrained shear strength gradient, k (kPa/m)	0.5–4.5	2.5–3.5
s_u increase at upper and lower clay layer interface, s_{uL} (kPa)	0–15	0–20
Depth of lower clay layer from toe, h_L (m)	0	0–10
Depth of firm base from toe, h_B (m)	10	20
Undrained Young's modulus, E_u (MPa)	10	10
Undrained Poisson's ratio, ν_u	0.495	0.495

3.6 Results

In order to calibrate the developed FE model, the results obtained from FE analysis are first compared with an analytical solution developed by Koppula (1984) and the solution obtained from limit equilibrium methods using Slope/W software. For brevity, analyses are shown only for Set A geometry (Fig. 3.2) with soil properties listed in Table 3.1. Two shear strength profiles are considered for these analyses. In case 1, the initial undrained shear strength of both clay layers (S1 and S2) increases with depth as s_{u0} = 30 (kPa) + kz, without any step increase of s_{u0} at the interface between S1 and S2. Here, s_{u0}, k and z are in kPa, kPa/m and meters, respectively. For case 2, the shear strength

profile is the same as in case 1 except for a step increase of s_{u0} at the interface of the clay layer (s_{uL} = 10 kPa and 15 kPa).

The process of failure is shown by plotting the accumulated plastic shear strain (ε_q^p, PEEQAVG in the software). ε_q^p represents the integration of the plastic deviatoric strain rate tensor over the period of analysis, which is related to the plastic shear strain in simple shear condition (γ^p) as $\varepsilon_q^p = \gamma^p / \sqrt{3}$.

3.6.1 Case 1: Effects of linear increase of undrained shear strength

Generally, the ratio of resisting force to the driving force is used to calculate the factor of safety (F_s). For linearly increasing shear strength profile, Koppula (1984) developed the following relationship between F_s, shear strength parameters, and stability number (m).

$$m = \frac{s_{ug}}{\gamma H} \frac{1}{F_s} \tag{3.3}$$

Based on the work of Koppula (1984), F_s is 2.3 for this case of analysis where s_{ug} = 30 kPa, β = 26.57°, H = 10 m, and k = 4.5 kPa/m. Limit equilibrium analysis is also conducted using Slope/W software for this slope geometry and soil conditions and the minimum F_s of 2.4 is obtained using the Morgenstern–Price method. The location of the critical failure plane is shown in Fig. 3.3 (green line). The difference in analysis method between the analytical solution and the LE method gives slightly different results. The critical slip surface in Slope/W analysis passes through the toe, which is consistent with the assumption used for developing the analytical solution by Koppula (1984).

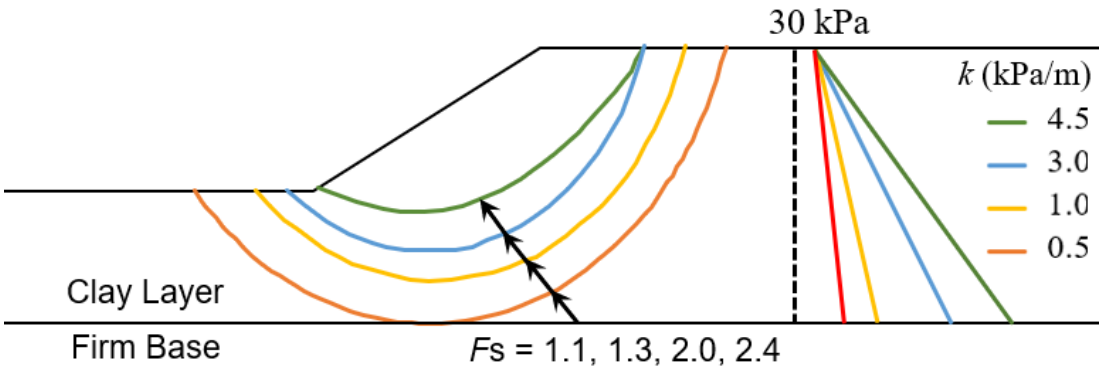

Figure 3.3: Effect of increasing shear strength gradient on critical failure circle (Slope/W analysis)

To examine the influence of an increasing shear strength gradient on the failure circle, several Slope/W analyses have been performed, with the strength gradient ranging from 0.5 to 4.5 kPa/m (Fig. 3.3). The failure circle is a deep-seated midpoint circle for k = 0.5, and the F_s is 1.1 in this case. When the shear strength gradient is increased to 1.0 kPa/m, the F_s increases to 1.3 and the failure circle shifts upwards. With a further increase in shear strength gradient to 3.0 kPa/m, the slip circle almost resembles a toe circle. The F_s rises from 1.3 to 2.0. Finally, increasing the shear strength gradient to 4.5 kPa/m strengthens the slope significantly, with the F_s reaching 2.4. In this case, the failure circle is a toe circle. This set of Slope/W analysis shows the change in location of the critical failure plane and F_s with shear strength gradient.

3.6.2 Case 1: Comparison of FE simulation results with LE analysis

In the FE model with strength gradient factor k = 4.5 kPa/m, a toe circle develops at *SRF* = 2.4. For similar slope geometry and geotechnical properties, $F_s \sim 2.4$ is observed in LE analysis (black dashed line shown in Fig. 3.4(a)). At *SRF* = 2.4, a large, curved plastic shear zone develops, causing downslope movement of the soil above this, as observed from instantaneous velocity vectors (Fig. 3.6). The plastic shear zone developed due to downslope movement of the soil above the failure plane is shown in Fig. 3.4(a). The main advantage of the present Eulerian-based FE model is that the

accumulation of plastic shear strain can be presented for a large deformation without causing any mesh distortion issue. The extent of the plastic shear strain increases with an increase in *SRF*, as shown in Fig. 3.4(b) for *SRF* = 2.9 when global failure has occurred. The location of the plastic shear zone and critical failure plane obtained from Slope/W analysis is similar, which shows the performance of the present FE modelling technique that is used for further analysis, presented in the following sections.

For k = 0.5 kPa/m, the shear strength increases only a small amount with depth (almost similar to a uniform undrained shear strength profile). In this case, all the parameters used in the analytical solution are same as before except C_R = 0.167, and m = 0.135 for k = 0.5 kPa/m. The F_s using the analytical solution of Koppula (1984) is found to be 1.11.

At SRF = 1.1, a large, curved plastic shear zone forms, which causes the soil above it to move downslope, as shown by instantaneous velocity vectors (Fig. 3.7). The large, curved plastic shear zone developed due to the downslope movement of the soil above the failure plane is shown in Fig. 3.5(a). In FE analysis using the SRF technique, a deep-seated failure surface also develops. Using the SLOPE/W software, based on the limit equilibrium (LE) method, the same slope is examined, and Fs = 1.1 is found. A similar deep-seated midpoint circle is observed in the LE analysis (black dashed line in Fig. 3.7(a)). Saha et al. (2014), Karmaker and Hawlader (2018) observed a similar deep-seated failure zone for uniform undrained shear strength profile, where the failure plane always passes near the bottom boundary. As shown in Fig. 3.7(b), large plastic shear strains are generated in a narrow zone at SRF = 1.4, along with significant movement of the failed soil, allowing the location of the failure plane to be better identified in FE analysis.

In addition, FE simulations are performed for k = 3.0 kPa/m and compared to Slope/W analysis. At SRF = 2.0, a large, curved plastic shear zone forms, which causes the soil above it to move downslope. The FE simulation result shown in Fig. 3.8 closely matches the LE analysis results. The LE results are shown by the black dashed line in Fig. 3.8(a). Using the SLOPE/W software, based on the limit equilibrium (LE) method, the same slope is examined, and Fs = 2.0 is found. As shown in Fig. 3.4 (b), large plastic shear strains generate in a narrow zone at SRF = 2.5, along with significant movement of the failed soil, allowing the location of the failure plane to be better identified in FE analysis. In the current FE model, a failure surface similar to the toe circle of the LE analysis is observed. There is a small deviation in the shear band propagation and the critical circle (LE analysis). The slight difference in the failure circle could be due to the inability of the LE method to assess the stress and deformation of the slope, whereas the Eulerian-based FE method can deform without any numerical issues due to mesh distortion.

The present comparison shows a clear understanding of the effect of the shear strength gradient on the failure mechanisms. The failure or critical circle moves upward as the shear strength gradient increases. The LE methods cannot model the progressive failure, and the SRF techniques used in FE analysis cannot predict the measured strains at large deformations (Wang et al. 2021). For this reason, the behaviour of a retrogressive landslide initiated by toe erosion with strain softening, as well as the strain rate effect, are thoroughly investigated in chapter 4.

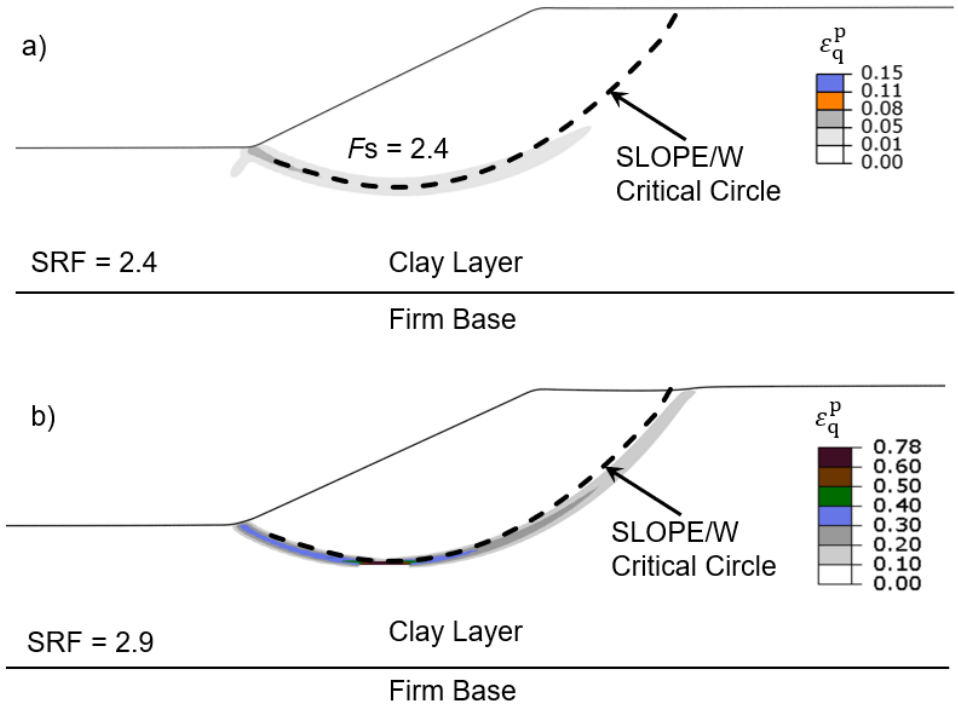

Figure 3.4: Comparison between FE simulation and LE analysis results for k = 4.5 kPa/m

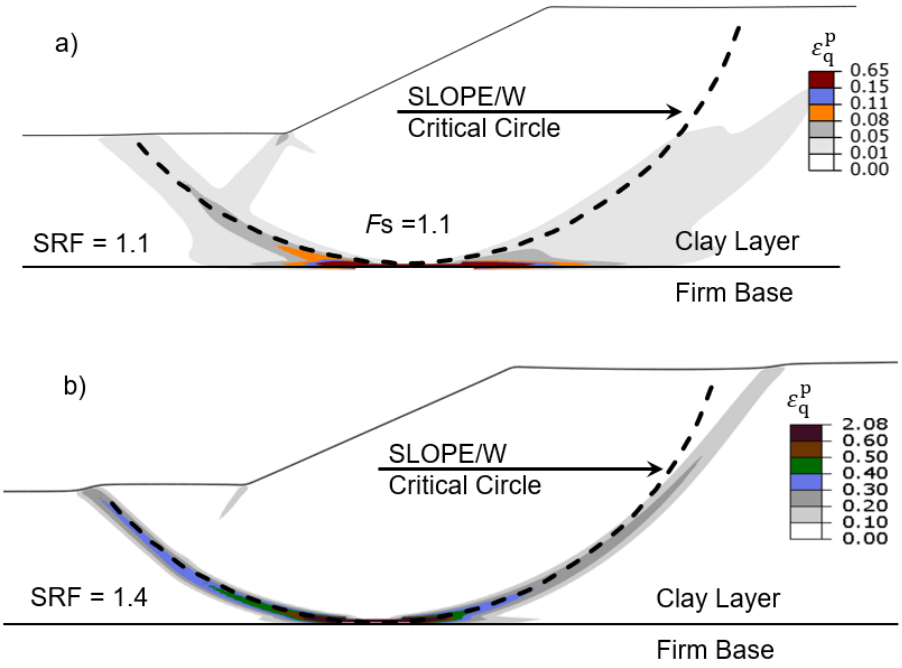

Figure 3.5: Comparison between FE simulation and LE analysis results for k = 0.5 kPa/m

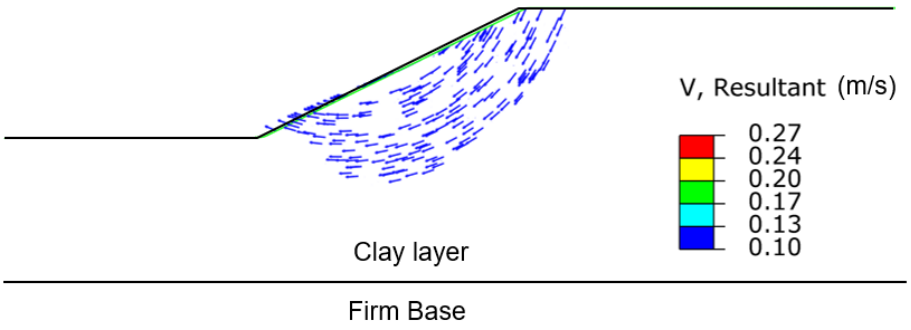

Figure 3.6: Direction of instantaneous velocity vectors for k = 4.5 kPa/m

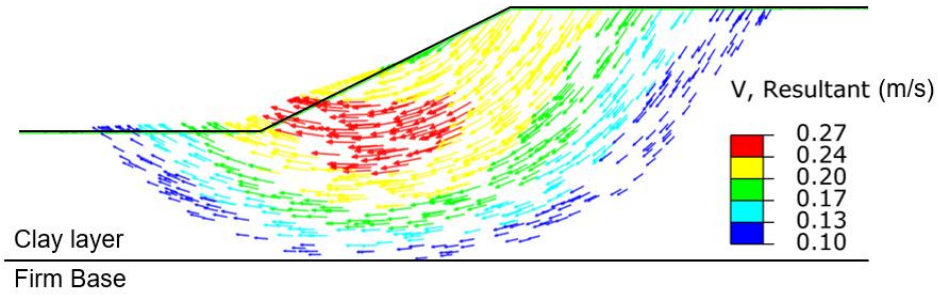

Figure 3.7: Direction of instantaneous velocity vectors for k = 0.5 kPa/m

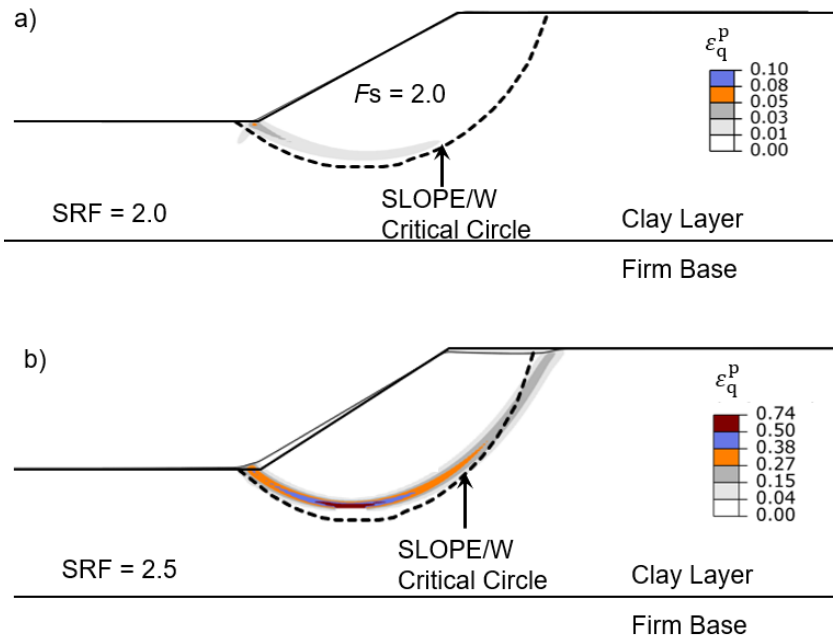

Figure 3.8: Comparison between FE simulation and LE analysis results for k = 3.0 kPa/m

3.6.3 Case 2: Effects of increasing shear strength in the lower clay layer

Locally increased undrained shear strength has been observed below the failure plane in some cases (e.g., Saint-Jude landslide, Locat et al. 2017; Rigaud landslide, Carson 1979). Due to the gradual increase in shear strength, the failure depth could not be estimated by observing the shear strength profile in those studies. It is possible that the undrained shear strength of the lower clay layer may be higher than that of the upper clay layer due to different soil compositions (Locat et al. 2019). However, in the simulations presented in this section, higher shear strength profiles are used for the lower clay layer, which are respectively 10 kPa and 15 kPa higher than the upper clay layer, as shown by the dashed line in Fig. 3.2. The upper clay layer, S1, has the same properties as before. Simulations are performed by placing the top of the lower clay layer at the toe level (case 2).

To determine the effects of higher shear strength in the lower clay layer on the failure circle, a number of LE analyses are conducted for k values ranging from 0.5 to 4.5 kPa/m.

For strength gradient factor k = 0.5 kPa/m, it is observed in Slope/W analysis that an increase in the undrained shear strength profile at a depth below the toe has a significant effect on the factor of safety. When higher shear strength is not used in the lower clay layer, the failure circle is a deep-seated midpoint circle, and the F_s is 1.1 (shown by the red line in Fig. 3.9). A factor of safety of 1.3 is found for case 2, which used 10 kPa higher undrained shear strength in the soil layer below toe level. The failure circle shifts upward when shear strength is increased by 10 kPa below the toe (green line in Fig. 3.9). The failure circle develops at a shallower depth when a higher shear strength in the lower clay layer is used. Increasing shear strength profile up to 15 kPa below the toe does not make a significant difference in the failure circle but the F_s rises to 1.6 (blue line in Fig. 3.9).

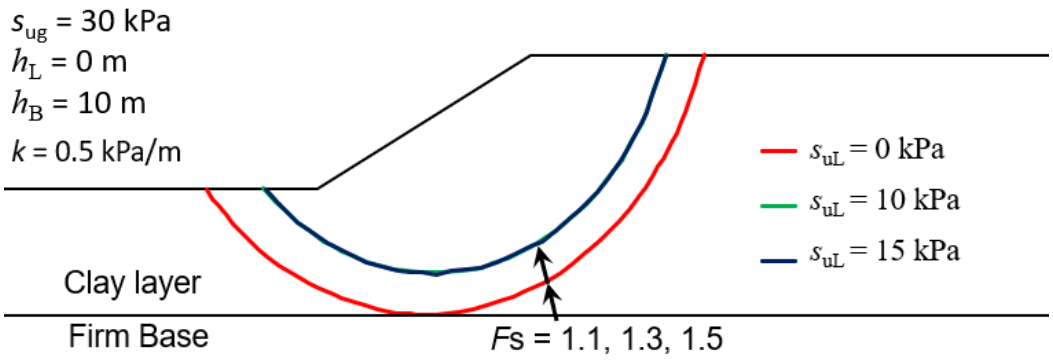

Figure 3.9: Effect of increasing shear strength in lower clay layer

When only the shear strength gradient is increased from 0.5 kPa/m to 1.0 kPa/m, the F_s increases from 1.1 to 1.3 and the failure circle shifts upwards. When shear strength is increased by 10 kPa in the lower clay layer at the level of the toe, the critical circle becomes shallower and resembles a toe circle. The F_s also rises from 1.3 to 1.5. A further increase in shear strength profile (15 kPa) below the toe forms a slope failure circle with F_s of 1.6. (Fig. 3.10).

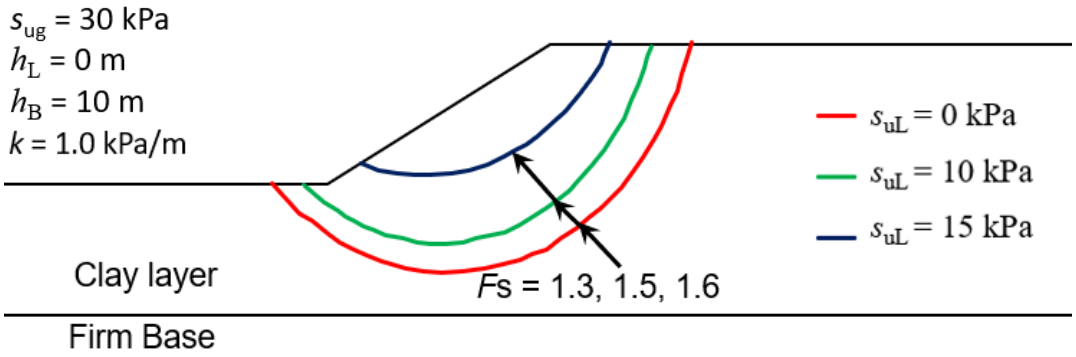

Figure 3.10: Effect of increasing shear strength in lower clay layer

For the shear strength gradient of 3.0 kPa/m, the F_s is found to be 2.0 when a higher shear strength is not used in the lower clay layer. The failure circle resembles a toe circle. The failure circle shifts upward when shear strength is increased by 10 kPa in the lower clay layer at the level of the toe. The critical circle becomes shallower, and a slope failure circle is formed. The F_s rises from 2.0 to 2.2.

Further increase of shear strength profile (15 kPa) below the toe does not make a significant difference in F_s (Fig. 3.11) but the critical circle becomes shallower.

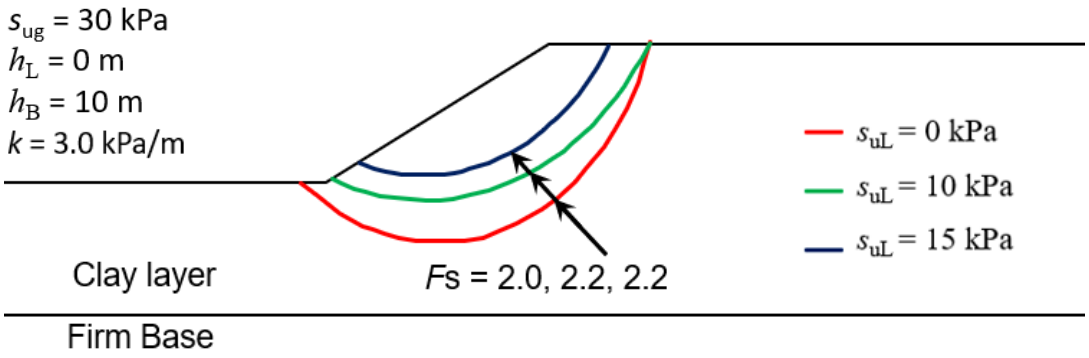

Figure 3.11: Effect of increasing shear strength in lower clay layer

For shear strength gradient k = 4.5 kPa/m, a factor of safety of 2.4 is found when higher shear strength is not used in the lower clay layer. The failure circle is a toe circle. There is little to no change in the failure depth for a 10 kPa increase in the shear strength profile below the toe level. The failure circle, also known as the critical slip circle, remains unchanged. A similar toe failure develops near the toe of the soil. Although increasing the shear strength strengthens the slope significantly, with the F_s rises from 2.4 to 2.6. Further increases in shear strength profile in the lower clay layer (15 kPa), move the failure circle upward, transforming a toe failure into a slope failure. (Fig. 3.12). All the parameters were the same as listed in table 3.1 (Set A) except for using higher shear strength at a depth below the toe in the shear strength profile. So, when the shear strength gradient is high, the effects of using a higher shear strength profile in the lower clay layer are less significant than when the shear strength gradient is low.

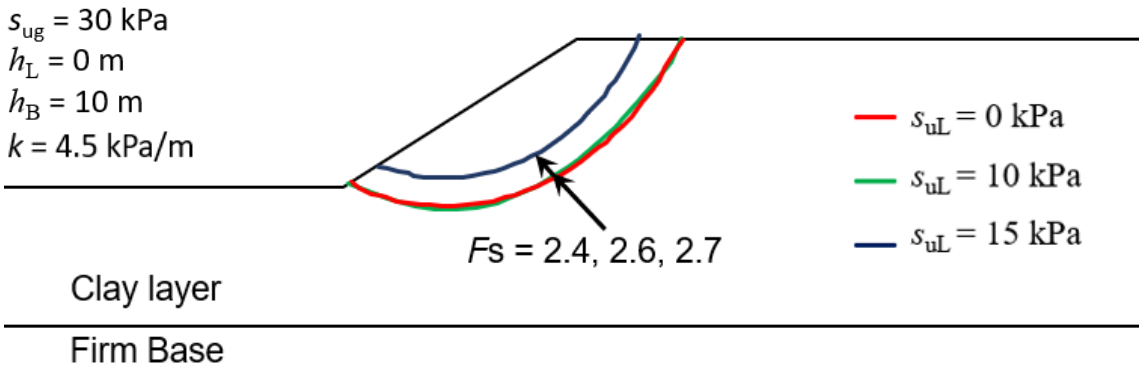

Figure 3.12: Effect of increasing shear strength in lower clay layer

As a result, it can be concluded that a higher shear strength in the lower clay layer has an effect on the depth of the failure circle. When a higher shear strength profile is used, the failure circle usually shifts upward. In general, the failure or critical circle transitions from a midpoint circle to a toe circle and then to a slope failure when a higher shear strength profile is used.

The traditional limit equilibrium (LE) methods cannot model the progressive failure, and the typical Lagrangian-based finite element (FE) modelling technique cannot simulate the complete process of sensitive clay landslides because of significant mesh distortion around the failure planes. The finite element (FE) method used in this study could overcome some of the limitations. While the described simplified approaches could be easily used in practical engineering, they are not suitable for analyzing large landslides in sensitive clays for several reasons, including the following: (i) the failure surface is not circular (e.g., in the spread or the failure of a soil block due to toe erosion); (ii) failure occurs by progressive formation of shear bands, which cannot be modelled by LE methods; and (iii) strain-softening plays a major role in failure. Further investigation of the role of the effects of the shear strength profile on retrogressive landslides using a large deformation finite element (FE) modelling technique is discussed in the next chapter.

3.6.4 20 m slope

In previous studies (for example, Saha et al. 2014; Griffiths and Yu 2015), a slope height of 10 m was taken into consideration for the analysis of slope stability. However, many natural slopes' heights are typically higher. In numerical simulations, a slope height of 20 m was used for a sensitive clay landslide (Dey et al. 2015; Wang et al. 2020). The primary goal of this study is to investigate the effects of a stronger lower layer on slope failure mechanisms, particularly for sensitive clay slopes, and compare these with the observed behaviour in the field. For this reason, additional LE analysis has been carried out for a slope of 20 m in order to compare the results of FE simulation obtained from the retrogressive analysis with LE analyses. The values for all of the parameters that are being used in this section can be found in Table 3.1 (Set B). The figures in sections 3.6.4.1–3.6.4.5 are generated using the SLOPE/W software, based on the limit equilibrium (LE) method.

3.6.4.1 Effect of slope angle

The undrained shear strength at the crest is 40 kPa, and the firm base layer is located 10 m below the toe. Since $h_L = h_B$, higher shear strength in the lower clay layer is not considered here. Figure 3.13 shows that a decrease in slope angle makes the slope more stable: thus, the factor of safety increases. When the slope angle is increased from 2:1 to 2.5:1, the factor of safety rises from 1.4 to 1.54. The factor of safety increases further to 1.66 when the slope angle is increased to 3:1. Despite the fact that a toe circle is formed at all three slope angles, as the slope angle increases, the failure circle shifts downward and covers a larger area. This chapter focuses on the effects of slope angle on failure patterns and depth of the critical failure plane using the LE method. Later in Chapter 4, the effects of similar slope angles for retrogressive landslides using FE analysis are discussed.

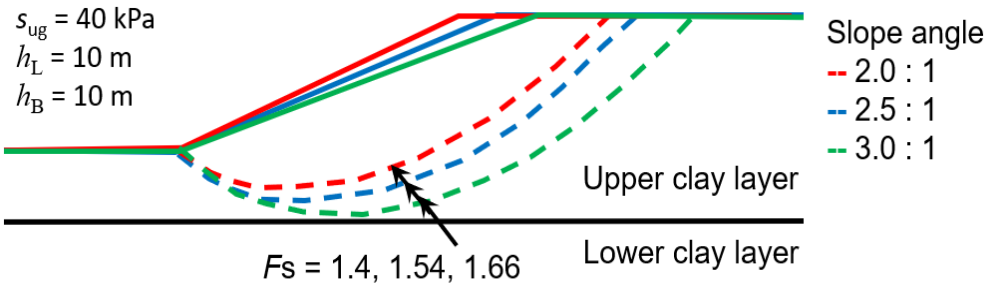

Figure 3.13: Effect of increasing slope angle

3.6.4.2 Effects of increasing shear strength gradient

The present study shows the effects of increasing shear strength gradients (k) ranging from 1.0 to 3.5 kPa/m on the failure depth of a slope. Figure 3.14 shows simulations for shear strength gradients (k) of 1.0, 2.5 and 3.5 kPa/m for a 20 m slope. The undrained shear strength at the crest is 40 kPa, and the firm base layer is located 5 m below the toe. Since $h_L = h_B$, higher shear strength in the lower clay layer is not considered here. All the parameters are the same in three soil profiles except for the k. In contrast to a 10 m slope (Fig. 3.3), increase in the shear strength gradient has little effect on the failure circle in a 20 m slope. The failure circle almost remains constant, or in other words, does not shift upward as the shear strength gradient increases. However, as the shear strength gradient increases, the factor of safety also increases.

Slope	**Critical Circle**
2:1	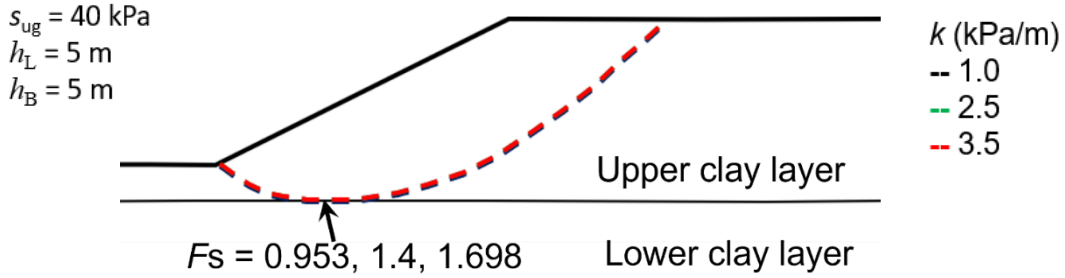

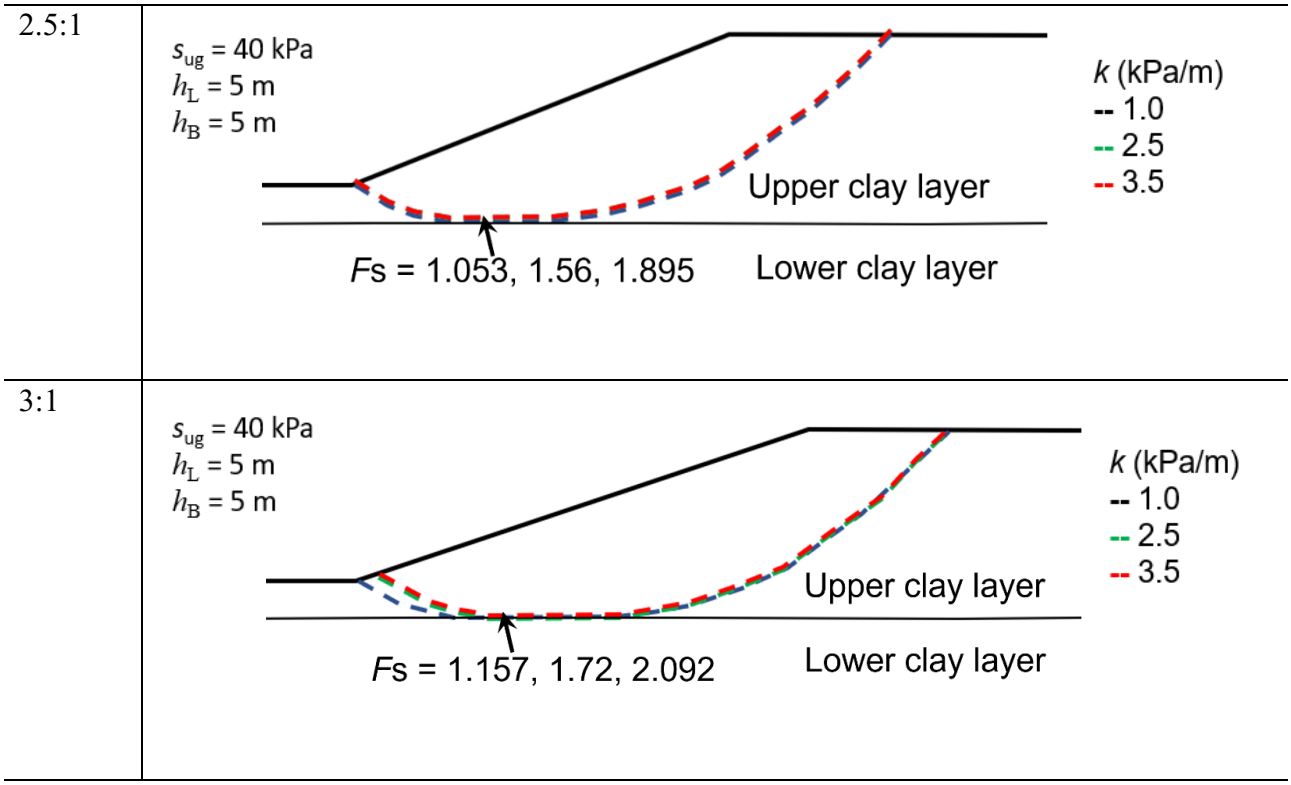

Figure 3.14: Effect of increasing slope angle

3.6.4.3 Effect of higher shear strength in lower clay layer

The undrained shear strength of the lower clay layer may be higher than that of the upper clay layer due to different soil compositions (Locat et al. 2019). In the analyses presented in this section, a higher shear strength profile is used for the lower clay layer, which is respectively 10 kPa and 20 kPa higher than the upper clay layer, as shown by the dashed line in Fig. 3.2. The undrained shear strength at the top of the crest is 40 kPa. Analyses are performed by placing the top of the lower clay layer at a depth of 5 m below the toe, and the firm base layer is placed 10 m below the toe. The upper clay layer has the same properties as before. To determine the effect of higher shear strength in the lower clay layer on the failure circle, a number of LE analyses are conducted for different slope angles and k = 2.5 kPa/m.

For a slope of 2:1, a 10 kPa increase in shear strength profile at a depth of 5 m below the toe has no significant effect on the failure depth. However, if it is increased by another 10 kPa, the critical circle becomes shallower and shifts upward. With an increase in shear strength in the lower clay layer, the toe circle transforms into a slope failure. Nonetheless, when the shear strength profile is increased at 5 m depth below the toe for 10 and 20 kPa, the factor of safety increases in all cases.

Similar failure patterns are observed for increase of 10 and 20 kPa in shear strength profiles at a layer below the toe for slope 2.5:1. The factor of safety also increases with the shear strength profile by 10 and 20 kPa.

For a slope of 3:1, an increase in the shear strength profile (10 and 20 kPa) at a depth of 5 m below the toe has no significant effect on the failure depth. However, with an increase in shear strength in the lower clay layer, the toe circle becomes shallower and transforms into a slope failure. Nonetheless, when the shear strength profile is increased at 5 m depth below the toe for 10 and 20 kPa, the factor of safety increases in all cases.

Slope	**Critical Circle**
2:1	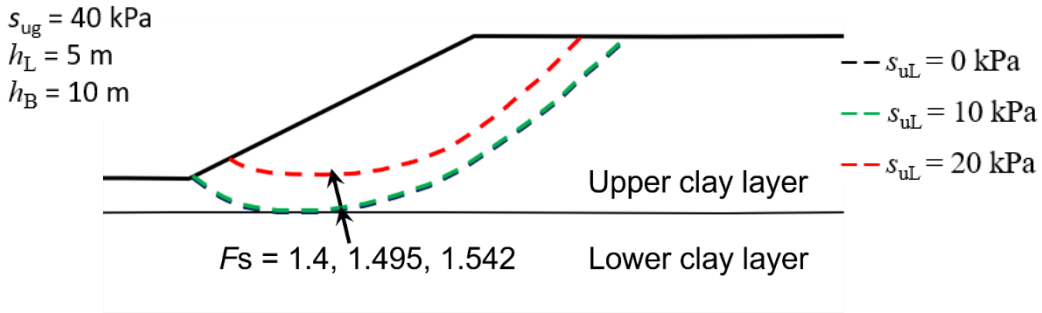

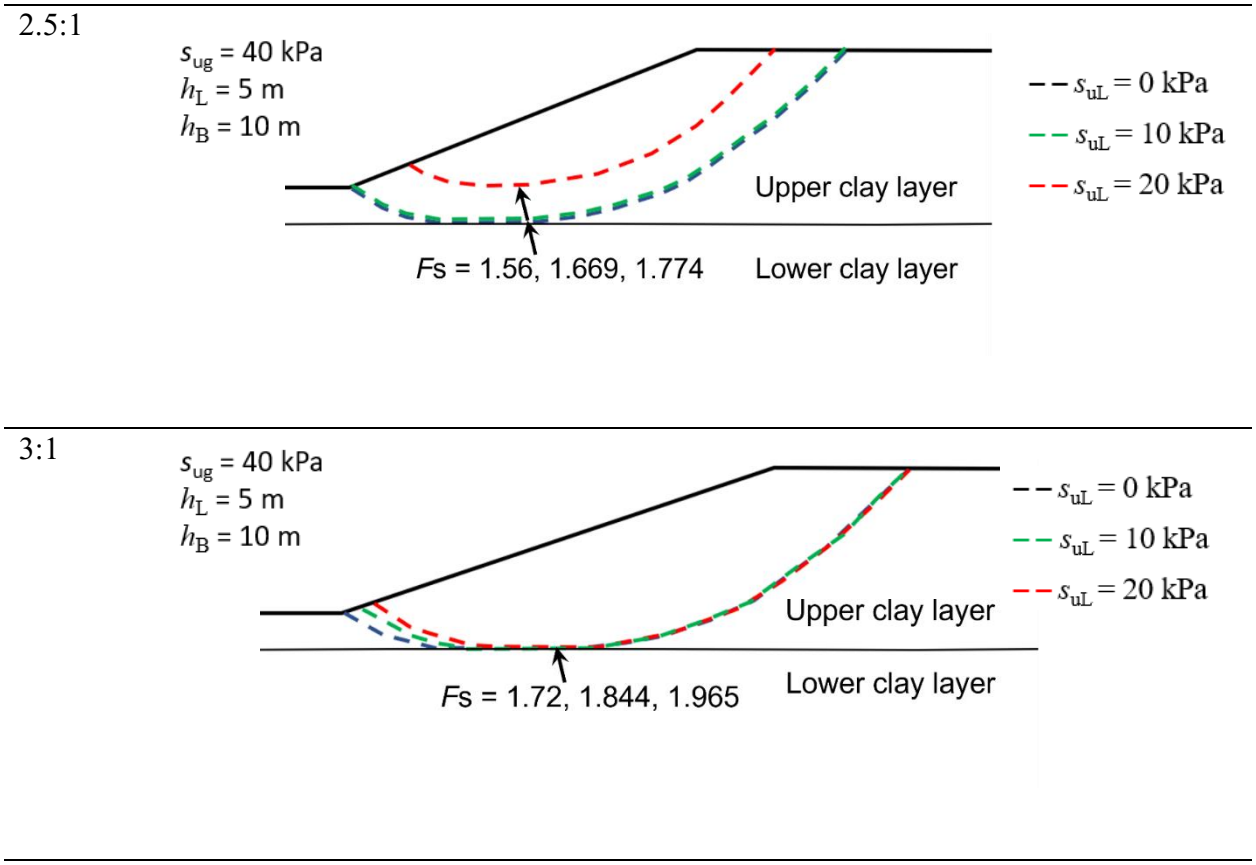

Figure 3.15: Effect of increasing shear strength in lower clay layer

3.6.4.4 Effect of toe erosion

Previously, in this study, LE analysis is performed under idealized conditions in which toe erosion is not considered. In this section, the toe erosion is modelled by excavating the shaded circular zone shown in fig. 3.16. Here, the effect of toe erosion is considered for s_{ug} = 40 kPa and k = 2.5 kPa/m. When there is no toe erosion, the factor of safety is as high as 1.54, as shown in Fig. 3.13. However, if toe erosion occurs, the factor of safety drops to 1.29 for k = 2.5 kPa/m (Fig. 3.16). Except for toe erosion, all of the parameters used in both cases (Figs. 3.13 and 3.16) are the same. It is also seen for other shear strength gradients like k = 3.0, 3.5 kPa/m that toe erosion reduces the stability of the slope.

As failure of a riverbank slope due to toe erosion is a common occurrence, it is necessary to consider the consequence.

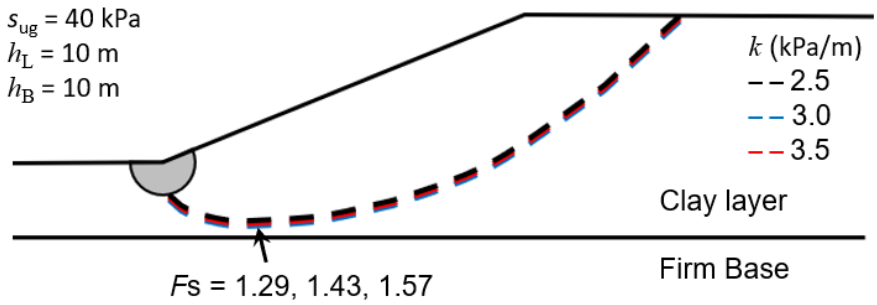

Figure 3.16: Effect of toe erosion

3.6.4.5 Influence of the depth ratio

The depth ratio (D) is the ratio of the vertical distance from the top of the slope to the firm base (DH) to the height of slope (H) (Das and Sobhan 2006). Figure 3.17 shows the effect of a firm base on the factor of safety and the location of the critical failure surface. The optimization method in SLOPE/W software is used to obtain solutions. Four failure regions are identified for different positions of firm base layers with s_{ug} = 40 kPa and k = 2.5 kPa/m. In this analysis, the position of the firm base layer is changed to see how that affects the pattern and depth of failure. If the firm base is placed considerably far from the toe (10 m) it does not affect the failure or critical circle and a deep seated (D) critical circle is formed (Fig. 3.17(a)). If the depth of the firm base from the toe is reduced to 5 m, the critical circle becomes a base circle where the critical circle is tangential to the firm base layer and emerges from the left side of the toe (Fig. 3.17(b)). If the firm base is placed near the toe (at 3 m depth below the toe), the failure circle transforms into a toe circle that is tangential to the firm base but starts at the toe of the slope (Fig. 3.17(c)). If the firm base placed at the level of the toe, a slope failure circle is formed where the critical circle passes through the slope and is tangential to the firm base layer. (Fig. 3.17(d)). Thus, it can be said that the position of the firm base layer at or below the toe affects the failure pattern and failure depth of a slope.

(a)

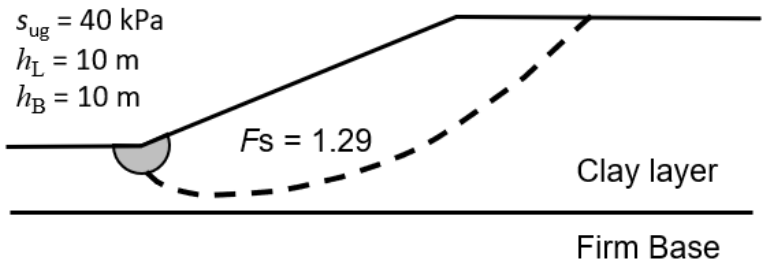

(b)

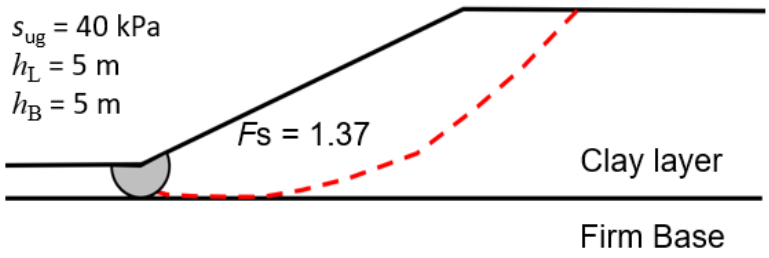

(c)

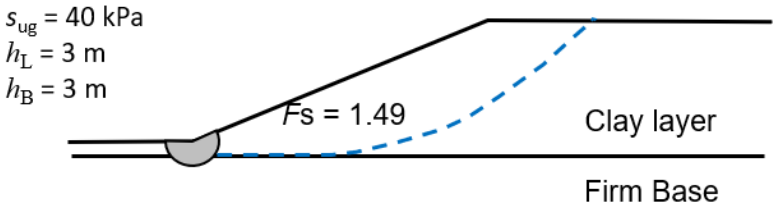

(d)

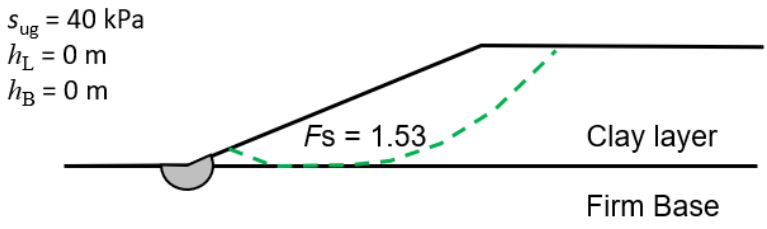

Figure 3.17: Effect of depth ratio (k =2.5 kPa/m and slope angle =21.8°)

Hunter and Schuster (1968) introduced a dimensionless strength gradient parameter *M*, which can be written as

$$M = \frac{s_{ug}}{kH} \tag{3.4}$$

and Griffiths and Yu (2015) provided a chart that gives a dimensionless stability number *N* as a function of slope angle, *D* and *M*. From *N* and *D*, the critical circle failure pattern can be classified into four distinct zones.

In Fig. 3.18, the dimensionless stability number *N*, is determined from the chart provided by Griffiths and Yu (2015) using the values of slope angle, *D*, and *M*, and the critical circle failure pattern is classified into four distinct zones using the SLOPE/W software based on the values of *N* and *D*. Four failure regions are identified for various *D* ranges with s_{ug} = 40 kPa and *k* = 1.0 kPa/m. In the region labelled "D" where $D \geq 1.4$, the critical failure surface emerges to the left of the toe, but it is not tangential to the strong layer below, which has no effect on the result. As *D* is decreased ($1.4 > D \geq 1.3$), the firm base begins to influence the critical circle in the region marked "B". At this stage, the critical circle is tangential to the firm base layer and emerges from the left side of the toe. If *D* is decreased further ($1.1 < D < 1.3$) it becomes a toe circle "T" which is very similar to a base circle. The critical circle in "T" is a tangent to the firm base but starts from the toe of the slope. When $D < 1.1$, the critical circle is a slope circle "S" that passes through the slope and is tangential to the firm base layer.

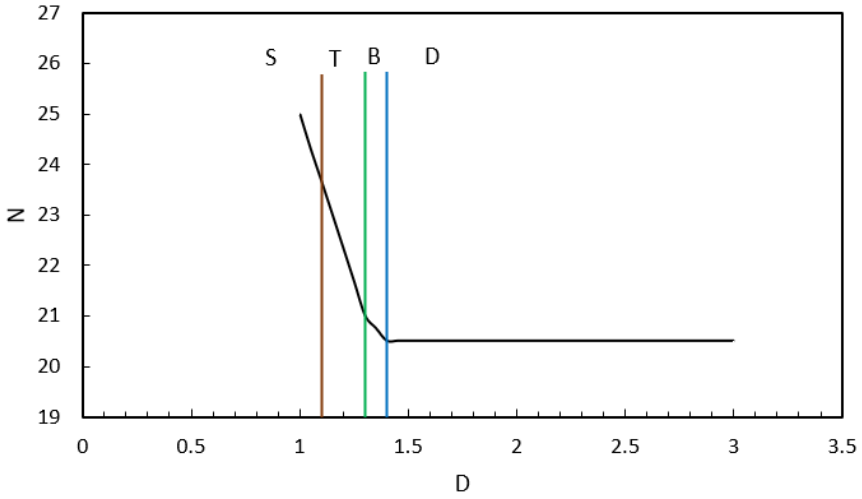

Figure 3.18: Typical result for slope with $M = 2$ and slope angle = 21.8°; S, slope; T, toe; B, base; D, deep

3.6.4.6 Comparison of LE results with FE simulation

In addition to different soil compositions, the undrained shear strength of the lower clay layer might be higher than in the upper clay layer. In the simulations presented in this section, an idealized shear strength profile, shown by the dashed line in Fig. 3.2, is used for the lower clay layer S2, which is 20 kPa higher than in the previous cases. For the upper clay layer S1, s_{u0} is the same as before. Simulations are performed by placing the top of the soil layer S2 at: (i) 10 m below the toe (Fig. 3.19) and (ii) 3 m below the toe (Fig 3.20).

In Fig. 3.19, the top of the soil layer S2 is placed at a deeper location (10 m below the toe). The maximum depth of the failure plane of the first soil block is 29 m from the crest, which means that the shear band did not reach the soil layer S2. The failure pattern is very similar to that obtained for the LE analysis (28.8 m). This implies that the lower clay layer does not have any influence on the failure if it is considerably far from the toe.

In Fig 3.20, the top of the soil layer S2 is placed at a deeper location (3 m below the toe). The failure also initiates from the bottom of the erosion block, and the global failure of the first soil block

occurs by forming a curved failure plane (Fig. 3.20). The maximum depth of the failure plane of the first block is 28 m, which is the same as that obtained in the LE analysis.

Comparing these cases, it can be concluded that the higher strength of the lower clay layer could influence the failure depth only if it is not too deep. However, the failure of the subsequent soil blocks in a retrogression landslide cannot be explained by LE analysis.

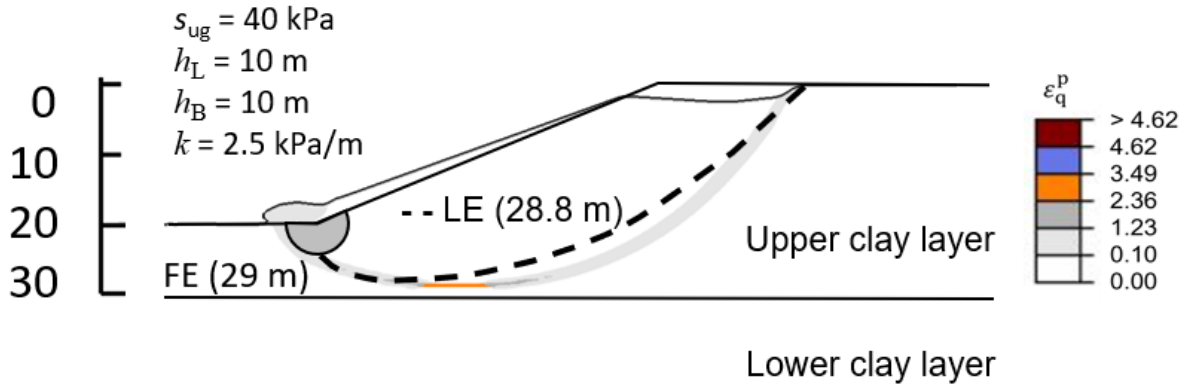

Figure 3.19: Comparison of LE analysis results with FE simulation (h_L = 10 m)

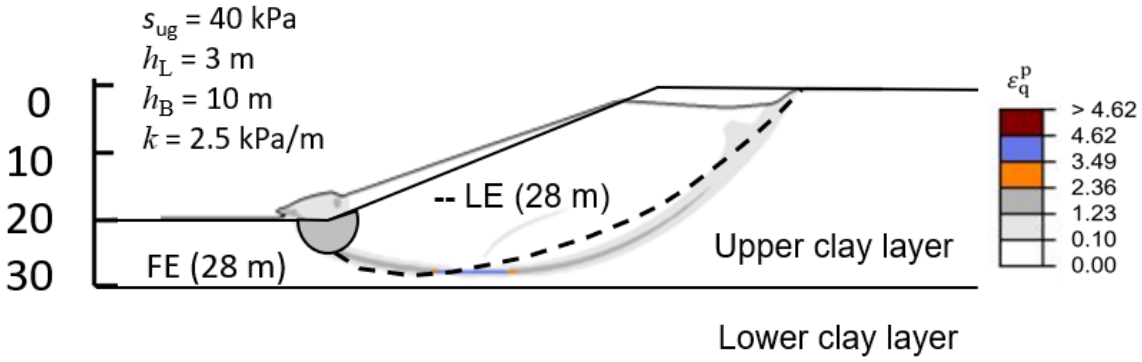

Figure 3.20: Comparison of LE analysis results with FE simulation (h_L = 3 m)

Previous research using LE analysis (e.g., Saha et al. 2014) assumed the base to be elastic and placed at the level of the toe, which does not represent the true soil behaviour below the toe. The shear band cannot pass through the elastic soil layer. For this reason, the effect of the lower clay layer is considered in this study. Instead of using an elastic base or a homogeneous high shear strength for the soil layer below the toe, a slightly increased shear strength in the linearly increasing shear strength profile, reaching the bottom, may be representative of the actual soil behaviour below the toe.

3.7 Summary

This chapter presents a comparative study of stability analyses on the effects of linearly increasing shear strength gradients using analytical, LE, and FE solutions. As the shear strength gradient increases, the failure circle shifts upward. A good agreement is observed in the factor of safety and the location critical failure circle of a clay slope using these methods. An increase in shear strength profile in the lower clay layer influences the stability analysis for low shear strength gradients of soil for varied slope heights. However, the effect is insignificant for a stronger soil or a higher shear strength gradient with depth.

Finally, it is to be noted that only a few simulations are performed in this study; although the results show some interesting trends that could be useful, these models are not very useful for large-scale landslides, because the LE method cannot determine the stress and deformation of the slope. However, the Finite Element (FE) method could overcome some of the limitations. A Eulerian-based FE method does not have any numerical issues related to mesh distortion. Further investigation of the role of the effects of the shear strength profile with strain softening and strain rate effects on retrogressive landslides using a large deformation finite element (FE) modelling technique is discussed in the next chapter.

Chapter 4: Effects of Undrained Shear Strength Profile on Retrogressive Landslides in Sensitive Clays

4.1 General

The undrained shear strength of normally and lightly overconsolidated clays generally increases linearly with depth, which could significantly influence the failure of a slope. For sensitive clays, the strength profile could affect the progressive failure mechanisms, including the formation of shear bands. The traditional limit equilibrium (LE) methods cannot model the progressive failure, and the typical Lagrangian-based finite element (FE) modelling technique cannot simulate the complete process of sensitive clay landslides because of significant mesh distortion around the failure planes. The present study investigates the effects of the shear strength profile on failure patterns through Eulerian-based FE simulations. Higher shear strength and slower softening of the soil in the lower part of the sensitive clay layer could change the failure pattern and increase the retrogression distance.

4.2 Introduction

Field investigations show a wide range of variations of undrained shear strength of clay with depth. A weathered crust is observed in many cases near the ground surface. Below the crust, the undrained shear strength generally increases almost linearly with depth (Quinn et al. 2011; Locat et al. 2015; Perret et al. 2019). Slope stability for the undrained conditions ($\phi = 0$) was the focus of some previous studies (e.g., Gibson and Morgenstern 1962; Hunter and Schuster 1968; Booker and Davis 1972; Koppula 1984; Griffiths and Yu 2015). An idealized linearly increasing soil profile is considered in these studies without considering the crust and softening of sensitive clays. Assuming circular failure planes, analytical solutions were developed in those studies based on the limit equilibrium (LE) methods. Some of those studies compared the location of the critical failure plane obtained from LE

methods with FE simulation results (e.g., Griffiths and Yu 2015). The results were presented in the form of a stability chart as a function of the stability number.

While these-simplified approaches could be easily used in practical engineering, they are not suitable for analyzing large landslides in sensitive clays for several reasons, including the following: (i) the failure surface is not circular (e.g., in the spread or the failure of a soil block due to toe erosion); (ii) failure occurs by progressive formation of shear bands, which LE methods cannot model; and (iii) strain-softening plays a major role in failure.

Based on post-slide investigations of large-scale sensitive clay landslides, the location of the failure surface was inferred from field tests (e.g., piezocone tests) (Delisle and Leroueil 2000; Locat et al. 2008; Locat et al. 2019). These studies confirmed the formation of non-circular failure planes. The failure surface often starts from a point near the toe of the slope and propagates quasi-horizontally into the intact soil deposit (Locat et al. 2013).

In addition to an increase in the undrained shear strength with depth, post-slide investigation of large-scale landslide areas also shows different soil units above and below the failure planes. For example, Bélanger et al. (2017) presented geophysical and geotechnical investigations of an area located upstream of Vases Creek Valley where numerous sensitive clay landslides occurred. The authors found two sensitive clay layers. Below the crust, the soil is highly sensitive, having high clay content, less silt content, high liquidity index and low residual shear strength. However, the soil layer, a few meters below the bottom of the valley, is relatively less sensitive, and has less clay content but higher silt content, lower liquidity index and higher residual shear strength. A similar pattern was found in other sensitive clay landslide areas; the soil layer below the sliding plane is somehow different in terms of particle size distribution and liquidity index (e.g., Locat et al. 2017). In some

cases, locally increased undrained shear strength is observed below the failure plane (e.g. Saint-Jude landslide, Locat et al. 2017; Rigaud landslide, Carson 1979).

The failure process might be affected by different soil units approximately below and above the toe level, for at least two reasons. First, the undrained shear strength could be slightly higher in the lower clay layer, as observed in some field investigations. Second, the rate of strain-softening might be lower when the clay content is lower. For example, during Ormen Lange gas field development in offshore Norway, Kvalstad et al. (2005) showed that marine clay (clay content 45%–65%) exhibits significant strain-softening behaviour while glacial deposits (clay content 30%–40%) show very little or no softening.

The objective of the present study is to investigate the effects of the shear strength profile and rate of strain-softening on retrogressive landslides using a large deformation finite element (FE) modelling technique.

4.3 Problem definition

A 2:1 (horizontal to vertical) slope is used for numerical simulations (Fig. 4.1). The height of the slope is 20 m. There is a 3-m weathered crust near the ground surface. Below the crust, there are two sensitive clay layers of a total 47 m thickness. The thickness of the upper sensitive clay layer (S1) is h_1, which has high clay content, and strain softening occurs rapidly compared to those for the lower sensitive clay layer (S2). The top surface of the lower sensitive clay layer S2 is at or below the toe of the slope. In some simulations, a lower rate of softening or higher shear strength (s_{uL}) is given, as shown by the dashed line of the shear strength profile in Fig. 4.1. The soil is very strong at a large depth (50 m below the crest level), and this soil is modelled as an elastic material.

The groundwater table is at the ground surface and along the slope. The effects of the opposite bank in the case of a riverbank slope are not modelled. The debris might move along the river, which could not be modelled in this two-dimensional simulation; therefore, the left boundary is placed 100 m far from the toe so that the debris does not accumulate near the toe.

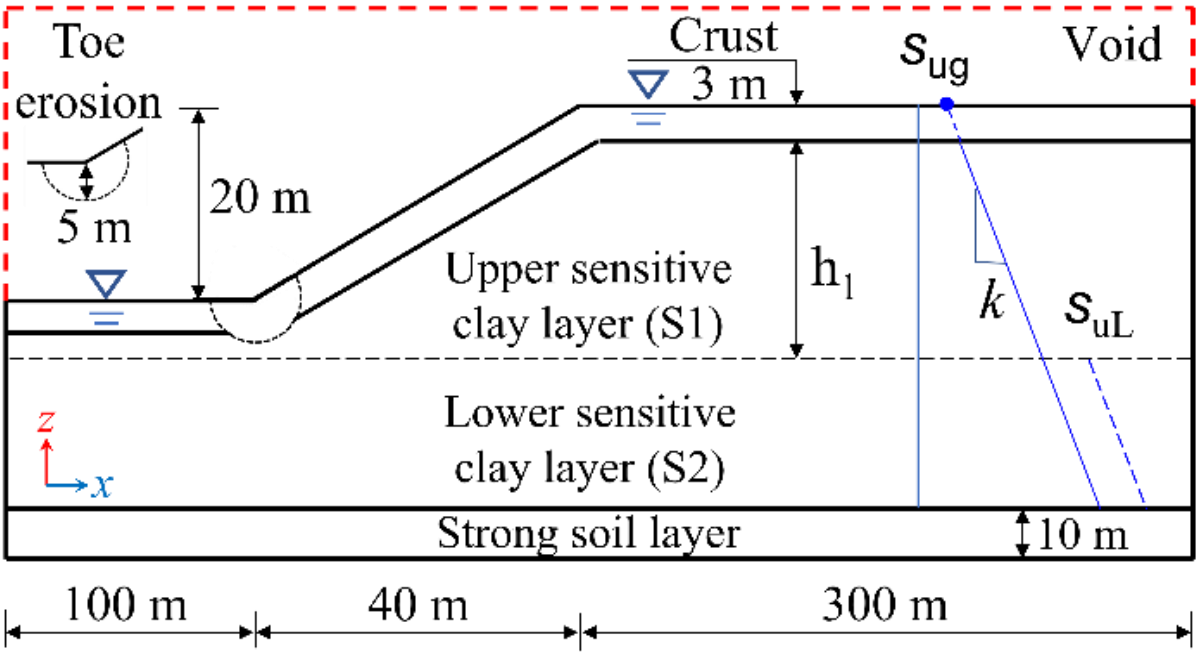

Figure 4.1: Geometry used in finite element analysis (not to scale)

The right boundary is placed at 300 m from the crest, which is sufficiently far from the failure zone and does not affect the results. The landslide is triggered by the failure of a circular soil block of 5 m depth from the toe, which is called "toe erosion" in this chapter (Fig. 4.1).

4.4 Finite element modelling

Most of the FE models available in the literature for slope stability analysis were developed in a Lagrangian framework (Griffiths and Lane 1999; Loukidis et al. 2003). The present study utilizes the Eulerian-based FE technique in Abaqus 6.19 software in which the Eulerian material (soil) can flow

through the fixed mesh without causing numerical issues related to mesh distortion, even at very large deformations.

In numerical modelling, zero velocity boundary conditions are applied in all directions (i.e., $v_x = v_y = v_z = 0$) at the bottom of the soil model (Fig. 4.1). A zero velocity boundary condition is also applied to all of the vertical faces of the domain except for the left side, where $v_x = 0$ is applied only to the elements below the toe level. There is no velocity boundary condition along the soil–void interface, which allows the soil to move into the void space when needed.

Only three-dimensional elements are available for Eulerian FE simulations. Therefore, the modelling is performed with a single element in the out-of-plane direction to simulate the plane strain conditions. The Eulerian domain is discretized into 0.5-m cubical elements using EC3D8RT in the software, which are 8-node linear brick elements of multi-materials with reduced integration, thermally coupled and hourglass controlled. The mesh size regularization technique is used to reduce mesh sensitivity issues (Karmaker and Hawlader 2022). The Eulerian Volume Fraction (EVF) tool is used to define the soil and voids: EVF = 1 for the elements filled with Eulerian material (clay), EVF = 0 for the void, and $0 < EVF < 1$ for the elements partially filled with soil.

The analysis consists of three steps. The first step is to apply a geostatic load to bring the soil to the in-situ stress conditions. Wang et al. (2021) developed a method to define the in-situ stress conditions in the Eulerian-based FE simulations, which consists of seepage analysis and effective stress-based in-situ stress modelling prior to total stress-based undrained landslide simulations. In the present study, their approach is used to define the in-situ stress conditions. By specifying the initial condition in this manner, the simulation can be run for K_0 greater than 1, as observed in some sensitive clays in eastern Canada. At the end of the gravitational step, shear stress is generated in soil elements

close to the slope; however, K_0 remains constant in soil elements distant from the slope, where retrogressive failure occurs (Wang et al. 2021). In the second step, the failure is triggered by toe erosion by reducing the undrained shear strength of the erosion block from its intact shear strength to 0.1 kPa in 5 seconds. In the final step, the failed soil is allowed to move downslope for 30-50s without applying any external load. The instantaneous velocity of the failed soil is negligible at the end of this step.

4.5 Undrained shear strength of sensitive clays

The mobilized undrained shear strength (s_u) of the sensitive clay layers (S1 & S2) is modelled as:

$$s_u = f_1 f_2 s_{uy} \tag{4.1}$$

where f_1 is a strain-softening factor, f_2 is a strain-rate factor, and s_{uy} is undrained shear strength at a very low shear strain rate.

4.5.1 Strain Softening Effects

The strain-softening factor f_1 can be defined by a linear or exponential function of accumulated plastic shear strain or plastic shear displacement (δ) (Locat et al. 2013; Dey et al. 2016; Wang et al. 2020). In this study, f_1 is defined using Eq. (4.2), which consists of an exponential decrease of s_u for $0 \leq \delta < 2\delta_{95}$ (similar to Einav and Randolph 2005) followed by a linear degradation at $2\delta_{95} \leq \delta < \delta_{ld}$ before becoming constant at large shear displacements ($\delta > \delta_{ld}$).

$$f_1 = \begin{cases} \dfrac{s_{uR}}{s_{u0}} + \left(1 - \dfrac{s_{uR}}{s_{u0}}\right) e^{-3\delta/\delta_{95}} & \text{if } 0 \le \delta < 2\delta_{95} \\ \dfrac{s_{uR}}{s_{u0}} - \dfrac{s_{uR} - s_{uld}}{s_{u0}} \dfrac{\delta - 2\delta_{95}}{\delta_{ld} - 2\delta_{95}} + c & \text{if } 2\delta_{95} \le \delta < \delta_{ld} \\ \dfrac{s_{uld}}{s_{u0}} + c & \text{if } \delta > \delta_{ld} \end{cases} \quad (4.2)$$

where s_{u0} is the peak undrained shear strength at the reference shear strain rate $(\dot{\gamma}_{ref})$ before softening; s_{uR} is the value of s_u at a sufficiently large value of δ; δ_{95} is the value of δ at which 95% reduction of $(s_{u0} - s_{uR})$ occurs; s_{uld} is the value of s_u at a completely remoulded state at a very large value of δ; and $c = (1 - s_{uR}/s_{u0})e^{-6} \approx 0$. In the FE program, adopting the von Mises criterion, the initial yield strength (= $2s_{u0}$) is given. In each time increment, the equivalent plastic shear strain (ε_q^p) is employed, which is then used to define strain-softening using Eq. (2). Further details of Eq. (4.2), numerical implementation, and model parameter selection are available in previous studies (Dey et al. 2015; Dey et al. 2016; Wang et al. 2020).

4.5.2 Strain Rate Effects

In general, the undrained shear strength increases with shear strain rate ($\dot{\gamma}$). In the FE program, ε_q^p is used in each time increment, and $\dot{\gamma}$ is calculated as $\dot{\gamma} = \sqrt{3}\Delta\varepsilon_q^p/\Delta t$, where Δt is a time interval.

Several models have been proposed in the past to capture strain-rate effects on undrained shear strength. Zhu and Randolph (2011) proposed an "additive power-law model" combining the Herschel–Bulkley (fluid mechanics) and the power-law (geotechnical approach) models, which can better capture the behaviour of soil from its intact state to the fluidized remoulded conditions, as occurs in sensitive clay landslides.

$$f_2 = 1 + \eta \left(\frac{\dot{\gamma}}{\dot{\gamma}_{\text{ref}}} \right)^{\beta} \tag{4.3}$$

where η and β are soil parameters (Randolph et al. 2012; Wang et al. 2021). At the reference strain rate (i.e. $\dot{\gamma} = \dot{\gamma}_{\text{ref}}$)

$$s_{\text{uy}} = s_{\text{u0}}/(1+\eta) \tag{4.4}$$

Field vane shear tests are commonly used to determine undrained shear strength. The average shear strain rate of a vane shear test for a rotation rate of 0.1 °/s is ~0.05 s^{-1} for a soil having a 10% increase in undrained shear strength per log cycle (Einav and Randolph 2006; Boukpeti et al. 2012). In this study, $\dot{\gamma}_{\text{ref}} = 0.05\ \text{s}^{-1}$ is used. Attempts have been made to examine the effects of rotation rate on vane shear strength. Dutta et al. (2015) compiled test results and showed that the strain rate effect is higher at higher strain rates and in softer soils. Also, while laboratory tests (e.g. triaxial) could be performed at a very low strain rate, the undrained conditions cannot be maintained in the field when tests are performed at a slow rate of rotation (partial drainage occurs). Roy and Leblanc (1988) presented field vane shear test results on two sensitive clays in Canada and showed that the shear strength increased at a slower rate of rotation, which was due to partial drainage during shearing. In this study, the strain rate effects are neglected (i.e. $f_2 = 1$) when $\dot{\gamma} \leq \dot{\gamma}_{\text{ref}}$. The initial undrained shear strength (s_{u0}) of both sensitive clay layers (S1 & S2) increases linearly with depth as

$$s_{\text{u0}} = s_{\text{ug}} + kz \tag{4.5}$$

where s_{ug} is constant (in kPa), which represents the value of the linear shear strength profile extrapolated to the ground surface (Fig. 4.1); k is the shear strength gradient (kPa/m) with depth (z) measured from the crest level.

4.6 Material parameters

Table 4.1 below shows the geotechnical parameters used in the "base case" finite element simulations.

Table 4.1: Geotechnical parameters used for numerical simulation

Parameter	Sensitive clay	Crust	Base
Total unit weight, γ (kN/m^3)	17	17	17
Initial undrained shear strength, s_{u0} (kPa)	40 + 2.5z	75	-
Undrained Young's modulus, E_u (MPa)	21	21	50
Undrained Poisson's ratio, ν_u	0.495	0.495	0.495
Reference shear strain rate, $\dot{\gamma}_{ref}$	0.05	-	-
δ_{95} (m)	0.05	-	-
δ_{pc} (m)	0.004	-	-
δ_{ld} (m)	2.0		
η	0.5	-	-
β	0.1	-	-

4.7 Results

Figure 4.2 shows the progressive formation of the failure planes for the base case where the initial undrained shear strength of both sensitive clay layers (S1 and S2) increases with depth as s_{u0} = 40 + 2.5z (solid line of the shear strength profile in Fig. 4.1). In this simulation, the strain-softening parameters are the same for both clay layers, as listed in Table. 4.1. The process of failure is shown

by plotting the accumulated plastic shear strain (ε_q^p). PEEQVAVG or ε_q^p represents the integration of plastic deviatoric strain rate tensor over the period of analysis, which is related to plastic shear strain in simple shear condition (γ^p) as $\varepsilon_q^p = \gamma^p/\sqrt{3}$. As the materials involve strain softening, significant strain localization occurs near the failure planes, and the shear bands form with the progress of the simulation.

For the base case (Fig. 4.2), the failure initiates from the lower part of the curved erosion block and propagates downward. The shear band propagates in a circular path, and after reaching a depth of 29 m from the crest level, it then curves upward and reaches the upslope ground surface, which causes global failure of the soil block M1 (Fig. 4.2(a)). The failed soil block rotates and tries to climb up above the toe with time. The displacement and rotation of M1 increase the backscarp height, and, at one stage, another small soil block, M2, fails (Fig. 4.2(b)). The failure of this soil block starts from a shallower depth (20 m below the crest level). Note that the slope of the backscarp is higher than the original slope (2:1); therefore, the failure of M2 could occur at a shallower depth. The displacement and rotation of the failed soil block stops at t ~ 27 s (Fig. 4.2(c)). The retrogression distance (L_R) is 40 m, which measures the horizontal distance between the crest and the furthest point where the final failure plane intersects the upslope ground surface.

4.7.1 Effects of strain-softening of the lower sensitive clay layer

As mentioned in the introduction, the deeper soils (e.g. S2 in Fig. 4.1) might have different particle size distribution, including lower clay content, than the upper sensitive clay layer. Field investigations do not show an abrupt change in undrained shear strength, although some increases have been reported (e.g., Locat et al. 2017). Therefore, three more simulations are performed for the same s_{u0} profile as in the base case and with the soil parameters listed in Table 4.1, but using a higher δ_{95} (= 1.0 m). This implies that the strain-softening of soil S2 occurs slowly in these simulations as

compared to the base case simulation. The top of the soil layer S2 is placed at three depths: (i) very close to the level of the toe: 3.25 m below the toe (case 1), (ii) moderately far from the toe: 5.25 m below the toe (case 2), and (iii) very far from the toe: 9.75 m below the toe (case 3).

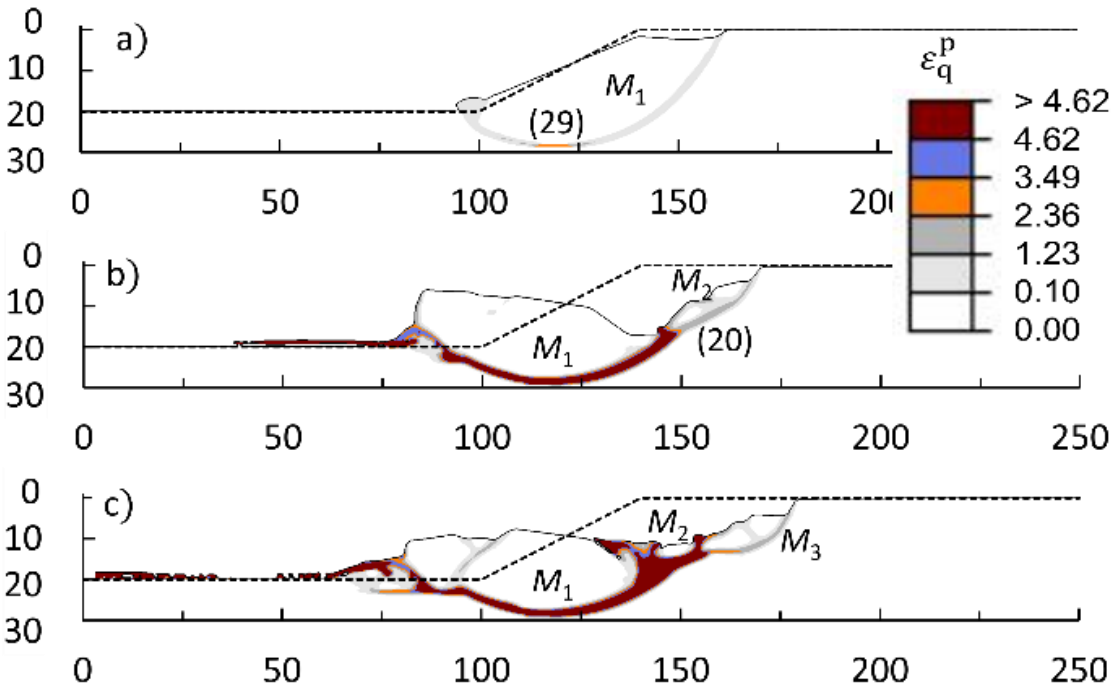

Figure 4.2: Soil failure in base case simulation

Figure 4.3 shows the failure pattern for case 1. Unlike base-case results, the failure due to toe erosion initiates from a shallower depth. The shear band propagates almost horizontally above the S2 layer for about 25 m and then curves upward and causes global failure of a soil block. The landslide stops after the successive failure of seven soil blocks with a retrogression distance of 90 m. The maximum depth of the failure planes is approximately at the top surface of the soil layer S2, except for the last block.

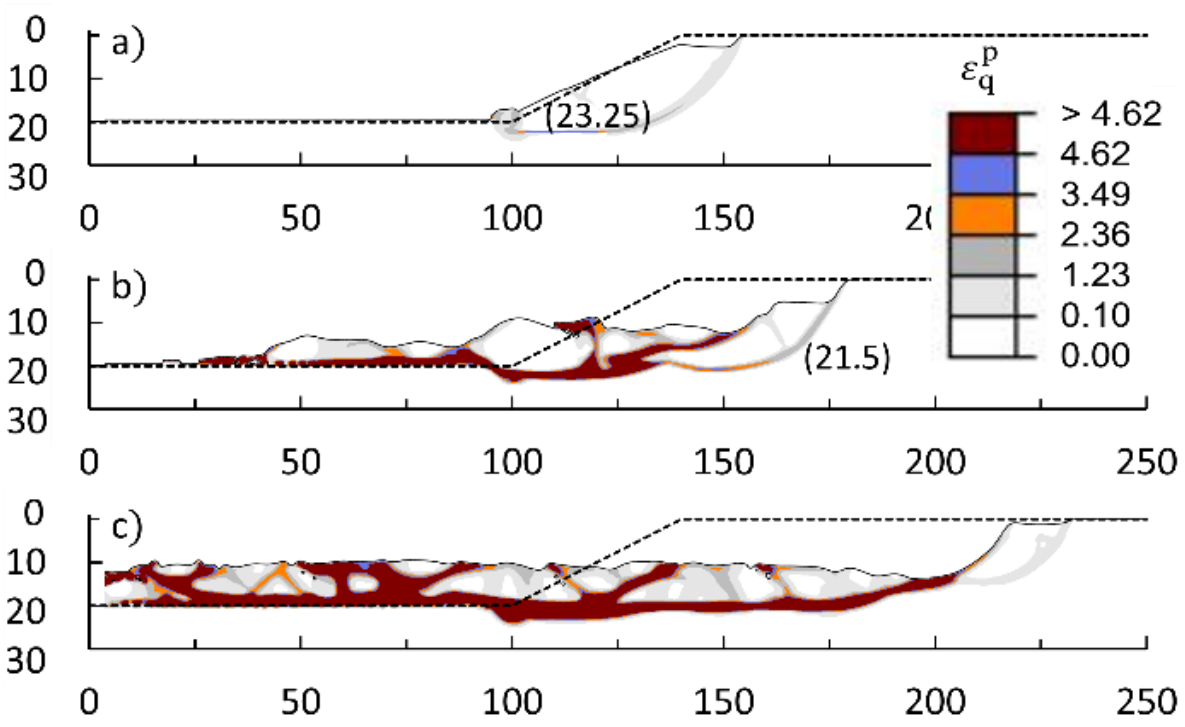

Figure 4.3 Soil failure in case 1 simulation

Figure 4.4 shows the simulation results for case 2. In this case, the failure initiates from a point around the bottom of the erosion block. The shear band then propagates horizontally immediately above the soil layer S2, approximately about 25 m, and then curves upward, causing the global failure of the first soil block. The failure of the second soil block starts ~5 m above the top of the S2 layer. The maximum depth of failure of the subsequent soil blocks becomes shallower. The retrogression distance, in this case, is 66.5 m.

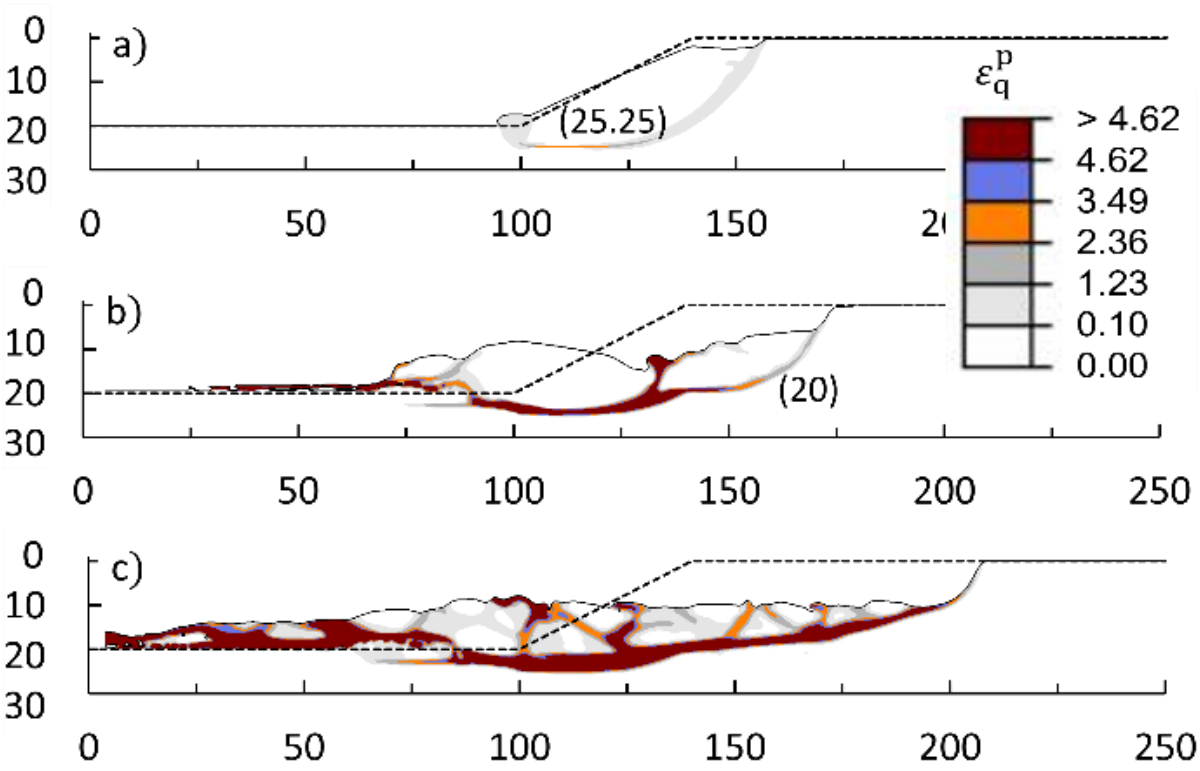

Figure 4.4: Soil failure in case 2 simulation

When the top of the soil layer S2 is placed at a deeper location (9.75 below the toe, case 3), the failure pattern is very similar to that obtained for the base case (Fig. 4.2). The maximum depth of the failure plane of the first soil block is 29 m from the crest, which means that the shear band did not reach the soil layer S2. This implies that the lower clay layer does not have any influence on the failure if it is considerably far from the toe.

A comparison of the simulation results of these four cases (base case and cases 1-3) shows that the maximum retrogression occurs when the S2 layer is placed close to the toe (case 1). In this case, the first shear band forms at a shallower depth through the upper clay layer S1 because the rate of softening is low for S2, although the undrained shear strength is the same near the interface between the two layers. The first soil block that failed at a shallower depth could displace easily in the

downslope direction, as compared to a soil block that fails through deeper soil (e.g. M1 in Fig. 4.2). The higher potential of displacement of the first soil block facilitates the failure of the subsequent soil blocks and results in larger retrogression in the case 1 simulation. In summary, the rate of softening could significantly change the failure patterns and thereby the retrogression distance.

4.7.2 Effects of increasing shear strength in the lower clay layer

In addition to different soil compositions, the undrained shear strength of the lower clay layer might be higher than in the upper clay layer. The local change in soil type (e.g., particle size) might give varying shear strengths. However, in the simulations presented in this section, an idealized shear strength profile, shown by the dashed line in Fig. 4.1, is used for the lower clay layer S2, which is 20 kPa higher than in the previous cases. For the upper clay layer S1, s_{u0} is the same as before. Simulations are performed by placing the top of the soil layer S2 at: (i) the level of the toe (case 4) and (ii) 3.25 m below the toe (case 5).

For case 4, Fig. 4.5 shows that the failure initiates from the bottom of the erosion block, and the global failure of the first soil block occurs by the formation of a curved shear band. The maximum depth of the failure plane is 28 m from the crest level. One important observation is that, although the soil is stronger below the toe (S2 layer), the shear band propagates to this stronger soil. With the displacement of this failed soil block, three more soil blocks failed, and the failure stopped after a retrogression distance of 62 m.

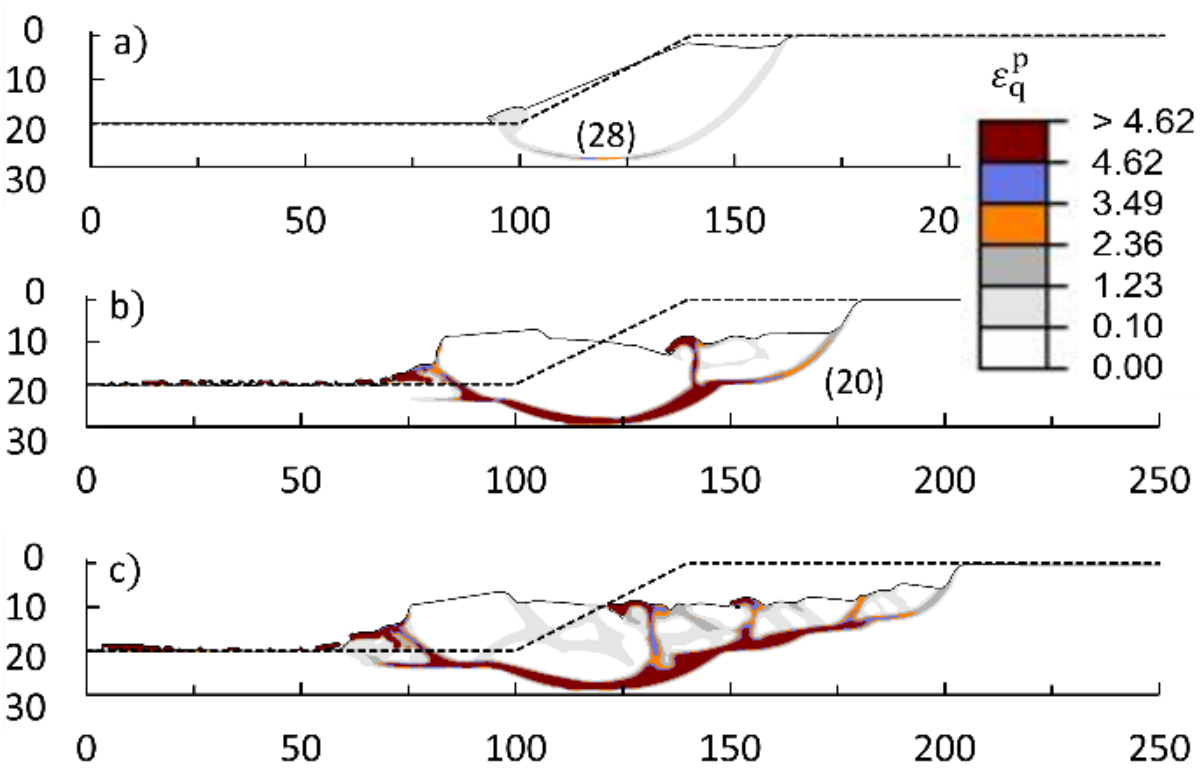

Figure 4.5: Soil failure in case 4 simulation

For case 5, the failure also initiates from the bottom of the erosion block, and the global failure of the first soil block occurs by forming a curved failure plane (Fig. 4.6). The maximum depth of the failure plane of the first block is 28 m, which is the same as that obtained in the case 4 simulation, although the S2 layer in case 5 is 3.25 m deeper than that in case 4. The effect of increasing shear strength at or below the toe level is primarily visible in the depth at which subsequent soil blocks form following the failure of the first block. With the displacement of the failed soil blocks, three more soil blocks fail, and the landslide stops after a retrogression distance of 67 m.

Comparing the results of these two simulations (cases 4 and 5) with the base case (Fig. 4.2), it can be concluded that the higher strength of the lower clay layer could also influence the progressive failure and increase the retrogression distance.

Finally, comparing case 1 (Fig. 4.3) and case 5 (Fig. 4.5), it can be concluded that the rate of softening has more effect on retrogression distance than the increase in shear strength of the lower clay layer.

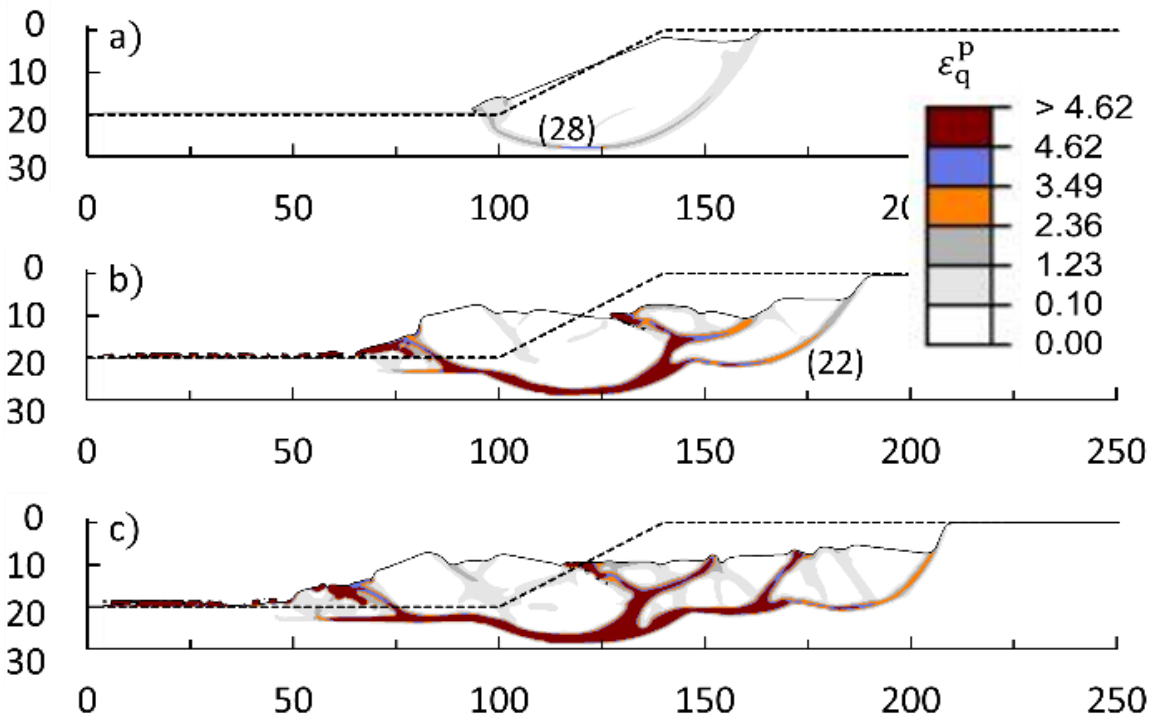

Figure 4.6: Soil failure in case 5 simulation

4.7.3 Effect of slope angle

The geometry of the slope is a key factor in progressive failure. Steep slopes may be more prone to progressive failure (Lo and Lee, 1973; Locat et al., 2013). Slopes of 2:1, 2.5:1, and 3:1 are used here to investigate the effect of slope angle on failure patterns.

The simulations for slopes 2.5:1 and 3:1 are shown in Figs. 4.7 and 4.8. Except for the slope angle, all other parameters in these two slopes are the same as in case 4 shown in Fig. 4.4. The failure process of a typical flowslide can be seen on all three slopes.

Four rotational slides occur successively when the slope is 2.5:1, as shown in Fig. 4.7. Reduction of shear strength of the eroded block triggers the sensitive clay to form a horizontal shear band. The shear band propagates some distance horizontally, and then curves upward, causing the global failure of the first soil block. The failure of the second soil block starts ~5 m above the top of the S2 layer. The subsequent soil blocks fail at a shallower depth than the one before. The retrogression of the landslide finally stops after reaching a retrogression distance of 49 m.

For slope 3:1, the failure pattern of the first block is very similar to the failure pattern described above. After propagating some distance horizontally, the shear band curves upward to the ground surface and causes the rotational failure of a soil block (Fig. 4.8). When the slope is 3:1, only three soil blocks fail. The subsequent soil blocks fail at a shallower depth than the one before. The retrogression of the landslide stops after reaching a retrogression distance of 33 m.

Simulation results for slope 2:1 are already shown in Fig. 4.4. For slope 2:1, five rotational slides occur successively, as shown in Fig. 4.4. The maximum depth of the failure surface for the slope is 2:1 and reduces slightly for a subsequent rotational slide, and the retrogression of the landslide eventually stops after reaching a retrogression distance (L_R) of 66.5 m.

Previous research has shown that an increase in the horizontal-to-vertical stress ratio, a decrease in soil brittleness, and slope angle collectively change the failure pattern from a flowslide to a spread failure (Wang et al. 2020). Since only the change in slope angle has been considered here, the change in failure pattern from flowslide to spread is not visible. The failure process of a typical flowslide can be seen on all three slopes.

The key observation from the simulations is that a steeper slope angle causes a higher retrogression distance and a higher number of failed blocks during the landslides. After the first block failure, a higher backscarp is observed for a steeper slope.

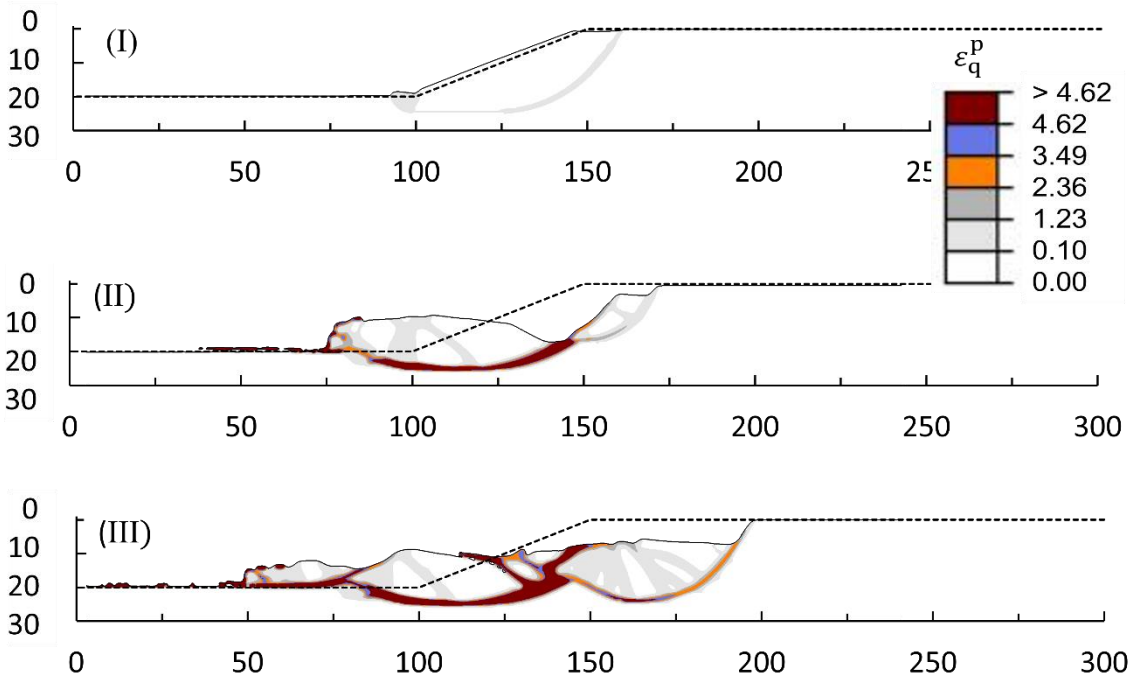

Figure 4.7: Propagation of plastic shear band for slope 2.5:1 (K_0 = 1.0)

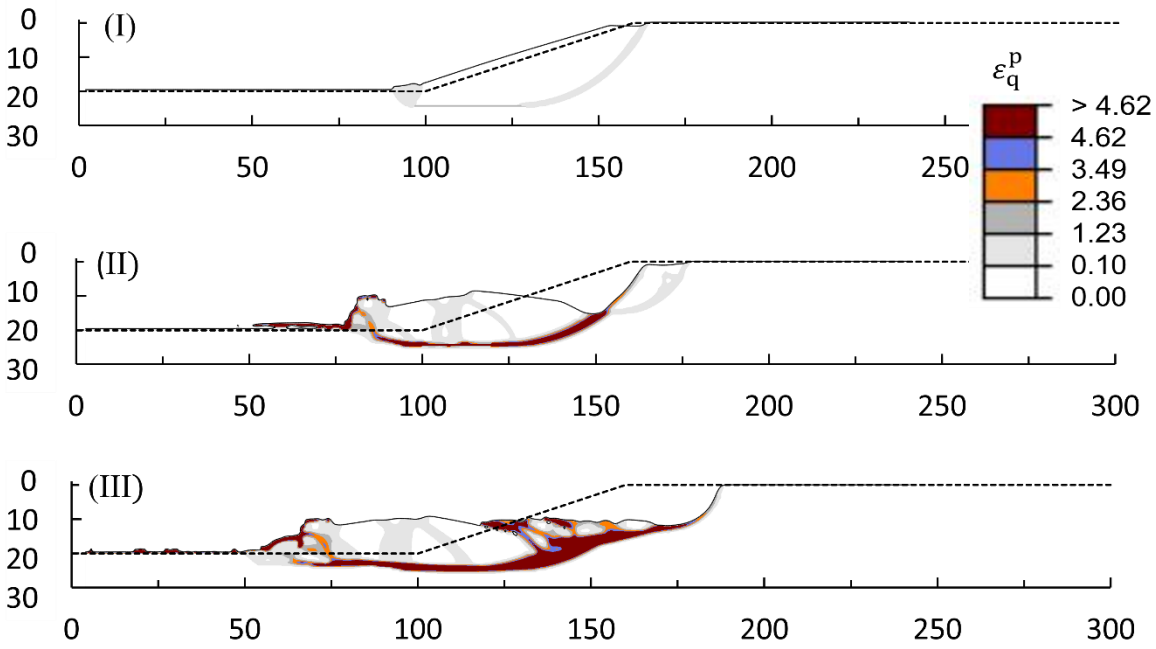

Figure 4.8: Propagation of plastic shear band for slope 3:1 (K_0 = 1.0)

4.7.4 Effect of shear strength gradient

The present study shows the effects of increasing shear strength gradients (k) ranging from 2.0 to 3.0 kPa/m on a large retrogressive landslide. Figures 4.9 and 4.10 show simulations for shear strength gradients (k) of 2.0 and 3.0 kPa/m, respectively. The results for k = 2.5 kPa/m are previously shown in Fig. 4.8. All the parameters are the same in the three soil profiles except for the k. In these simulations, a failure pattern resembling a flowslide is observed as K_0 = 1.0 is used. Wang et al. (2021) investigated the numerical analysis of a retrogressive landslide in sensitive clay and observed that the flowslide occurred when the earth pressure coefficient in terms of effective stress (K_0) was less than or equal to 1.

Figure 4.9 shows that for k = 2.0 kPa/m, four (4) rotational blocks fail before the backscarp stabilizes. Due to the reduction in shear strength, the material of the erosion block collapses and flows downslope, resulting in the initiation of a horizontal shear band. The shear band curves upward to the

ground surface after propagating some distance horizontally. The upward moving shear band touches the ground surface, resulting in global block failure of the first block. Following the failure of the first block, the soil blocks are displaced further, resulting in a flowslide type of failure pattern. Following the failure of the first block, the depth of subsequent failed soil blocks decreases. In comparison to the other two strength gradients used in this study, the soil blocks fail more quickly for shear strength gradient *(k)* = 2.0 kPa/m and deteriorate over a greater retrogression distance of 46.5 m.

As shown in Fig. 4.10, increasing the shear strength gradient (k ~ 3.0 kPa/m) reduces the distance of subsequent failed soil blocks. In comparison to k = 2.0 kPa/m, the global failure of the first block occurs relatively slowly. Only two blocks of soil fail with a retrogression distance of 30 m, resulting in a flowslide type of failure. As a result, it can be seen that increasing the shear strength gradient makes the slope more stable, and thus it takes a longer time to fail.

In Fig. 4.8, the soil profile with a shear strength gradient of k = 2.5 kPa/m clearly shows that after the first soil block fails, the depth of succeeding blocks decreases. The retrogression of the landslide comes to an end after three (3) blocks of soil collapse over a distance of 33 m.

It is in agreement with Wang et al. (2021) that a decrease in k causes the retrogression distance to increase. Some key observations from this analysis are: i) as the strength gradient increase, the slope becomes more stable; ii) the retrogression distance reduces as the k increases; iii) if the shear strength gradient is low, the soil blocks will fail quickly.

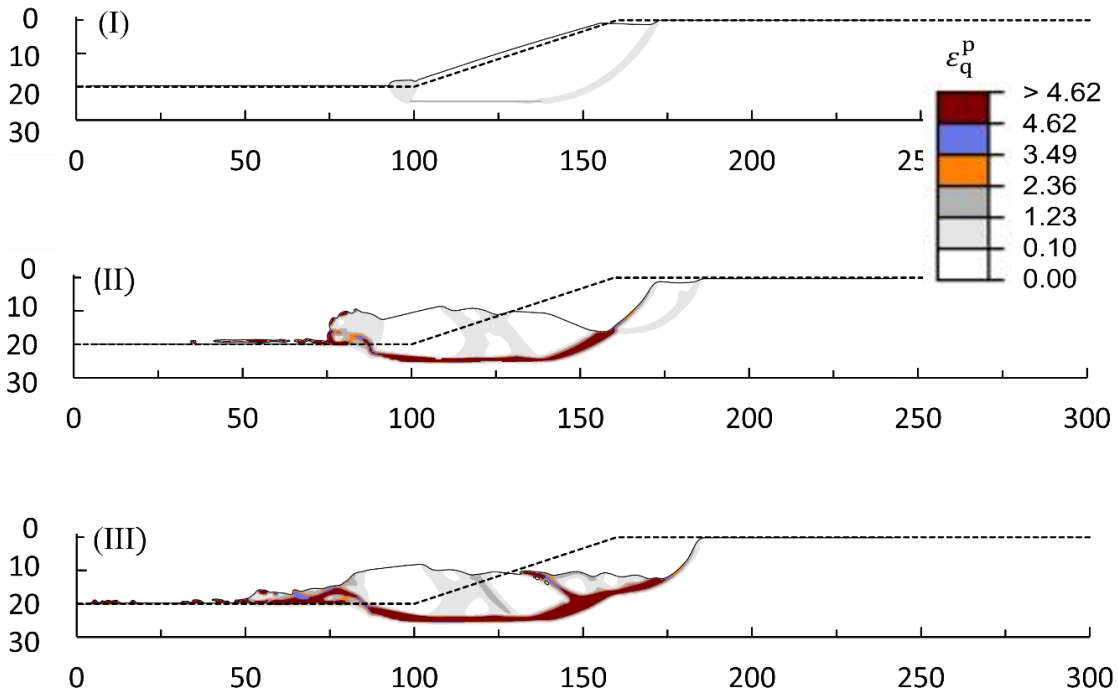

Figure 4.9: Propagation of plastic shear band for shear strength profile, k = 2.5 kPa/m

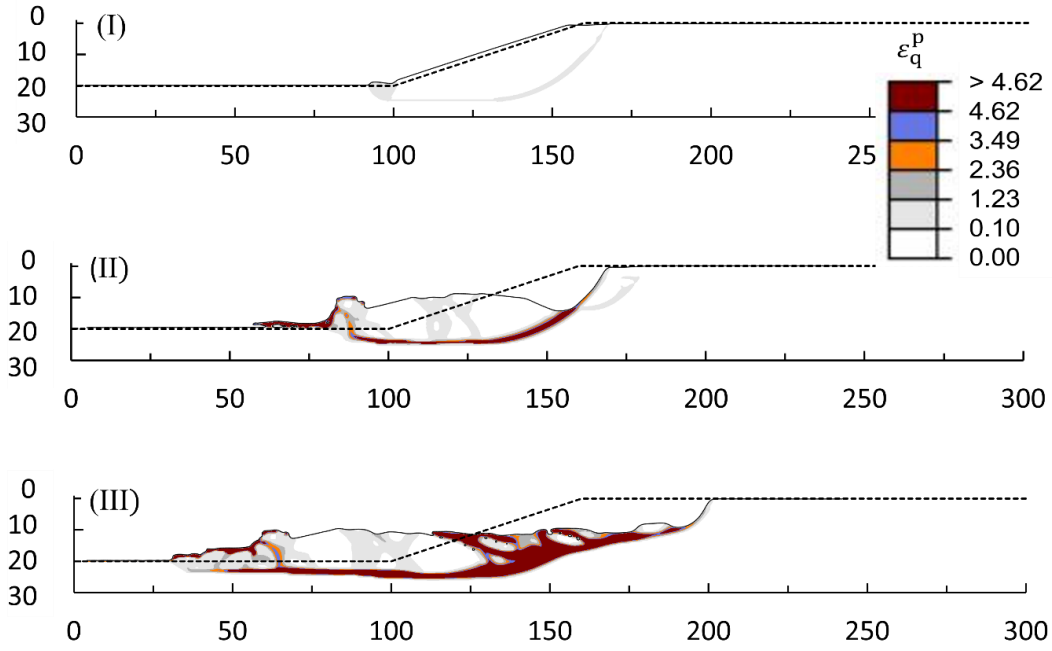

Figure 4.10: Propagation of plastic shear band for shear strength profile, k = 3.0 kPa/m

4.7.5 Effect of Earth Pressure Coefficient at Rest, K_0

Previous studies show that the earth pressure coefficient K (or K_0) is an important factor that affects the failure pattern of a slope of strain-softening materials (Lo & Lee, 1973; Locat et al., 2013; Potts et al., 1997). To investigate the effect of the earth pressure coefficient at rest, K_0, on the failure patterns, simulations are performed for a higher $K_0 = 1.5$ (Fig. 4.11) and compared with the results of $K_0 = 1.0$ (Fig. 4.8), considering the other parameters as the same.

Figure 4.11 shows several horsts and grabens form as the soil debris moves further away from the toe. The successive formation of horsts and grabens represents a typical spread failure. For $K_0 = 1.5$, seven blocks of horsts and grabens form successively. The failure of the successive soil blocks occurs at a shallower distance, and the retrogression of the landslide eventually stops after reaching a retrogression distance of 122 m.

When $K_0 = 1.5$, it is found that the first block globally fails at a greater distance than when the K_0 is equal to 1.0 (Fig. 4.8). The retrogression distances for $K_0 = 1.0$ and 1.5 are, respectively, 33 m and 122 m. A flowslide type of failure pattern is observed for $K_0 = 1.0$, as shown in Fig. 4.8. However, the spread type of failure is observed for $K_0 = 1.5$ as shown in Fig. 4.11. Nevertheless, in both cases, since the backscarp slope is steeper than the original slope (3:1), subsequent block failure occurs at a shallower depth.

A slope with high lateral stress stores more strain energy, and once it is released, for instance by the local failure triggered by toe erosion, the soil layer has a tendency to expand laterally (Bjerrum, 1964). This explains the formation of horizontal shear bands in Figure 4.11, rather than upward curves as in Figure 4.8. Geertsema et al. (2006) considered that spreads might occur on slopes where s_{u0} and

k are higher than what is needed for a flowslide. This consideration was based on a number of historical landslides in eastern Canada and Scandinavia.

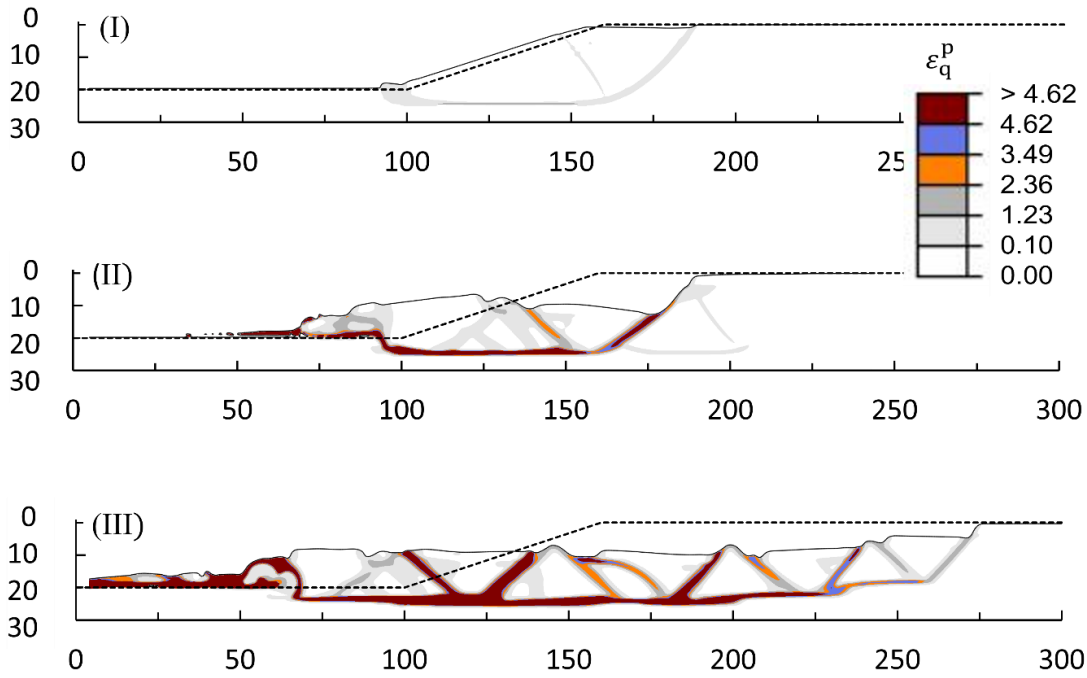

Figure 4.11: Propagation of plastic shear band for slope 3:1 ($K_0 = 1.5$)

Based on the current FE simulation, a higher earth pressure coefficient, which is a sign of a higher s_{u0}, could be a cause of a spread.

An increased shear strength gradient (k) changes the failure plane development and thereby reduces L_R in flowslides; however, k has less effect on retrogression in the formation of spreads. Thus, from this analysis, it can be concluded that the earth pressure coefficient at rest is a significant factor that affects both failure pattern and retrogression distance.

4.7.6 Effect of rate of softening (δ_{95})

To investigate the effect of the rate of softening, analysis is carried out for δ_{95} = 0.01 m (Fig. 4.12) and compared with δ_{95} = 0.05 m. Simulations for δ_{95} = 0.05 m have already been presented in Fig. 4.8.

Figure 4.12 shows that the reduction of shear strength of the eroded block triggers the sensitive clay to form a horizontal shear band which then curves upward towards the surface crust. Two upward-moving shear bands touch the ground surface after shear band initiation. The soil blocks are displaced further in this way, resulting in a flowslide type of failure pattern. For lower δ_{95}, a faster degradation of shear strength leads to the failure of five successive blocks of soil block and the retrogressive distance of 56 m. However, for a higher value of δ_{95} (0.05), the retrogression distance is small and it stops at 33 m (Fig. 4.8). The retrogression distance increases by 23 m when δ_{95} is reduced to 0.01 m from 0.05 m. This is because the resistance of brittle soil reduces very fast with the accumulated plastic strain and hence becomes unable to form a larger horizontal shear band. As a result, the shear band moves upward to the soil with relatively lower strength. In comparison to Figs. 4.8 and 4.12, a relatively lower backscarp is observed for δ_{95} = 0.01 m.

To summarise, the increase in brittleness (i.e. a decrease in δ_{95}) causes the post-peak degradation of undrained shear strength to occur quickly, resulting in the failure of a large mass of soil over a large retrogression distance. It also concurs with Locat et al. (2013) that soils with a high level of brittleness (lower δ_{95}) are more prone to cause large retrogressive landslides.

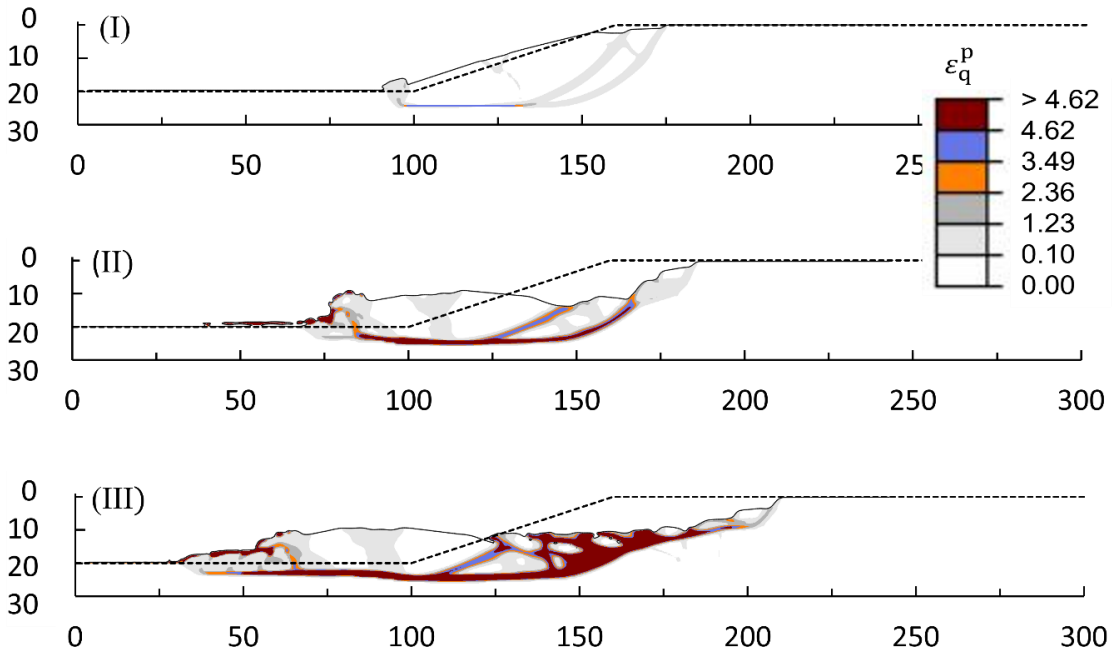

Figure 4.12: Effect of δ_{95} for slope 3:1

4.7.7 Effect of depth of the eroded block

The depth of the eroded block may also influence the failure patterns. Two analyses are performed in order to investigate this for the following conditions: the slope in Fig. 4.13 has an erosion block depth of 3 m, while in Fig. 4.8 has an erosion block depth of 5 m. Except for the depth of the eroded block, all other parameters are the same as those shown in Fig. 4.8.

As shown in Fig. 4.13, a horizontal shear band forms as a result of the reduction of shear strength of a 3 m eroded block. Global failure occurs when the shear band moves upward and reaches the crust. The first block failure causes a series of flowslides to form. The surface crust at the left of the toe is not affected due to the erosion of the 3 m soil block near the toe, as shown in Fig. 4.13. The soil becomes more remoulded in comparison to the previous 5 m block erosion, and thus more soil block fails. The retrogression distance increases as the depth of the eroded block decreases.

When the depth of the eroded block is 3 m, three blocks of soil fail, and the retrogression distance is 48.5 m. The retrogression distance for a 5 m erosion block is 33 m, but only two blocks fail. The eroded block that failed at a shallower (3 m) depth could displace easily in the downslope direction, as compared to an eroded block that fails through deeper soil (5 m) (Fig. 4.8). The higher potential of displacement of the shallower eroded block facilitates the failure of the subsequent soil blocks and results in larger retrogression. However, because of the greater depth of the eroded block (5 m), the surface crust at the left of the toe is affected. The debris from the failed soil block moves away from the toe with the surface crust material as the flowslides form (Fig. 4.8).

From the comparison of these two conditions (Figs. 4.8 and 4.13), it can be concluded that a sufficiently large amount (greater depth) of toe erosion is required to affect the surface crust (downslope) at the left of the toe. A small amount (less depth) of erosion could cause global failure, but the failed soil mass moves over the surface crust. The simulation results also reveal that toe erosion depth has an effect on retrogression landslide failure distance.

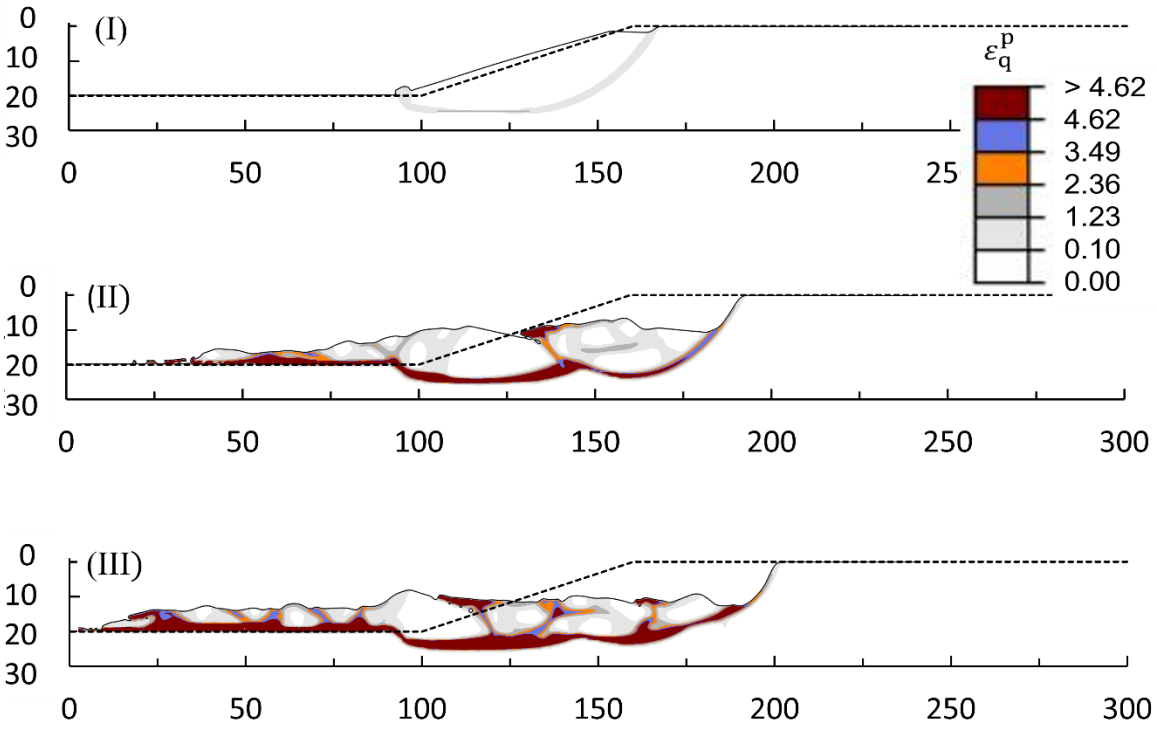

Figure 4.13: Effect of depth of eroded block (3 m)

4.8 Summary

Many large-scale landslides occur in sensitive clays. The shear strength of the sensitive clay layer generally increases with depth. Several post-slide investigations show different soil units above and below the failure plane, at least, in terms of particle size distribution, clay/silt content and liquidity index. The present study investigates the effects of the undrained shear strength and softening rate on the progressive failure of sensitive clay slopes. It is observed that a slower rate of softening of the soil below the level of the toe could cause the shallower failure of soil blocks and larger retrogression. Furthermore, it has been noticed that a relatively higher initial undrained shear strength of the soil in the lower clay layer also could increase the retrogression distance. However, the effects of softening are more significant than shear strength increase on retrogression distance.

Finally, it is to be noted that only a few simulations are performed in this study, although the results show some interesting trends that could be useful for further investigation of the role of the deeper clay layer on slope failure mechanisms and the extent of landslides.

Chapter 5: Conclusions and Recommendations

5.1 Conclusions

Many large-scale landslides occur in sensitive clays. The shear strength of the sensitive clay layer generally increases with depth. Several post-slide investigations show different soil units above and below the failure plane, at least, in terms of particle size distribution, clay/silt content, and liquidity index. The present study primarily focuses on the effects of the undrained shear strength and softening rate on the progressive failure of sensitive clay slopes. Limit equilibrium (LE) analysis and finite element (FE) analyses are performed in this study. The LE methods cannot determine the stress and deformation of the displacing soil. Existing Lagrangian-based FE cannot simulate large deformations. A Eulerian-based FE method is used in this study which does not have any numerical issue related to mesh distortion.

LE and FE analyses of elastic perfectly plastic clay slopes are presented in chapter 3, which show that:

- Critical failure surface shifts upward with an increase in shear strength gradient. The critical circle is a midpoint circle and toe circle for low and high shear strength gradients.
- When the shear strength gradient is high, the effects of using a higher shear strength profile in the lower clay layer are less significant than when the shear strength gradient is low.
- Increasing shear strength in the lower clay layer also has an effect on the depth of the failure circle. When a higher shear strength profile is used, the failure circle usually shifts upward. However, for a mild slope angle, an increase in the shear strength profile below the toe has no significant effect on the failure depth.
- Increasing shear strength in the lower clay layer also has an effect on the depth of the failure circle. When a higher shear strength profile is used, the failure circle usually shifts upward.

However, for a mild slope angle, an increase in the shear strength profile below the toe has no significant effect on the failure depth.

- A higher strength of the lower clay layer could influence the failure depth. However, the failure of the subsequent soil blocks in a retrogression landslide cannot be explained by LE analysis.
- The position of the firm base layer at or below the toe affects the failure pattern and failure depth of a slope.

The effects of strain-softening and strain rate on undrained shear strength, and thus the progressive formation of failure planes and large-scale landslides in sensitive clays, are presented in chapter 4. This set of analyses shows that:

- A slower rate of softening of the soil below the level of the toe could cause the shallower failure of soil blocks and larger retrogression.
- A relatively higher initial undrained shear strength of the soil in the lower clay layer also could increase the retrogression distance. However, the effects of softening are more significant than the shear strength increase on retrogression distance.
- A steeper slope angle results in a greater retrogression distance and an increased number of failed blocks during landslides. After the initial block failure, a steeper slope is found to have a larger backscarp.
- An increase in strength gradient (k) makes the slope more stable and reduces the retrogression distance. However, if the shear strength gradient is low, more soil block failure is expected.
- Earth pressure coefficient at rest is a significant factor that affects both failure pattern and retrogression distance.

- An increase in the rate of softening (i.e., a decrease in δ_{95}) causes the post-peak degradation of undrained shear strength to occur quickly, resulting in the failure of a large mass of soil over a large retrogression distance. It also shows that soils with a high level of brittleness are more prone to cause large retrogressive landslides.

5.2 Recommendations

The current study presents large deformation FE modelling of clay slopes. The FE results are also compared with limit equilibrium methods. The present FE modelling has many advantages and can explain deformation and progressive failure that LE methods cannot. However, the present study has some limitations. The following are some recommendations for future studies.

- Despite the fact that the analyses in this study were conducted for a specific geometry, triggering factors, and undrained conditions, the existing modelling technique could be improved further using other loading conditions and geometries.
- Although the element size scaling rule is used to reduce the mesh size dependency of the solution, additional research might be carried out to develop a more effective approach.
- The landslide in this study is modelled in the plane-strain condition. However, in reality this is a three-dimensional problem. Three-dimensional modelling of retrogressive landslides would be computationally expensive but could reveal more about their mechanisms.
- The effects of anisotropy are not considered in the present study, which could be significant in sensitive clays.
- A detailed investigation of the role of the effects of the surficial crust on retrogressive landslides using a large deformation finite element (FE) modelling technique is required.

References

Andresen, L. and Jostad, H. P. 2002. A constitutive model for anisotropic and strain-softening clay. In *Numerical Models in Geomechanics,* 79–83.

Andresen, L. and Jostad, H. P. 2007. Numerical Modeling of Failure Mechanisms in Sensitive Soft Clay — Application to Offshore Geohazards. In *Off. Technology Conf. (pp. 1–7)*. Texas: OTC 18650.

Benson, D. J. and Okazawa, S. 2004. Contact in a multi-material eulerian finite element formulation. *Computer Methods in Applied Mechanics and Engineering*, 193(39–41): 4277–4298.

Bélanger, K., Locat, A., Fortier, R. and Demers, D. 2017. Geophysical and geotechnical characterization of a sensitive clay deposit in Brownsburg, Quebec, In *Landslides in sensitive clays: From research to implementation*, Springer, Cham, Switzerland, edited by V. Thakur, J.-S. L'Heureux, and A. Locat, 77–86.

Bjerrum, L. 1967. Progressive failure in slopes of overconsolidated plastic clay and clay shales. Terzaghi Lecture. *Journal of the Soil Mechanics and Foundations Division*, ASCE. 93(5): 3–49.

Booker, J.R. and Davis, E. H. 1972. A note on a plasticity solution to the stability of slopes in inhomogenous clays, *Géotechnique,* 22(3): 509–513.

Boukpeti, N., White, D. J., Randolph, M.F. and Low, HE 2012. Strength of Fine-grained Soils at the Solid–fluid Transition, *Géotechnique*, 62(3): 213–226.

Carson, M.A. 1979. On the retrogression of landslides in sensitive muddy sediments: reply, *Canadian Geotechnical Journal*, 16(2): 431–444.

Chai, J., Igaya, Y., Hino, T. and Carter, J. 2013. Finite element simulation of an embankment on soft clay–Case study. *Computers and Geotechnics*, *48*: 117–126.

Chen, W. F. 1975. Limit Analysis and Soil Plasticity. *Elsevier*, Amsterdam, Netherlands.

Cheng, Y. M., Lansivaara, T. and Wei, W. B. 2007. Two-dimensional slope stability analysis by limit equilibrium and strength reduction methods. *Computer and Geotechnics*, 34: 137–150.

Das, B. M. and Sobhan, K. 2006. Principles of geotechnical engineering, ed. *Cengage Learning,* Boston, USA. 771p.

Davis, E. H. and Booker, J. R. 1971. The effect of increasing strength with depth on the bearing capacity of clays. *Research Report R175*, School of Civil Engineering, University of Sydney.

Davis, E. H. and Booker, J. R. 1973. The effect of increasing strength with depth on the bearing capacity of clays. *Géotechnique*, 23(4) : 551-563.

Dawson, E. M., Roth, W. H. and Drescher, A. 1999. Slope stability analysis by strength reduction. *Géotechnique*, 49(6) : 835–840.

Delisle, M. C. and Leroueil, S. 2000. Détection, à l'aide du piézocône, de zones ramollies dans des pentes argileuses et évaluation de leur comportement mécanique, *Report GCT2000-07 prepared for the Ministère des Transports du Québec*, Université Laval, Québec.

Demers, D., Robitaille, D., Locat, P., and Potvin, J. 2014. Inventory of large landslides in sensitive clay in the province of Québec, Canada: preliminary analysis. In Landslides in Sensitive Clays *Springer*, Dordrecht, 77–89.

Dey, R., Hawlader, B., Phillips, R. and Soga, K. 2015. Large Deformation Finite-element Modelling of Progressive Failure Leading to Spread in Sensitive Clay Slopes, *Géotechnique*, 65(8): 657–668.

Dey, R., Hawlader, B., Phillips, R. and Soga, K. 2016. Modeling of Large-Deformation Behaviour of Marine Sensitive Clays and Its Application to Submarine Slope Stability Analysis, *Canadian Geotechnical Journal*, 53(7): 1138–1155.

Dutta, S., Hawlader, B. and Phillips, R. 2015. Finite element modeling of partially embedded pipelines in clay seabed using Coupled Eulerian–Lagrangian method, *Canadian Geotechnical Journal*, 52(1): 58–72.

Einav, I. and Randolph, M. F. 2005. Combining upper bound and strain path methods for evaluating penetration resistance, *International Journal for Numerical Methods in Engineering,* 63(14): 1991–2016.

Einav, I. and Randolph, M. F. 2006. Effect of Strain Rate on Mobilised Strength and Thickness of Curved Shear Bands, *Géotechnique*, 56(7): 501–504.

Fredlund, D. G. and Krahn, J. 1977. Comparison of slope stability methods of analysis. *Canadian Geotechnical Journal*, 14(3): 429–439.

Gibson, R. E. and Morgenstern, N. 1962. A note on the stability of cuttings in normally consolidated clay, *Géotechnique,* 12(3): 212–216.

Geertsema, M., Clague, J. J., Schwab, J. W. and Evans, S. G. 2006. An overview of recent large catastrophic landslides in northern British Columbia, *Canada Engineering Geology,* 83(1–3): 120–143.

Griffiths, D. V. and Lane, P. A. 1990. Finite element analysis of the shear vane test. *Computers & structures*, 37(6): 1105–1116.

Griffiths, D. V. and Kidger, D. J. 1995. Enhanced visualization of failure mechanisms by finite elements. *Computers & Structures*, 55(2): 265–268.

Griffiths, D. V. and Lane, P. A. 1999. Slope stability analysis by finite elements, *Géotechnique*, 49(3): 387–403.

Griffiths, D. V. and Yu, X. 2015. Another look at the stability of slopes with linearly increasing undrained strength, *Géotechnique*, 65(10): 824–830.

Han, J. and Leshchinsky, D. 2004. Limit equilibrium and continuum mechanics-based numerical methods for analyzing stability of MSE walls. In *Proc. of the 17th ASCE Engineering Mechanics Conference*, University of Delaware, Newark, DE, 1: 1–8.

Ho, I. 2014. Parametric Studies of Slope Stability Analyses Using Three-Dimensional Finite Element Technique: Geometric Effect. *Journal of GeoEngineering*, 9(1): 33–43.

Huang, M. and Jia, C. Q. 2009. Strength reduction FEM in stability analysis of soil slopes subjected to transient unsaturated seepage. *Computers and Geotechnics*, 36(1–2): 93–101.

Hunter, J. H. and Schuster, R. L. 1968. Stability of simple cuttings in normally consolidated clay, *Géotechnique,* 18(3): 372–378.

Karmaker, R. and Hawlader, B. 2018. Modeling of Pile Stabilized Clay Slopes Using a Large Deformation Finite-Element Method, *7th Canadian Geohazards Conference*, paper no-155.

Karmaker, R. and Hawlader, B. 2022. Large deformation finite-element modeling of pile jacking in sensitive clay, *Proceedings of 20th International Conference on SMGE*, Sydney, Australia.

Koppula, S. D. 1984. On stability of slopes in clays with linearly increasing strength, *Canadian Geotechnical Journal*, 21(3): 577–581.

Kvalstad, T. J., Andresen, L., Forsberg, C. F., Berg, K., Bryn, P. and Wangen, M. 2005. The Storegga Slide: evaluation of triggering sources and slide mechanics, *Marine and Petroleum Geology*, 22(1-2): 245–256.

Leshchinsky, D. and Smith, D. S. 1989. Deep-seated failure of a granular embankment over clay: stability analysis. *Soils and foundations*, *29*(3): 105–114.

Lo, K. Y. and Hinchberger, S. D. 2006. Stability analysis accounting for macroscopic and microscopic structures in clays. In *Proceeding of 4th International Conference on Soft Soil Engineering*. Vancouver, Canada, 3–34.

Lo, K. Y. and Lee, C. F. 1973. Stress analysis and slope stability in strain-softening materials. *Géotechnique,* 23(1) : 1–11.

Locat, P., Leroueil, S. and Locat, J. 2008. Remaniement et mobilité des débris de glissements de terrain dans les argiles sensible de l'est du Canada, In *Proceedings of the 4th Canadian Conference on Geohazards* : *From Causes to Management*, Presse de l'Université Laval, Québec, Canada, 97–106.

Locat, A., Leroueil, S., Bernander S., Demers, D., Jostad, HP. and Ouehb, L. 2011. Progressive failures in eastern Canadian and Scandinavian sensitive clays. *Canadian Geotechnical Journal*, 48(11): 1696–1712.

Locat, A., Jostad, H. P. and Leroueil, S. 2013. Numerical Modeling of Progressive Failure and Its Implications for Spreads in Sensitive Clays, *Canadian Geotechnical Journal*, 50(9): 961–978.

Locat, A., Leroueil, S., Fortin, A., Demers, D. and Jostad, H.P. 2015. The 1994 landslide at Sainte-Monique, Quebec: geotechnical investigation and application of progressive failure analysis, *Canadian Geotechnical Journal*, 52(4): 490–504.

Locat, J., Turmel, D., Locat, P., Therrien, J. and Létourneau, M. 2017. The 1908 disaster of Notre-Dame-de-la-Salette, Québec, Canada: Analysis of the landslide and tsunami. In *Landslides in Sensitive Clays*, Springer, Cham, 361–371.

Locat, A., Locat, P., Demers, D., Leroueil, S., Robitaille, D. and Lefebvre, G. 2017. The Saint-Jude landslide of 10 May 2010, Quebec, Canada: Investigation and characterization of the landslide and its failure mechanism, *Canadian Geotechnical Journal*, 54(10): 1357–1374.

Locat, A., Locat, P., Michaud, H., Hébert, K., Leroueil, S. and Demers, D. 2019. Geotechnical characterization of the Saint-Jude clay, Quebec, Canada, *AIMS Geosciences*, 5: 273–302.

Loukidis, D., Bandini, P. and Salgado, R. 2003. Stability of seismically loaded slopes using limit analysis, *Géotechnique*, 53(5): 463–479.

Maula, B. H. and Zhang, L. 2011. Assessment of embankment factor safety using two commercially available programs in slope stability analysis. *Procedia Engineering*, 14: 559–566.

Perret, D., Mompin, R., Demers, D., Lefebvre, G. and Pugin, A.J.M. 2013. Two large sensitive clay landslides triggered by the 2010 Val-Des-Bois earthquake, Québec (Canada)–implications for risk management. Poster, First Int. In *Workshop on Landslides in Sensitive Clays (IWLSC)*, Québec, Canada, 28–30.

Perret, D., Therrien, J., Locat, P. and Demers, D. 2019. Influence of surficial crusts on the development of spreads and flows in eastern Canadian sensitive clays, *Proceedings of the 72nd Canadian geotechnical conference*, GeoSt.John's, St. John's, NL, Canada.

Potts, D. M., Dounias, G. T. and Vaughan, P. R. 1990. Finite element analysis of progressive failure of Carsington embankment. *Géotechnique*, 40(1): 79–101.

Potts, D., Kovacevic, N. and Vaughan, P. 1997. Delayed collapse of cut slopes in stiff clay. *Géotechnique*, 47(5): 953–982.

Quinn, P. E., Diederichs, M. S., Rowe, R. K. and Hutchinson, D. J. 2011. A new model for large landslides in sensitive clay using a fracture mechanics approach, *Canadian Geotechnical Journal*, 48(8): 1151–1162.

Randolph, M. F., White, D. J. and Yan, Y. 2012. Modelling the Axial Soil Resistance on Deep-water Pipelines, *Géotechnique*, 62(9): 837–846.

Rayhani, M. H., Yanful, E. K. and Fakher, A. 2007. Desiccation-induced cracking and its effect on the hydraulic conductivity of clayey soils from Iran. *Canadian Geotechnical Journal*, 44(3), 276–283.

Roy, M., Blanchet, R., Tavenas, F. and Rochelle, P. L. 1981. Behaviour of a sensitive clay during pile driving. *Canadian Geotechnical Journal*, *18*(1): 67–85.

Roy, M. and Leblanc, A. 1988. Factors Affecting the Measurements and Interpretation of the Vane Strength in Soft Sensitive Clays, In *Vane Shear Strength Testing in Soils: Field and Laboratory Studies*, ASTM STP 1014, A.F. Richards Ed., Philadelphis, 117–128.

Saha, B., Hawlader, B., Dey, R. and McAffee, R. 2014. Slope Stability Analysis using a Large Deformation Finite Element Modeling Technique. In *67th Canadian Geotechnical Conference GeoRegina*.

Shen, J. M. and Brand, E. W. 1985. On stability of slopes in clays with linearly increasing strength: Discussion. *Canadian Geotechnical Journal*, *22*(3): 419–421.

Steward, T., Sivakugan, N., Shukla, S. K. and Das, B. M. 2011. Taylor's slope stability charts revisited. *International Journal of Geomechanics*, 11(4): 348–352.

Sully, J. P. 1993. Interpretation of field vane strength of an anisotropic soil: Discussion. *Canadian Geotechnical Journal*, 30(4): 720–722.

Taylor, D.W. 1937. Stability of earth slopes. *Journal of Boston Society of Civil Engineers*, 24: 337–386.

Thakur, V., Degago, S. A., Oset, F., Aabøe, R., Dolva, B. K., Aunaas, K., Nyheim, T., Lyche, E., Jensen, O. A., Sæter, M. B., Robsrud, A., Viklund, M., Nigussie, D. and L'Heureux, J. S. 2014. Characterization of post-failure movements of landslides in soft sensitive clays. In *Landslides in sensitive clays–from geosciences to risk management* (eds J. S. L'Heureux, A. Locat, S. Leroueil, D. Demers and J. Locat), Dordrecht, the Netherlands: Springer, 91–103.

Tu, Y. L., Liu, X. R., Zhong, Z. L., Li, Y. Y. and Drescher, A. 2016. New criteria for defining slope failure using the strength reduction method. *Engineering Geology*, 212: 63–71.

Ugai, K. and Leshchinsky, D. 1995. Three-dimensional limit equilibrium and finite element analyses: a comparison of results. *Soils and Foundations*, 35(4): 1–7.

Wang, C. and Hawlader, B. 2017. Numerical modeling of three types of sensitive clay slope failures. In *Proceedings of the 19th International Conference on Soil Mechanics and Geotechnical Engineering*, Seoul, South Korea, 871–874.

Wang, C., Saha, B. and Hawlader, B. 2015. Some factors affecting retrogressive failure of sensitive clay slopes using large deformation finite element modeling. In *Proceedings of the 68th Canadian Geotechnical Conference and the 7th Canadian Permafrost Conference*, Quebec City, Canada, 1–6.

Wang, C., Hawlader, B., Perret, D. and Soga, K. 2021. Effects of Geometry and Soil Properties on Type and Retrogression of Landslides in Sensitive clays, *Géotechnique*, 1–15.

Yu, H. S., Salgado, R., Sloan, S. W. and Kim, J. M. 1998. Limit analysis versus limit equilibrium for slope stability. *Journal of Geotechnical and Geoenvironmental Engineering*, *124*(1): 1–11.

Zhu, H. and Randolph, M.F. 2011. Numerical analysis of a Cylinder Moving Through Rate-dependent Undrained Soil, *Ocean Engineering*, 38(7): 943–953.

Zolfaghari, A. R., Heath, A. C., and Mccombie, P. F. 2005. Simple genetic algorithm search for critical non-circular failure surface in slope stability analysis. *Computer and Geotechnics*, 32: 139–152.